N82-19358 UNCLAS

MICROCOPY RESOLUTION TEST CHART
NATIONAL BUREAU OF STANDARDS-1963-A

NASA Contractor Report 165827

Evaluation of Superplastic Forming and Co-Diffusion Bonding of Ti-6Al-4V Titanium Alloy Expanded Sandwich Structures

G. H. Arvin, L. Israeli, J. H. Stolpestad, and G. W. Stacher

North American Aircraft Operations
Rockwell International Corporation
El Segundo, California

September 1981

NASA

National Aeronautics and
Space Administration

Langley Research Center
Hampton, Virginia 23665

PREFACE

One of the outstanding new technologies applicable to airframe structures is the Superplastic Forming/Diffusion Bonding (SPF/DB) process. This innovative manufacturing process in the field of titanium structures has already shown important reductions in weight and fabrication cost. SPF/DB has the potential of becoming the technology breakthrough to produce the needed low-cost, lightweight, reliable titanium airframe structures required for the next generation of air vehicle systems.

The program presented in this report is a continuation of previous NASA programs oriented towards the application of the SPF/DB process to supersonic cruise research (SCR). The present program is the verification of the performance of an SPF/DB structure designed to meet the requirements of an inner wing area of the NASA arrow-wing advanced supersonic transport concept (a Boeing design used as the baseline).

The program consists of selection of structural concepts and their optimization for minimum weight, SPF/DB process optimization, fabrication of representative specimens, and specimen testing and evaluation.

The structural area used for this research includes both upper and lower wing panels, where the upper wing panel (mainly designed under compression loads) is used for static test evaluation, and the lower panel (mainly designed under tension loads) is used for fracture mechanics evaluations.

Individual test specimens were cut from six 1143 mm (45 in.) by 1372 mm (54 in.) panels and consist of 39 static specimens, 10 fracture mechanics specimens, and one each full size panel for static and fracture mechanics testing. Traceability is maintained from the large "source" panels to the individual small specimens. Tests are performed at temperatures of -54° C (-65° F), R. T., and 260° C (500° F).

Key Rockwell personnel associated with this program are as follows:

G. H. Arvin	Program Manager
L. Isreali	Project Engineer
J. Stolpestad	Fatigue and Fracture Mechanics
G. Stacher	Material and Producibility
F. Keoller	Material and Producibility
C. Lappen	Quality and Reliability Assurance
C. Moore	Static Tests
S. Storm	Dynamic Tests

i

TABLE OF CONTENTS

Section I

INTRODUCTION

BACKGROUND

This program was one basic facet of an ongoing long-range NASA program consisting of interrelated supersonic cruise research (SCR) efforts directed toward advancing aerospace technology applicable to future supersonic cruise aircraft.

The NASA SCR program is specifically directed toward development of a strong technology base to provide decision making rationale for future supersonic aircraft, including aerodynamics, propulsion, systems, and structural studies to increase efficiency of the aircraft while also providing for environmental concerns. Under the SCR program, advances in aerospace technology are showing that supersonic cruising vehicles can become economically viable in the future.

Of the technologies being explored, the aircraft structure is among the most important because it requires high reliability, structural efficiency, and low cost. Several options are available for these structures, including advanced metallics and composites. The most likely approach to SCR structures will probably include an optimum combination of advanced metallics and composites to produce an efficient low-cost aircraft with minimal risk. The most promising advanced metallic structure that will have direct application to SCR is a new emerging technology using superplastic forming and diffusion bonding (SPF/DB) properties of metals, particularly titanium. This technology promises to become the technological breakthrough required to produce low-cost, lightweight, reliable SCR structures.

OBJECTIVES

The objectives of this program were to:

1. Demonstrate the applicability of the titanium alloy SPF/DB expanded sandwich structure to future supersonic cruise aircraft

2. Establish state-of-the-art procurement specifications and optimize process parameters for titanium SPF/DB

3. Supplement the design data base for a titanium SPF/DB sandwich in the areas of static design allowable strength, fatigue and crack growth characteristics, and crack arrestment techniques

APPROACH

This program demonstrated that SPF/DB is capable of producing titanium structures that will meet durability and structural requirements of future SCR vehicles

As reported in recent studies (references 1 and 2) which determined the impact of SPF/DB technology on typical large, supersonic cruise aircraft, cost savings approaching 70 percent and weight savings approaching 50 percent, when compared with more conventional titanium manufacturing processes, may be possible. Design concepts heretofore considered uneconomical or impractical because of high costs and fabrication difficulties, including sandwich structures, beaded panels, corrugated or sine wave spars, frames, and panels with integral frames, are now possible using the SPF/DB process. Complex configurations which could otherwise not be fabricated by conventional methods have been produced in titanium by the SPF/DB process in a single cycle.

Superplasticity in titanium is a phenomenon in which very large tensile elongations may be realized because, under the proper conditions of temperature and strain rate, local thinning (necking) does not occur. (See figure 1a.) Diffusion bonding (DB) is the joining of titanium under pressure at elevated temperatures without melting or use of bonding agents. Fortunately, DB of titanium is accomplished under identical conditions to that of superplastic forming (SPF). This is the basis for the combined SPF/DB process.

Combining of SPF with DB, using stopoff in selected areas to prevent bonding, and using argon gas to expand the DB parts, provides a wide range of structural shapes from simple two-sheet construction to extremely complex integral skin-stringer-frame shapes (reference 1). The fabrication of a three-sheet sandwich structure is illustrated in figure 1b. Yttria compound (stopoff) is applied to both sides of the core sheet to prevent DB where desired. The titanium pack is then heated to approximately 927° C (1,700° F), argon gas pressure is applied to the sheets causing DB, followed by the sandwich being formed by expanding the pack with argon gas injected between the two face sheets.

SCHEDULE

The program schedule is illustrated in figure 2. The four interdependent tasks shown are described in "Program Structure."

LIST OF SYMBOLS

A	sandwich cross section area
D	bending rigidity of facing sheets about sandwich centroidal axis
E_c	compression modulus of elasticity
F_c	column buckling stress
F_{ci}	initial buckling stress
F_{cs}	crippling stress (subscript indicates individual section components)
F_{cy}	compression yield stress
F_s	core web initial shear buckling stress
$F_{s_{ult}}$	core web failure stress
F_s'	core shear stress corresponding to core web initial buckling stress
$F_{s_{ult}}'$	core shear failure stress
G	material shear modulus
G_c'	core shear modulus
I	section moment of inertia
I_{2p}	moment of inertia for 2p sandwich width
I_{LT}	moment of inertia for LT sandwich width
L	beam length between supports
M	moment
P	applied test load
P_{cr}	highest test load in the elastic range
P_c	column buckling load
c_e	crippling coefficient (function of edge support and material)
e	distance from the neutral axis to the midfiber of the compressed facesheet of the sandwich
f	applied stress

LIST OF SYMBOLS (Concl)

f_{cr}	applied stress at which buckling occurred
f_{ult}	applied failure stress
f'_{cr_S}	applied core shear corresponding to core web initial buckling
f'_{ult_S}	applied ultimate core shear
K	buckling coefficient
K_S	buckling coefficient for core web shear
ℓ_1	force arm (moment = force x arm)
t_{F_C}	thickness of the compressed facesheet
$t_{F_{min}}$	thinnest facesheet thickness
W	effective width
δ	combined bending and shear deflection
δ_B	bending deflection
δ_S	shear deflection
μ	Poisson's ratio
η	plasticity correction factor
ρ_0	radius of gyration
ρ_C	material density
ρ''_C	reduced core density (core webs considered only as core component)
ϵ	strain

Subscripts

L or X	parallel to core orientation
T or Y	perpendicular to core orientation
cr	buckling
cs	crippling

4

Section II

PROGRAM DEVELOPMENT

PROGRAM STRUCTURE

In order to achieve the program objectives in a logical sequence of efforts, a program organization consisting of four interdependent tasks was established.

Task 1 - Structural Concept Selection

Task 2 - Process Optimization and Test Specimen Fabrication

Task 3 - Design Allowables Data

Task 4 - Structural Panel Performance

In task 1, one expanded sandwich configuration was selected and sized to meet specified requirements. Panels were designed and detai'ed for fabrication as a source of test specimens for tasks 3 and 4. Design allowable test specimens were designed to be cut from some of the panels.

In task 2, processing parameters for the SPF/DB operation were optimized and specimen panels were fabricated and, where appropriate, cut into smaller test specimens. A complete quality assurance program was developed and used for the titanium material, processing operation, and final product.

In task 3, a comprehensive test program for selected design allowables data was developed. Tests included short column, bending, core shear, durability, and crack growth rate. Data have been evaluated and compared with existing data on expanded sandwich.

In task 4, a test program was established for the behavior of large expanded sandwich panels of the configuration established in task 1. One panel was statically tested in compression, and one was fatigue tested in tension, simulating a key location on the upper and lower wing surface, respectively. Test results were evaluated and compared to theory and appropriate published data.

Activities in the four program tasks are described in detail in the following sections.

5

TASK 1 - STRUCTURAL CONCEPT SELECTION

PROTOTYPE STRUCTURAL APPLICATION

The prototype structure specified to be the basis for this program is the upper and lower wing surface (at point 4) of the Boeing supersonic transport (SST) study aircraft defined in NASA CR145111. The location of point 4 and associated loading conditions are shown in figure 3 and table I. The wing upper surface, critical in compression, was selected as the basis for compression strength and panel stability static testing; the wing lower surface, critical in tension, is the basis for fatigue (crack growth) and crack arrestment specimens.

SANDWICH GEOMETRY SELECTION

Earlier optimization studies of SPF/DB sandwich configurations compared truss, sine wave, and dimpled core characteristics, properties, and efficiencies. The results of these studies (prior to this program) led to the selection of a truss-core configuration as optimum for the requirements and load levels of this program. It is considered a simple and efficient concept for a ratio of more than 3:1 between the two biaxial compression loads. The truss core was oriented along the highest of the two edgewise compression loads, resulting in a spanwise core orientation for the upper wing panel and a chordwise orientation for the lower wing panel. (See figure 4 for panel sizes and core orientation.)

CONFIGURATION SIZING

Effort was performed to reconfirm and finalize the geometric parameters selected in Rockwell precontract studies. (See figure 5.) Preliminary optimization of the upper and lower covers of the wing at point 4, the location selected for consideration in this program, was performed by hand. An existing Rockwell computer program, designed to optimize truss-core sandwich geometry under wide-column conditions, was used to finalize the lower wing cover sizing. This computer program was then expanded to cover compression biaxial and shear loaded panels and used to finalize the upper wing cover. Upper and lower panel original configurations were improved and their combined weight reduced by about 4.3 percent.

PANEL DESIGN

In designing the panels to be fabricated for this program, it was decided the panels should be as large as feasible to reduce fabrication costs and normalize as much as possible the source of the small test specimens while not unduly increasing tooling costs and fabrication complexity. After weighing all relevant considerations, including the state-of-the-art of SPF/DB, an overall panel size of 1,200 by 1,500 mm (4 by 5 feet) was selected, with a usable uniform sandwich area of approximately 990 by 1,220 mm (39 by 48 inches).

To satisfy the requirements of the test plans developed and described in tasks 3 and 4, a six-panel layout was adopted.

1. Two panels for static test elements (task 3)

2. Two panels for fatigue test elements (task 3)

3. One panel for static panel test (task 4)

4. One panel for fatigue panel test (task 4)

The task 3 test elements were cut from the panels in accordance with an optimal specimen distribution layout. Figure 6 shows a typical test specimen layout. Special attention was given to the specimen marking procedure to insure traceability of all specimens along the entire process from panel cutting operation to test evaluation.

TASK 2 - PROCESS OPTIMIZITION AND TEST SPECIMEN FABRICATION

PROCESS OPTIMIZATION

Although one of the objectives of this program was to optimize SPF/DB process parameters, it was decided early in the program that this objective had already been accomplished by the Air Force BLATS program. Consequently, these newly improved procedures, which represented a forefront in the state-of-the-art, were selected for this program to insure the best quality available in the panels to be fabricated. These new improvements consisted of:

1. Kiss plates around the panel between the container and the cover plate to limit the squeeze effect on the sealing contour

2. Time extension of internal argon pressure over a portion of the cooling stage to reduce core deformations after the end of the forming process

3. Container installation on top of the cover plate for easy release of the SPF/DB panel from the container and to enable unrestricted panel rest on the flat cover area

4. Breakthrough and reverse breakthrough simultaneous rapid start of the core forming process over the entire panel area

A step-by-step description of the SPF/DB process as applied to panel fabrication in this program is provided in a subsequent section of this report.

MATERIAL PROCUREMENT

Because of the inordinately long procurement time for titanium sheet, the material for this program was obtained from numerous existing reserve stockpiles. However, exact sheet thicknesses desired were not available in all cases and DB of two or three sheets to form one sandwich face was necessary. This supplementary operation was performed concurrent with panel fabrication in order to have a low impact on the cost of the program. This procedure had been successfully accomplished prior to this program, and no program problems or data contamination were expected or experienced.

Coupons from each sheet of material (figure 7) were made and furnished to the Rockwell Science Center for material characterization to set exact process parameters for the SPF/DB process for each panel.

TOOLING

The most expensive tooling for this program would have been the steel panel container for the SPF/DB panel fabrication process. Fortunately, an existing container for the Space Shuttle windshield frame was made available to this program and saved the cost of machining a new container. The Space Shuttle container and cover plate (figure 8) were of a size easily adaptable to this program except for the cavity depth, which was greater than the panel thickness desired. This problem was easily solved by fabricating a depth-reducing insert to be placed in the cavity.

The Space Shuttle container was inspected and measurements of the container depth indicated a bow in the center of the tool. A nominal depth was calculated, and the insert design was predicated on that measurement. The insert shown in figure 9 was machined of low carbon steel plate.

SPF/DB PROCEDURE

The improved SPF/DB process used in fabricating the expanded sandwich panels for this program is illustrated by the following step-by-step sequence.

1. The argon tubes are installed on one face. (See figure 10.)

2. The core sheet is slotted for argon tube access into the panel. (See figure 11.)

3. Argon tube location in core sheet slot. Holes for argon access to both sides of the core are provided as well. (See figure 12.)

4. The two silk screens are ready for yttria application on both sides of the core sheet. (See figure 13.)

5. One silk screen is positioned over the core sheet for yttria application. (See figure 14.)

6. The core sheet with yttria applied on both sides is aligned with the first face (guide bolts). The argon tubes are tightened with titanium strip welded to the core sheet. (See figure 15.)

7. The second sandwich face is laid down. (See figure 16.)

8. The clamped pack is tack welded together. The long pipes are temporary supports for the argon pipes. (See figure 17.)

9. The pressure plate and container are prepared for processing. The slots for argon tubes can be seen. (See figure 18.)

10. The container insert is installed. (See figure 19.)

11. The container is placed on the heating platen. (See figure 20.)

12. The pack with the picture-frame seal is laid on the container. (See figure 21.)

13. The entire system (pack, container, pressure plate, platens, insulating material, pipes, and thermal sensors) is installed into the 4,500-ton press. Gas and liquid argon supply vessels are on the right side. (See figure 22.)

14 The control unit especially designed for the SPF/DB process is ready to monitor panel fabrication.

15. The end product is cut and cleaned. (See figure 24.)

PANEL FABRICATION

All six panels were fabricated, radiographically evaluated, and dimensionally inspected. The panels were made on a 4,500-ton press, using basically the same procedure as described in the preceding paragraphs, with exceptions described in the following paragraphs.

Fatigue Test Panels

Fatigue panels 1 and 2 (F-100 and F-200) showed a smooth surface with only little grooving at the edges. Because the grooves were located out of the test specimen area, they did not affect the test results. The X-ray survey performed on these two panels showed some very minor core buckling, but the buckling level was found acceptable according to previously established BLATS standards. No ruptures of the core were found.

Panel 3 (F-300) was fabricated in the same manner as the previous two panels. Evaluation of panel F-300 by radiographic means showed slight core distortion and some small core ruptures. However, the ruptures were in the boundary area, which was not used to make any of the individual test specimens. The three completed fatigue panels are shown in figure 25.

Two examples of radiographics are shown in figures 26 and 27.

Panels 1, 2, and 3 (F-100, F-200, and F-300), fabricated for fatigue, crack growth, and crack arrest tests, were chem-milled to final dimensions, and specimens were cut, end filled, and set up for testing. (Testing is described under tasks 3 and 4.) The small specimens are shown in figure 28 and the full panel in figure 29.

Static Test Panels

Panel 4 (S-100 first static panel) was produced following identical procedures used on the previous three fatigue panels. This panel has the core sheet thickness, as well as the core configuration, modified to satisfy static panel requirements. Sealing problems were encountered because of using several smaller heating platens of various thicknesses. As a result, the DB cycle was conducted at a lower pressure level 1.72 MPa (250 psi) instead of 2.07 MPa (300 psi), and the time was extended correspondingly to 4 hours instead of 2 hours, as covered by "Manufacturing Process Procedures."

Problems arose during the forming cycle as a consequence of accidental complete pinching of both inlet argon supply needles. The breakthrough process was substantially delayed until the problem was located; thereafter, the two outlet argon needles were used for supply. The panel, consequently, was formed with argon pressure and without argon flow.

The part was completed, and a visual inspection showed a well-formed part with slight surface grooving. However, radiographic inspection revealed numerous internal defects.

After the S-100 panel was produced, inspection of the container showed an important out-of-plane deformation of the insert toward the edges and especially in the corner areas. A decision was made to continue the use of this container without repairs to the insert in order to avoid a possible additional delay caused by the impending return of the container to the Space Shuttle program for a spare-parts run. It was assumed that the specimens to be obtained from the remaining panels would not be affected by deformation at the panel edges.

Panels 5 and 6 (S-200 and S-300) were fabricated using identical processing procedures as those used for previous panels. The DB cycle was typical, breakthrough was rapid at low pressures, the identical pressure/temperature cycle used in fabrication of panel 4 was applied, and removal and cool-down followed normal procedures. Both panels were well-formed and displayed only slight surface grooving. However, the sixth panel showed some core rupture on the X-ray inspection, while the fifth panel showed a good core. An investigation to determine usability of the sixth panel indicated that the necessary test specimens could be extracted from the good areas of the panel. The specimen layout was modified to avoid discrepant areas, and the specimens were then cut from the panel.

QUALITY ASSURANCE PLAN

A quality assurance program plan of action was established for this program. Related detail inspection instructions were established to implement the plan of action.

10

RADIOGRAPHIC INSPECTION RESULTS

In accordance with the inspection instructions, the six panels were checked for quality. Radiographic inspection of core sheets was used to verify the relationship of the pattern silk screened on opposing surfaces. Fully formed and bonded panels were radiographically inspected for core rupture, core thinning, core distortion, node nonbonds, and node spacing. Ultrasonic inspection normally used to evaluate gas bonded areas (closeout) was not applied to this program because all closeout structures are trimmed from the element test specimens. A summary of the type of discrepancies found in the six fabricated panels by nondestructive testing is shown in table II.

An evaluation of the core rupture in panels 4 and 6 was accomplished by comparison of the processing records of panels 4, 5, and 6. Records indicate that slight overtemperature conditions existed on panels 4 and 6 but not on panel 5. In addition, breakthrough anomalies were encountered on panels 4 and 6 and are considered to be the primary cause of the core rupture. Pinched or constricted gas needles resulted in nonoptimum breakthrough processes which directly affected application of the desired strain rates. Actual strain rates, as opposed to planned strain rates, were high because of the combination of nonuniform breakthrough times and pressures and the slightly overtemperature condition. The conclusion was drawn that for future panels greater emphasis must be placed on maintaining a maximum process temperature of 927° C (1,700° F) on any thermocouple, even at the expense of deviating on the minimum temperature requirement. In addition, it is apparent that locating and maintaining the gas needles in the proper position during pack buildup and tool transport into the hydraulic press will require special care in future operations.

TASK 3 - DESIGN ALLOWABLES DATA

STATIC TESTS

Static Test Plan and Specimen Geometry

The static test plan was established to provide preliminary design allowables data for short column, core shear, and bending beam loading, both longitudinal and transverse, for three temperatures. The static test plan is summarized in table III.

In the following subsections, each type of specimen will be individually discussed relative to its predicted strength, the data from the static tests, test/predicted strength correlation, and recommended semiempirical design strength formulae. In each of these subsections, standardized nomenclature will be used for algebraic representation of structural parameters and for sandwich geometry. Figures 30 and 31 illustrate the geometric nomenclature for this program; the parameters u 1 in the strength equations are defined in the List of Symbols.

11

The material properties used in the test evaluations are shown in table IV. The RT values were obtained from Reference 3 (page 1-10), the -54° C values from Reference 4 (pages 5-83 and 5-80), and the 260° C value from Reference 4 (pages 1-16 and 1-17) as an average between 204° C (400° F) and 316° C (600° F).

The test specimens for the short column, core shear, and bending beam tests are shown in figures 32, 33, and 34, respectively.

Short Column - Longitudinal Core

The longitudinal short column tests were conducted to verify the predicted values for:

a. Local stability stress (initial buckling F_{cr})

b. Failure stress (crippling F_{cs})

c. Compression modulus of elasticity (E_c)

A total of seven specimens were tested at low, room, and high temperatures, as shown in table III. The test results, the predicted values, and their correlation are shown in table V and figures 35 and 36.

Predicted Values

For local stability stress prediction, the conventional buckling formula was used:

$$\frac{F_{cr}}{\eta} = k \left(\frac{\pi^2 E_c}{12(1 - \mu^2)} \right) \left(\frac{t_{F_{min}}}{b_F} \right)^2 \; ; \; \text{Values for } k \text{ from Reference 8.}$$

For failure stress prediction, the conventional crippling formula was used:

$$F_{cs_i} = c_e \sqrt{F_{cy} E_c} \left(\frac{t_i}{b_i} \right)^{0.75}$$

where $c_e = .771$ for truss core sandwich made of Ti-6Al-4V alloy
(Reference 9)

Subscript i indicates the individual sandwich section component under consideration. Besides the aforementioned crippling formula, the following limitation must be considered:

$$F_{cs} \leq F_{cy}$$

The crippling stress calculated for individual components of the truss core section are combined in the following formula:

$$F_{cs} = \frac{\Sigma (F_{cs_i} A_i)}{\Sigma A_i}$$

where $A_i = t_i \times h_i$

Test Results

Test data consist of load versus deflection, gage readings, strain gage indications, and geometry of the individual specimens. The buckling and ultimate stresses were obtained by dividing the applied buckling and ultimate loads by the total transverse section area. The total transverse section area includes both face and core sheets.

$$f_{cr} = \frac{P_{cr}}{LT \, (t_{F_1} + t_{F_2} + t_N)}$$

$$f_{ult} = \frac{P_{ult}}{LT \, (t_{F_1} + t_{F_2} + t_N)}$$

The compression modulus of elasticity, E_c, was obtained by the conventional formula:

$$E_c = \frac{P_{cr}}{\epsilon LT \, (t_{F_1} + t_{F_2} + t_N)}$$

Test/Predicted Correlation

The test/predicted (T/P) ratios exhibited a narrow spread, indicating a good prediction capability. A general review of the ratio of test/predicted values shows:

	Average	Lowest	Highest
Load instability	1.01	0.94	1.09
Failure stress	1.08	0.99	1.18
Modulus of elasticity	1.03	0.93	1.16

Recommendations

A correction factor of 0.84 is recommended for design buckling stress and 0.90 for design crippling stress to bring the average margin of safety to 0.20. The average T/P modulus of elasticity ratio is 1.03 and the predicted E_c values are recommended to be considered adequate.

Therefore:

$$\frac{F_{cr}}{\eta} = 0.84\ K \frac{\pi^2}{12(1-\mu^2)} \left(\frac{t_{F_{min}}}{b_F}\right)^2 \quad ,\ K\ \text{from Reference 8.}$$

$$F_{cs_i} = 0.9\ c_e \sqrt{F_{cy}\ F_c} \left(\frac{t_i}{b_i}\right)^{0.75} \quad ;\ c_e = 0.71\ \text{(Reference 9)}$$

The little influence of the F_{cy} cutoff value in F_{cs} computation for the node was neglected. The weighted crippling stress formula remains unchanged. For modulus of elasticity, the data provided in table IV should be used.

Test values for 260° C indicate that the compression modulus of elasticity derived from Reference 4 for that temperature may be too low. The value of E_c (96.19 GPa) used in the foregoing test for 260° C would have to be increased to 106.77 GPa to bring the (T/P)$_{AV}$ to 1.00. However, since this observation is based on only three tests, it is recommended that future programs include a recheck of the compression modulus at 260° C.

Figure 37 shows a typical room temperature setup, while figure 38 illustrates the elevated temperature test equipment. Figures 39 and 40 show a typical specimen after failure.

Short Column - Transverse Core

The transverse short column tests were conducted to verify the predicted values for:

a. Local stability stress (initial buckling, F_{cr})

b. Failure stress (1.20 x initial buckling assumed)

c. Compression modulus of elasticity (E_c)

A total of seven specimens were tested at low, room, and high temperature, as shown in table III.

The test results, the predicted values and their correlation are shown in table VI and figures 41 and 42.

Predicted Values

For local stability stress prediction, the conventional wide column formula was used:

$$\frac{F_{cr}}{\eta} = K_c \frac{\pi^2 E_c}{12(1-\mu^2)} \left(\frac{t_{F_{min}}}{b_f}\right)^2 \quad ; \quad K_c \text{ from Reference 8.}$$

For failure stress prediction, 1.20 times initial buckling was used. The stress level was in the elastic range; therefore, the plasticity correction factor was equal to unity.

Test Results

Test data consist of load versus deflection, gage readings, strain gage indications, and geometry of the individual specimens.

The buckling and ultimate stress were obtained by dividing the applied buckling and ultimate loads by the transverse area of both face sheets.

$$F_{cr} = \frac{P_{cr}}{1.1\ (t_{F_1} + t_{F_2})}$$

$$F_{ult} = \frac{P_{ult}}{1.1\ (t_{F_1} + t_{F_2})}$$

The compression modulus of elasticity, E_c, was obtained by the conventional formula:

$$E_c = \frac{P_{cr}}{\varepsilon\, 1.1\ (t_{F_1} + t_{F_2})}$$

Figure 43 illustrates a typical specimen setup ready for test. Figures 44 and 45 show a typical specimen after failure.

Test/Predicted Correlation

The test/predicted (T/P) ratios exhibited a narrow spread, indicating a good prediction capability. A general review of the test/predicted values shows:

	Average	Lowest	Highest
Local instability	.84	.73	.99
Failure stress	1.02	.93	1.14
Modulus of elasticity	1.64	1.47	1.89

Recommendations

Although the correct test value for initial buckling is difficult to establish, the predicted values proved about 16% higher than the values obtained from tests. To correct this discrepancy and to provide a 20% margin of safety for design purposes, a correction factor of 0.84 x 0.8 = 0.65 is recommended to be used with the buckling formula. The resulting initial buckling design formula is:

$$\frac{F_{cr}}{\eta} = 0.65\, K_y\, \frac{\pi^2\, E_c}{12\,(1 - \mu^2)} \left(\frac{t_{F_{min}}}{b_f}\right)^2 \qquad ; \ K_y \text{ from Reference 8.}$$

For failure stress prediction, the initial buckling formula, increased by 20%, provided a test/predicted ratio around 1.02. Therefore, the initial buckling formula is considered suitable for design ultimate stress, providing a 20% margin of safety.

$$\frac{F_{ult}}{\eta} = K_y\, \frac{\pi^2\, E_c}{12\,(1 - \mu^2)} \left(\frac{t_{F_{min}}}{b_f}\right)^2 \qquad ; \ K_y \text{ from Reference 8.}$$

For elastic modulus, the test results provided moduli of elasticity between 47% and 89% higher than the predicted ones. For example, at room temperature the average test value was E_c = 176 GPa in contrast to the expected value of 113 GPa. The discrepancy is high but consistent, and indicates an unidentified influence that could not be traced to the computer or test machine readings. All seven tests are grouped in a narrow band. All test values reduced by a factor of 1.64 are shown in table VII in the next to last column. The test reduced value/predicted ratios are shown in the last column.

Since the longitudinal short column tests showed good correlation between test results and predicted values, and because modulus of elasticity is a material characteristic, the predicted values shown in the longitudinal short column evaluation are considered correct and recommended for design.

In a similar manner to the results of longitudinal short column tests, the transverse short column tests at 260° C indicate that the material $E_c = 96.19$ GPa is too low; further investigation is recommended.

Core Shear Beam - Longitudinal Core

The longitudinal core shear beam tests were conducted to verify the predicted values for:

a. Core shear stress (F'_{s_L})

b. Core shear modulus (G'_{c_L})

A total of seven specimens were tested at low, room, and high temperature as shown in table III.

The test results, the predicted values, and their correlation are shown in table VII and figures 46 and 47.

Predicted Values

For core shear instability, the computations are based on core web elements. The shear buckling stress was obtained by using the conventional plate shear formula:

$$\frac{F_s}{\eta} = K_s \frac{\pi^2 E_c}{12 (1 - \mu^2)} \left(\frac{t_c}{b_c}\right)^2 \quad ; \quad K_s \text{ from Reference 5.}$$

The K_s value obtained from Reference 5 considers the core web under combined shear and inplane web bending loading. The K_s value was obtained as a function of web aspect ratio and bending-to-shear stress ratio:

$$K_s = f\left(\frac{a}{b}, \frac{f_b}{f_s}\right) \qquad \text{(Reference 5)}$$

Using appropriate diagrams, the conversion from F_S/η to F_S was performed.

The core web shear stress was translated to core shear stress with the following formula:

$$F'_{S_L} = F_S \frac{t_c}{p}$$

For predicted elastic shear properties, the following material shear moduli were used:

$$G_{(-54^\circ C)} = \frac{E_{c(-54^\circ C)}}{E_{c(RT)}} \qquad G_{(RT)} = 45.82 \text{ GPa}$$

$$G_{(RT)} = 42.75 \text{ GPa (Reference 3)}$$

$$G_{(260^\circ C)} = \frac{E_{c(260^\circ C)}}{E_{c(RT)}} \qquad G_{(RT)} = 36.36 \text{ GPa}$$

The core shear properties were predicted by using two different formulas:

$$G'_{c_L} = \frac{\rho''_c}{\rho_c} G$$

$$G'_{c_L} = G \frac{p^2 t_N}{(h_c + b_N)(c - t_N)} \qquad \text{(Reference 6)}$$

where

$$\rho''_c = \left(1 - \frac{b_N}{p}\right)\frac{t_N}{c} \rho_c \quad ; \quad p = b_n + (c - t_N) \text{ctn } \theta$$

$$\rho_c = 276.48 \text{ lb/ft}^3$$

Comparing predicted values and test results, the second formula was found more appropriate and is recommended.

18

Test Results

Test data consist of load versus deflection, and geometry of the individual specimens. The buckling and ultimate core shear stress were obtained by dividing half of the applied load P/2 by the transverse area of the beam specimen.

$$f'_{si} = \frac{P}{2 H c}$$

$$f_{ult} = \frac{P_{ult}}{2 H c}$$

The elastic behavior was analyzed by considering both bending and shear deflections:

$$\delta = \delta_B + \delta_S$$

$$\delta = \frac{P L^3}{48 E_c I_c} + \frac{P L}{4 G'_{c_L} A_c}$$

where

$$A_c = \text{Shear section area} = H_c h$$

From the foregoing formula, the core shear modulus is obtained:

$$G'_{c_L} = \frac{P L / 4 A_c}{\delta - (P L^3 / 48 E_c I_c)}$$

Figure 48 groups the six longitudinal core shear specimens after failure, while figure 49 shows a closer failure detail of one typical specimen.

Test/Predicted Correlation

The "as fabricated" core web thickness was found to be substantially thicker than designed. Consequently, the core web shear stress reached the plastic range and the test/predicted evaluation results were distorted. Another factor which influenced the test/predicted results was the buckled core web resulting from fabrication. The buckled core was caused by a compressive load imposed by the container upon the SPF/DB panel after the core had been fully formed.

A general review of the test/predicted values shows:

	Average	Lowest	Highest
Core shear instability	.67	.60	.71
Core shear failure stress	.91	.78	1.01
Shear modulus	1.15	.84	2.02

The test results of specimen CSLHI have been discarded since the load was applied through a too narrow 6.35mm (1/4 inch)-wide metal strip. For the other specimens, a 25.4mm (1 inch)-wide metal strip was used for load application. It should be mentioned that the stabilizing filler in the load application area was inadvertently omitted from the high temperature specimens.

Recommendations

Plate shear tests are recommended in the future to avoid potential errors originating from the combined bending and shear loading. However, the present test results can be considered acceptable for preliminary design sizing.

For core shear stress, the initial buckling has an average test/predicted ratio of 0.67. To provide a 0.20 margin of safety for design purposes, a factor of 0.67 x 0.8 = 0.54 is recommended to be applied to the prediction formula discussed earlier:

$$\frac{F_{s_{cr}}}{\eta} = 0.54 \, k_s \, \frac{\pi^2 E_c}{12 (1 - \mu^2)} \left(\frac{t_c}{b_c}\right)^2 \; ; \; k_s \text{ from Reference 6.}$$

for buckling shear in core web.

The ultimate failure stress test/predicted ratio averaged 0.91. To provide a 0.20 margin of safety for design purposes, a factor of 0.91 x .80 = 0.73 is recommended to be applied to the prediction formula:

$$\frac{F_{s_{ult}}}{\eta} = 0.73 \, k_s \, \frac{\pi^2 E_c}{12 (1 - \mu^2)} \left(\frac{t_c}{b_c}\right)^2 \; ; \; k_s \text{ from Reference 6.}$$

For both initial buckling and ultimate stress, the $F_{S_{cr}}$ and $F_{S_{ult}}$ stresses in core webs are obtained in the following procedure:

Multiply $F_{S_{cr}}/\eta$ or $F_{S_{ult}}/\eta$ by $\sqrt{3}$. Obtain $\sqrt{3F_{S_{cr}}}$ or $\sqrt{3F_{S_{ult}}}$ from figure 50. Divide them by $\sqrt{3}$. If allowable core shear is required, multiply the core web shear stress by t_c/p:

$$F'_{S_{cr}} = F_{S_{cr}} \frac{t_c}{p} \; ; \quad F'_{S_{ult}} = F_{S_{ult}} \frac{t_c}{p}$$

Core shear modulus, G'_{C_L}, was obtained in a relatively scattered pattern. The high temperature tests showed higher than predicted values. It may be assumed that the modulus of elasticity is influenced much less by high temperature than indicated by present data available. Therefore, the $E_C = .96$ GPa should be checked in future programs. Similar recommendations were given in the preceding test evaluations.

The lower-than-predicted values for low and room temperature are presumably caused by the core being buckled from fabrication. An average for those tests indicates a test/predicted ratio for the core shear modulus of 0.85. It is recommended, therefore, that the prediction formula be reduced by this factor:

$$G'_{C_L} = 0.85 \; G \frac{p^2 \, t_N}{(b_C + b_N)(c - t_N)}$$

Core Shear Beam - Transverse Core

The transverse core shear beam tests were conducted to verify the predicted values for:

a. Core shear stress (F_{S_T})

b. Core shear modulus (G_{C_T})

A total of seven specimens were tested at low, room, and high temperatures as shown in Table III.

The test results, the predicted values, and their correlation are presented in Table VIII.

Predicted Values

For core shear stability, the computations are based on core web elements. The core web compression buckling stress is obtained by using the conventional wide column formula:

$$\frac{F_{w_{cr}}}{\eta} = K_c \frac{\pi^2 E_c}{12 (1 - \mu^2)} \left(\frac{t_c}{b_c}\right)^2$$

where

$K_c = 1$ (for pinned ends)
$K_c = 4$ (for fixed ends)

Since all the buckling stresses were found in the elastic range

$$F_{w_{cr}} = F_{w_{cr}}/\eta , \quad \text{or} \quad \eta = 1$$

The core web compression stress was translated to core shear stress by the following formula:

$$F'_{s_T} = F_{w_{cr}} \frac{t_c}{p} \cos \theta$$

The core shear elastic properties were predicted by using two different formulas:

$$G'_{c_T} = 1.85 \frac{E_c t_c \cos^3 \theta}{p(p - b_N)} \quad \text{(empirically derived from earlier tests)}$$

$$G'_{c_T} = \frac{(c - t_N) t_N}{(b_c + t_N)^2} \quad \text{(Reference 6)}$$

As in the longitudinal core shear evaluation, the second formula compared more favorable with test results.

Test Results

The same approach was used as for the longitudinal core shear tests with some alteration:

a. $(\overline{LL})$ is replaced by $(\overline{LT})$ and vice versa

b. G'_{c_L} is replaced by G'_{c_T}

Test/Predicted Correlation

The test/predicted (T/P) ratios exhibited a large spread, indicating limited prediction capability, with the entire field centered around a T/P average of about 0.43 for buckling stress, 0.54 for ultimate stress, and 0.70 for core shear modulus. A general review of the ratio of test/predicted values shows:

	Average	Lowest	Highest
Buckling stress	.43	.32	.61
Failure stress	.54	.43	.72
Core shear modulus	.70	.35	1.01

The wide spread and low T/P ratios obtained are attributed to the core web deformations resulting from fabrication. This initial eccentricity of the core web decreases considerably the column performance of each individual web element. The core web "as fabricated" deformation is a random phenomenon differing from web to web and along each web.

Recommendations

Plate shear tests are recommended in future programs to eliminate the bending deflection influence brought in by the core shear beam type of test. Although more expensive, plate shear tests offer the advantages of greater reliability and more direct data analysis. Improved manufacturing methods will reduce the initial core web deformations, increasing significantly the T/P values. On the basis of present tests, it is recommended that reduction factors be applied to reconcile the prediction formulas with the test results.

A correction factor of 0.35 is recommended for design buckling stress and 0.43 for design failure stress to bring the average margin of safety to 0.20. A reduction factor of 0.70 is recommended for core shear modulus. The resulting design equations then become:

$$\frac{F_{w_{cr}}}{\eta} = 0.35 \; K \; \frac{\pi^2 \, E_c}{12 \, (1 - \mu^2)} \left(\frac{t_c}{b_c}\right)^2 \qquad \text{(Design Buckling)}$$

$$\frac{F_{w_{cr}}}{\eta} = 0.43 \, K \, \frac{\pi^2 \, E_c}{12 \, (1 - \mu^2)} \left(\frac{t_c}{b_c}\right)^2 \quad \text{(Design failure)}$$

$$G'_{c_T} = 0.70 \, G \, \frac{(c - t_N) \, t_N}{(b_c + b_N)^2}$$

Bending Beam - Longitudinal Core

The longitudinal bending beam tests were conducted to verify the predicted value for:

    a. Local stability stress (initial buckling - F_{cr})

    b. Failure stress (crippling - F_{cs})

A total of five specimens were tested at low, room, and high temperatures, as shown in Table III.

The test results, the predicted values, and their correlation are presented in Table IX and Figures 51 and 52.

Predicted Values

For local stability stress and failure predictions, the conventional buckling and crippling formulas, respectively, shown in the longitudinal short column test evaluation were used.

Test Results

Test data consist of load versus deflection, gage readings, strain gage indications, and geometry of the individual specimens.

The applied buckling stress was obtained by using the bending stress formula:

$$F_{cr} = \frac{M_{cr} \, (2 \, c + t_{F_1} + t_{F_2})}{2 I_{\overline{LT}}}$$

The applied failure stress was obtained as above, but in the section properties computation the facesheet width (b_F) between nodes was reduced to the effective width (w). Similarly, the compression side of the core web width was reduced to $1/4$ b_c.

Figure 53 shows a typical test specimen in the test apparatus after failure, while figure 54 displays all of the failed bending beam specimens, both longitudinal and transverse.

Test/Predicted Correlation

The test/predicted (T/P) ratios exhibited a relatively narrow spread, indicating a good prediction capability. A general review of the ratio of test/predicted values shows:

	Average	Lowest	Highest
Local Instability	1.06	.92	1.24
Failure	1.32	1.02	1.62

Recommendations

A correction factor of 0.88 is recommended for design buckling stress, and 1.10 for design crippling stress to bring the average margin of safety to 0.20. Therefore:

Buckling design stress,

$$\frac{F_{cr}}{\eta} = 0.88 \ K_x \ \frac{\pi^2 \ E_c}{12 \ (1 - \mu^2)} \left(\frac{t_F}{b_F}\right)^2 \quad ; \ K_x \ \text{from Reference 8.}$$

Crippling design stress,

$$F_{cs} = 1.10 \ c_e \sqrt{F_{cy} \ E_c} \left(\frac{t_i}{b_i}\right)^{0.75} \quad ; \ c_e = 0.771 \ (\text{Reference 9})$$

$$F_{cs} \leq F_{cy}$$

The little influence of the F_{cy} cutoff value in F_{cs} computation for the node was neglected.

The combination crippling formula remained unchanged.

Bending Beam - Transverse Core

The transverse bending beam tests were conducted to verify the predicted values for:

    a. Local instability stress (initial buckling - F_{cr})

    b. Failure stress (F_{cs})

A total of five specimens were tested at low, room, and high temperatures, as shown in Table III.

The test results, the predicted values, and their correlation are shown in Table X and figure 55.

Predicted Values

For local stability stress prediction, refer to the transvese short column prediction discussion.

Test Results

Test data consist of load versus deflection, gage reading, strain gage indications, and geometry of the individual specimens.

The applied buckling stress was obtained by using a simplified bending stress formula where only the facesheets resist moment

$$F_{cr} = \frac{M_{cr}}{ht_{F(comp)}} \quad 1.1$$

$$M_{cr} = f(P_{cr})$$

P_{cr} was considered the load where the load versus strain curve separates from a straight line

The applied failure stress was considered equal to the buckling stress since the load versus strain curve separates from the straight line and the failure occurs immediately.

Figure 56 shows a typical specimen after failure.

Test/Predicted Correlation

The test/predicted (T/P) ratios exhibited a relatively narrow spread, indicating satisfactory prediction capability. A general review of the ratio of test/predicted values shows:

	Average	Lowest	Highest
Local instability	1.44	1.24	1.66

Recommendations

A correction factor of 1.20 is recommended for design buckling stress to bring the average margin of safety to 0.20. The equation for design buckling stress then becomes:

$$\frac{\sigma_{cr}}{\eta} = 1.20 \; K_y \; \frac{\pi^2 \; E_c}{12 \; (1 - \mu^2)} \left(\frac{t_F}{b_F}\right)^2 \quad ; \; K_y \; \text{from Reference 8.}$$

FRACTURE MECHANICS TESTS

The purposes of the fracture mechanics tests were twofold: (1) To determine the da/dN crack growth characteristics of superplastic formed and concurrently diffusion bonded Ti-6Al-4V titanium truss core sandwich panels subjected to constant amplitude load cycles, and (2) to demonstrate the durability, damage tolerance, and residual strength characteristics of a moderate size wing panel subjected to a load spectrum representative of a supersonic cruise vehicle.

Crack Growth Design Allowable Tests

Specimen Description

Nine crack growth design allowable tests were conducted at the load and temperature schedule listed in table XI. The test specimens were 190 mm (7.50 in.) wide, 610 mm (24 in.) long, and approximately 25 mm (1 in.) thick. All specimens contained a 2.5 mm (0.10 in.) long through-the-thickness crack created by electrical discharge machining (EDM) in one face sheet at midpanel. These flaws were precracked in three-point bending prior to test. Details of the panel cross-sections in the test area are shown in figure 57.

The specimen face sheet thickness dimensions listed in table XII were measured from the fracture face after failure and vary somewhat from the nominal drawing thickness dimensions. The measured dimensions were those used in determining the maximum test stresses listed in table XI. The resulting applied stresses for the constant amplitude tests were lower than the intended 231 MPa (33.5 Ksi) because of larger-than-normal face sheet thicknesses remaining after chem-milling.

Eight of the specimens were tested to a constant amplitude load cycle with a maximum axial tension stress of approximately 207 MPa (30 ksi) at an R-factor of zero. The ninth specimen was tested to the spectrum listed in table XIII, with a maximum spectrum stress of 231 MPa (33.5 ksi). All tests were conducted in an air environment at the temperatures noted in table XI with a cyclic rate of approximately 3 Hz. Crack lengths were measured and recorded after every 1.3 mm (0.05 inch) increment of growth up to failure.

Test Results

The crack growth curves for the longitudinal core specimens tested at temperatures of 21° C (70° F), -54° C (-65° F), and 260° C (500° F) are shown in figures 58, 59, and 60. Figure 61 shows the comparative curves for these three tests with the data normalized to a common initial crack length, C = 2 mm (.08 in.). Based on past experience with other materials, it was expected that the sub-zero temperature test would produce a slower growth rate and longer test life than the equivalent load room temperature test and that the reverse would be true of the elevated temperature test. These tests were run at the same load level to facilitate this comparison. The curves in figure 61 confirm the expected longer life at -54° C (-65° F) compared to room temperature, but also show the 260° C (500° F) test with greater life than the room temperature test. No explanation is offered for this. Each of the tests showed a moderate level of crack arrestment provided by the core nodes as they were approached by the growing crack. This is shown graphically by the change in slope of the curve as it approaches the first and then the second node. Figure 62 shows the growth curve of a similar specimen but with a crack-arrest strip chem-milled on the face sheet at the second node. No appreciable influence is shown by this strip in terms of additional crack arrestment beyond that provided by the core node since the crack was long at this point and growing at a controlled but fairly rapid rate compared to the size of the crack strip.

The crack growth data for the transverse core specimens tested at temperatures of 21° C (70° F), -54° C (-65° F), and 260° C (500° F) are shown in crack length versus cycles and in the traditional da/dN versus K formats, respectively, in figures 63 through 68. Figure 69 shows the comparative data for these three tests in da/dN versus K format. As in the case of the longitudinal core tests it was expected that the sub-zero test would produce the slowest growth rate and the elevated temperature test the fastest rate, with room temperature in between. Again, however, this trend was not demonstrated by the data. The growth rate lines of figure 69 confirm the expected slower growth rate at -54° C (-65° F) compared to room temperature, but also show the 260° C (500° F) test with a slower growth rate than either the room temperature or sub-zero tests. One common characteristic of each of the three transverse core tests was a slope of the da/dN line of approximately 2. Refer to figures 64, 66, and 68. This slope is substantially lower than a typical da/dN curve slope in the range of 3 to 3.5. One possible explanation is that a shallow slope is a characteristic of Ti-6Al-4V SPF/DB processed

28

material. Another contributing factor, and perhaps the predominant one, is that load is being progressively shed by the cracked face sheet through the diagonal core to the back, uncracked, face sheet. This thought is confirmed by limited strain gage data from test F-11 in which one strain gage on the back face gave progressively larger readings from 210.3 MPa (30.5 ksi) initially to a maximum of 248 MPa (36 ksi) as the front face crack grew from its initial size to a length of 88.9 mm (3.50 in.).

Figure 70 shows the growth curve for test F-11, a transverse core specimen with crack arrest strips on one face sheet. Figure 71 shows a comparison of test F-11 with test F-12, a similar transverse core panel but without crack arrest strips. Both tests had been run at the same cyclic stress level and had essentially the same initial crack length. The shaded area shows the influence of the crack arrest strips. The improvement in life was from 64,000 cycles on F-12 to 72,000 cycles on F.11, an increase of 12 percent.

Figure 72 shows the crack growth curve for spectrum test F-06. Failure occurred after 247,000 cycles of step 5 of the second lifetime. The crack had grown from an initial size of 4.1mm (0.16 in.) to a final size of 177.8mm (7.0 in.) at failure. A total of 1,709,000 load cycles had been applied at the time of failure, equivalent to 1.33 lifetimes. The most damaging load steps were climb segment steps 5, 6, and 7 of the first lifetime and ground-air-ground segment step 4 and climb segment step 5 of the second lifetime. The 1.0-g stress level for this test was (25 ksi) and the maximum stress (step 7) was (33.5 ksi).

TASK 4 - STRUCTURAL PANEL PERFORMANCE

STATIC TESTS

The static tests consisted of compression panel tests. One panel, 996 x 1143 mm (39 x 45 inches), was tested in the core longitudinal direction. The original test plan called for this panel to be tested in the transverse direction to limit load prior to performing the ultimate (failure) strength test in the longitudinal direction. In order to avoid the possibility of an unexpected failure or permanent distortion during the transverse loading, a decision was made to use a separate specimen 280 x 890 mm (11 x 35 inches) for the transverse loading and to test to failure.

Longitudinal Compression Panel

The static compression panel test was designed to verify the accuracy of the compression panel predicting method, applied to the uppercover conditions of point No. 4 of the supersonic transport vehicle. (See figure 3 and table I.)

The loading condition consisted of combined biaxial and shear loads on a very long panel (a/b ratio of 4.73). Since a test of this size of panel would be impractically expensive, a a/b = 1 panel was chosen. For panels with aspect ratio a/b = 1 and a/b = 4.72, the buckling coefficient is equal. Therefore, testing a panel with aspect ratio a/b = 1 is considered satisfactory.

To obtain general instability mode of failure, the maximum size of panel was chosen. The manufactured panel had a full size of 1524 x 1219 mm, of which 1241 x 1013 mm was expanded sandwich. The largest possible size of compression test specimen obtainable from this panel was 1143 x 1143 mm, including some non-sandwich edge area, for an a/b = 1.

Predicted Values

To predict the compression panel general instability, the method of reference 7, based on Rayleigh-Ritz energy method, was used. The "as-designed" 1143 x 1143 panel had the side flanges incorrectly cut and a 1143 x 996 panel was provided for test, with the long side parallel to the core. The stability equation is:

$$N_x = K_x \frac{\pi^2 D}{(\overline{LT})^2}$$

where

$$K_x = f(a/b, J) = 4$$

$$\frac{a}{b} = \frac{\overline{LL}}{\overline{LT}} = 1.15$$

$$J = \frac{U (\overline{LT})^2}{\pi^2 D} = 45.8$$

$$U = G'_{c_T} = 2.16 \times 10^7$$

$$G'_{c_T} = 0.7 G \frac{(c - t_N) t_N}{(b_c + b_N)} = 987 \text{ MPa}$$

$$b_c = \frac{c - t_N}{\sin \theta}$$

$$D = \frac{E_c t_F (c + t_F)^2}{2 (1 - \mu^2)} = 4.74 \times 10^4$$

The predicted value of the buckling load P_x for the "as-designed" specimen was 1.355 x 10^{6}N, so an available test machine with a maximum capacity of 1.779 x 10^{6}N was considered adequate for testing this specimen. However, the "as-fabricated" specimen had thicker face sheets than intended and the panel did not buckle even at maximum test machine capacity. A review of the predicted buckling load using actual face sheet thicknesses resulted in a new value of 1.879 x 10^{6}N. Unfortunately, no higher capacity test machine was free at that time to retest to the higher expected load. Consequently, a limited conclusion can be drawn that the panel showed no evidence of the onset of lateral deformation within 6 percent of the predicted buckling load.

Figure 73 shows the compression panel in the test machine.

Long Column - Transverse Core

The transverse long column test was conducted to verify the predicted values for:

a. The "wide column" behavior of a panel with high ratio of length/width

b. Local stability stress (initial buckling - F_{cr})

An 890 x 280 mm (35 x 11 inches) panel was tested as a long column at room temperature. The truss core was oriented along the 280 mm side and the ends were pinned. As mentioned previously, because of nondifferential face sheet chem-milling, the design face sheet thickness was obtained in certain areas only; in the remainder of the panel the face sheets were thicker than intended. In addition, because of the container deformation, the sandwich panel itself was thinner than designed, with the core webs less stretched (i.e., thicker) than intended. Consequently, the predicted specimen properties were recalculated for the "as fabricated" dimensions.

Predicted Values

For prediction of the local stability stress, the conventional buckling formula was used:

$$F_{cr} = K_y \frac{\pi^2 E_c}{12 (1 - \mu^2)} \left(\frac{t_{F_{min}}}{b_F}\right)^2$$

where

$$K_y = f\left(\frac{t_c}{t_{F_{min}}}, \theta\right) = 1.62 \text{ (Reference 8)}$$

$$\frac{t_c}{t_{F_{min}}} = \frac{t_N \cos\theta}{t_{F_{min}}} = 0.72$$

$$\theta = 51°$$

$$\frac{F_{cr}}{\eta} = 284.9 \text{ MPa}$$

Since the stress level is in the elastic range:

$$F_{cr} = 284.9 \text{ MPa}$$

$$P_{cr} = F_{cr}(t_{F_1} + t_{F_2})\overline{LL} = 204.9 \text{ KN}$$

For general stability, the conventional Euler formula was used:

$$\frac{F_c}{\eta} = \frac{\pi^2 E_c}{(\overline{LT}/\rho)^2}$$

where

$$\rho^2 = I/A = 118.9 \text{ mm}^2$$

$$\overline{LT} = 872.5 \text{ mm}$$

$$E_c = 113.08 \text{ GPa}$$

$$\frac{F_c}{\eta} = 247.9 \text{ MPa} = F_c$$

32

Load applied at general stability stress is:

$$P_c = F_c \, (t_{F_1} + t_{F_2}) \, \overline{LL} = 131.1 \text{ KN}$$

Comparing local and general stability, the column would be expected to fail in the general instability mode.

In different sources, Poisson's Ratio has different values; e.g., $\mu = .33$ (limited number of tests performed on SPF/DB Ti-6Al-4V material) or $\mu = .31$ (Reference 4).

Test Results

Test data consist of load versus deflection, gage readings, strain gage indications, and geometry of the specimen. The failure occurred in the general instability mode as predicted by analysis, followed almost instantly by local instability failure of one face sheet intranode element. The failure stress was obtained by dividing the failure load by the cross section area:

$$F = \frac{P}{(t_{F_1} + t_{F_2}) \, \overline{LL}} = \frac{180589}{(1.37 + 1.19) \, 281} = 2505 \text{ MPa}$$

A supplementary check of the modulus of elasticity was performed:

$$E_c = \frac{P_i}{\epsilon A} = \frac{133440}{0.5 \, (1083 + 1938) 10^{-6} \, (1.37 + 1.19) \, 281} = 122.8 \text{ GPa}$$

Poisson's Ratio was calculated on the basis of the strain readings, one along the load direction (strain gage No. 7) and the other perpendicular to it (strain gage No. 3).

Strain Gage \ Load (KN)	46.70	66.72	93.41	113.42	133.44
No. 3	119	173	245	299	351
No. 7	396	568	782	937	1083
μ(= No. 3/No. 7)	0.30	0.30	0.31	0.32	0.32
$\mu_{av.}$ = 0.31					

Figure 74 is a plot of load versus strain from strain gage No. 7 and illustrates clearly the abrupt onset of failure. Figure 75 shows the specimen ready for testing in the test machine, while figures 76 and 77 show the failed specimen after removal of the load.

Test/Predicted Correlation

The local instability failure stress test/predicted correlation value of:

$$\frac{250.5}{284.9} = 0.88$$

is closely in line with the transverse short column T/P buckling ratio of .84. The general instability failure stress test/predicted correlation value of:

$$\frac{250.5}{247.9} = 1.01$$

indicates a very accurate prediction capability. The modulus of elasticity T/P value is:

$$\frac{122.8}{113.08} = 1.086$$

Poisson's ratio test/predicted value:

$$\frac{0.31}{0.31} = 1 \quad \text{(for non-SPF/DB materials)}$$

$$\frac{0.31}{0.33} = 0.94 \quad \text{(for SPF/DB materials)}$$

In present computations, the Poisson's Ratio used was $\mu = 0.33$. The present value of $\mu = 0.31$ coincides with the value indicated in Reference 4 for non-SPF/DB material. However, the difference in values does not represent a significant difference in predicted buckling stress values:

$$\frac{(1 - 0.33^2)}{(1 - 0.31^2)} = 0.986$$

Recommendations

On the basis of the similarity to the local buckling test results obtained from transverse short column specimens, the corresponding recommendation will not be changed but rather considered confirmed. Also, local buckling in transverse loading should be considered as ultimate load. The modulus of elasticity obtained from test is 9 percent higher than predicted. This is not considered a significant deviation and the predicted value should be considered adequate for future design.

34

FRACTURE MECHANICS TESTS

Fatigue Panel

Specimen Description

A single large panel, figure 78, was tested in ambient laboratory air to the load spectrum of table XIII to determine the durability and damage tolerance characteristics of the structure. The panel was designed with a longitudinal core orientation and with four 3.0 x 12.7 mm (0.120 x 0.500 in.) wide crack-stopper strips diffusion bonded to the inside surface of one face sheet at the core nodes. The purpose of these strips was to study their influence on the growth rate of an approaching face sheet crack compared to the influence of adjacent unstiffened core nodes. Strain gages were mounted on the external side of the face sheet at each of the crack strips to measure the stress redistribution resulting from extension of the artificial crack that was induced at the beginning of the second lifetime.

Test Spectrum

The cyclic load spectrum applied to the fatigue structural performance panel is listed in table XIII. The same spectrum of stresses was also applied to crack growth test specimen F-06 but with a lower maximum load because of the narrower width of F-06. This spectrum consists principally of four-segment operational flights together with a small number of check flights. The table represents one design lifetime of 21,100 flights and includes 1,286,000 cycles. The steps were applied in full, sequentially as listed. This use of this spectrum and the manner in which it was applied were directed by the customer in order to facilitate comparison of Rockwell's test results with those of another contractor conducting a similar research program.

Test Results

The structural performance panel was tested in ambient laboratory air to the cyclic load spectrum of table XIII. The 1.0-g stress level for the test was 172 MPa (25 ksi) while the maximum stress in the spectrum was 231 MPa (33.5 ksi). The durability of the panel was demonstrated by the successful completion of the first lifetime without crack initiation. Prior to the start of the second lifetime an artificial crack was introduced by electrical discharge machining through the thickness of one face sheet at mid-point. Testing was continued with crack growth measured and recorded after periodic increments of growth. Failure of the panel occurred after 4215 cycles of step 7 of the second lifetime. A total of 950,000 cycles, approximately 75 percent of a lifetime, were applied in the second lifetime up to the time of failure. During this time the intentionally initiated crack grew from an initial length of 2.8 mm (0.11 in.) to 37.3 mm (1.47 in.). A plot of this growth is shown in figure 79. Failure did not occur in this primary test area. The crack that ultimately caused failure of the panel initiated at an edge of the panel approximately 230 mm (9 in.) above the mid-panel test area and progressed inward, undetected, on one face sheet for a distance of 76 mm (3 in.) prior to catastrophic failure. The general location of failure initiation was in one

face sheet along a raw edge of the panel which resulted when the specimen was cut to test configuration from a larger SPF/DB panel. Thus the resulting test panel did not have edge closeout members such as the type that would exist on production aircraft panels.

The strain gages mounted on the facesheet were read periodically from the beginning of the test to confirm the desired stress level. They did not, however, register any significant redistribution of stress from the growing mid-panel artificial crack because the test was terminated before the crack had grown into their area of influence.

Based on the inadvertent failure of this panel it should not be assumed that the SPF/DB process produces structurally deficient panels. Prior to the inadvertent failure, this test had successfully demonstrated one crack-free durability lifetime of 21,100 flights and 50,000 flight hours plus 3/4 lifetime of steady, non-catastrophic growth from an intentionally initiated crack at the mid-panel test area.

Because of the close proximity of the failure to the mid-panel test area it was deemed impractical to effect a repair that would not impact the subsequent distribution of the load in a continuing test, thus the notion of a repair was discarded and the test was terminated.

SECTION III

CONCLUSIONS

It is felt that all stated objectives of this program have been essentially satisfied. More specifically, in an examination of the program results with respect to the detail objectives (refer to Introduction), it can be concluded that:

1. SPF/DB titanium alloy expanded truss-core sandwich has been shown to be an applicable and qualified candidate for future supersonic cruise aircraft design in that basic structural allowables can be reliably predicted. (The relative cost/weight merits of SPF/DB titanium sandwich in comparison with other structural concepts are not within the scope of this program.) Test results from replicate specimens for the various loadings and temperatures tested showed a statistically acceptable repeatability and satisfactory correlation with analytical predictions. Where empirical factors need be applied to the analytical formulae, they are easily determined.

    It must be noted that in regard to evaluating the overall applicability of SPF/DB titanium sandwich to future supersonic cruise aircraft, this program contributes only a first step in that broad objective. The development of the technology of SPF/DB titanium sandwich structural design will require a carefully planned, multidirectional program of many phases to evolve a fully validated, competitive system.

2. State-of-the-art procurement specifications and optimized process parameters for SPF/DB titanium sandwich were established by the Air Force BLATS program in a virtually concurrent schedule with this program. This program corroborated that predetermined sandwich geometries can be consistently produced over relatively large panels. It is felt that the various quality discrepancies experienced were the result of economies inherent in a low-volume development program and would become negligible in a production environment with dedicated tooling. However, this program did emphasize the vital importance of precise process control and a rigid quality assurance specification.

3. The SPF/DB titanium sandwich design data base was supplemented by this program to the extent permitted by the limited range of variables encompassed. In static strength, the most important contribution was the demonstration of the validity of the analytical prediction techniques and the ability to generate straightforward empirical adjustment factors where necessary. In the area of fatigue strength and crack-growth characteristics, basic data were acquired. One crack-arresting design concept was investigated.

Section IV

REFERENCES

1. Sakata, I. F., and Davis, G. W., "Substantiating Data for Arrow-wing Supersonic Transport Configuration Structural Design Concepts Evaluation," vol. 1 NASA CR-132575-1, vol. 2 NASA CR-132575-2, vol. 3 NASA CR-132575-3, vol. 4 NASA CR-132575-4, October 1975.

2. Wright, B. R., Bruckman, F. A., Wilson, J. R., Guinn, W. A., and Sakata, I. F., "Supersonic Cruise Vehicle Technology Assessment Study of an Over/Under Engine Concept," NASA CR-145285, October 1977

3. "Preliminary Design and Material Allowables for SPF/DB Structure (BLATS)", Report No. NA-78-539-1, Rockwell International/Los Angeles Division, Contract F33615-77-C-3107, Sept. 1978.

4. MIL-HDBK-5C, "Metallic Materials and Elements for Aerospace Vehicle Structures", Sept. 1976.

5. Structures Manual, Publication 2546-N, Rockwell International/Space Division, 1974.

6. Ko, W. L., "Elastic Constants for Superplastically Formed/Diffusion-Bonded Corrugated Sandwich Core", NASA Technical Paper 1562, Dryden Flight Research Center, May 1980.

7. Harris, L. A., and Auelmann, R. R., "Stability of Flat, Simply-Supported Corrugated Core Sandwich Plates Under Combined Loads", IAS Paper, IAS National Summer Meeting, Los Angeles, June 1959.

8. Anderson, M. S., "Local Instability of the Elements of a Truss-Core Sandwich Plate," (Supersedes NACA TN 4292.) NASA/TR R-30, 1959.

9. Structures Manual, Report No. NA-72-1, Rockwell International/North American Aircraft Division, 1972.

DEFINITION CAPABILITY OF TITANIUM ALLOYS TO DEVELOP
EXTREMELY HIGH TENSILE ELONGATIONS AT
ELEVATED TEMPERATURES AND CONTROLLED
STRAIN RATES

• CONVENTIONAL MATERIAL
TENSILE ELONGATION
10-30%

• SUPERPLASTIC MATERIAL
TENSILE ELONGATION >THAN 1000%

ARGON PRESSURE

START

ARGON PRESSURE

30% DEFORMATION

ARGON PRESSURE

50% DEFORMATION

100% DEFORMATION
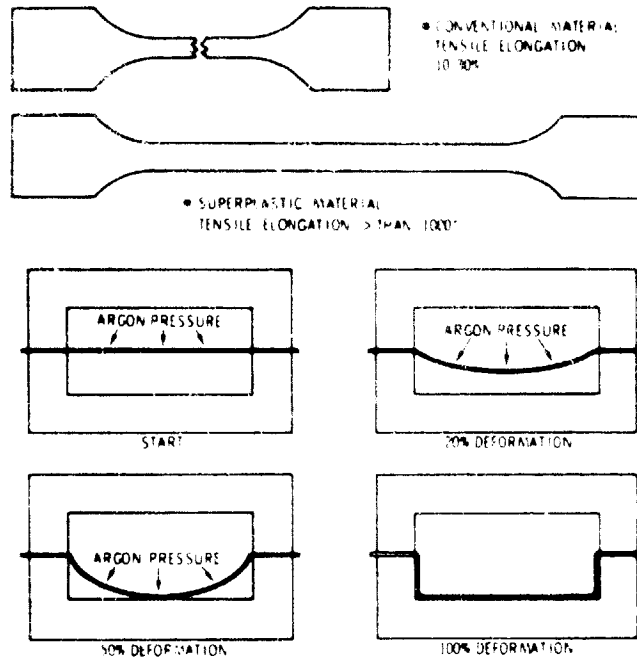
(a) PHENOMENON OF SUPERPLASTICITY

TITANIUM SHEET

STOPOFF

1. STOP OFF IS
APPLIED TO
PREVENT BONDING
IN SELECTED
AREAS

2. PARTS LAID UP

3. DIFFUSION BONDING
IS ACCOMPLISHED
WITH TEMPERATURE
AND GAS PRESSURE

GAS PRESSURE

GAS
PRESSURE

TOOLING

SANDWICH EXPANDS
STRETCHING CORE
TO DESIRED
CONFIGURATION

4.

GAS PRESSURE

5. SANDWICH WITH
CORRUGATED CORE
COMPLETELY
EXPANDED

GAS PRESSURE
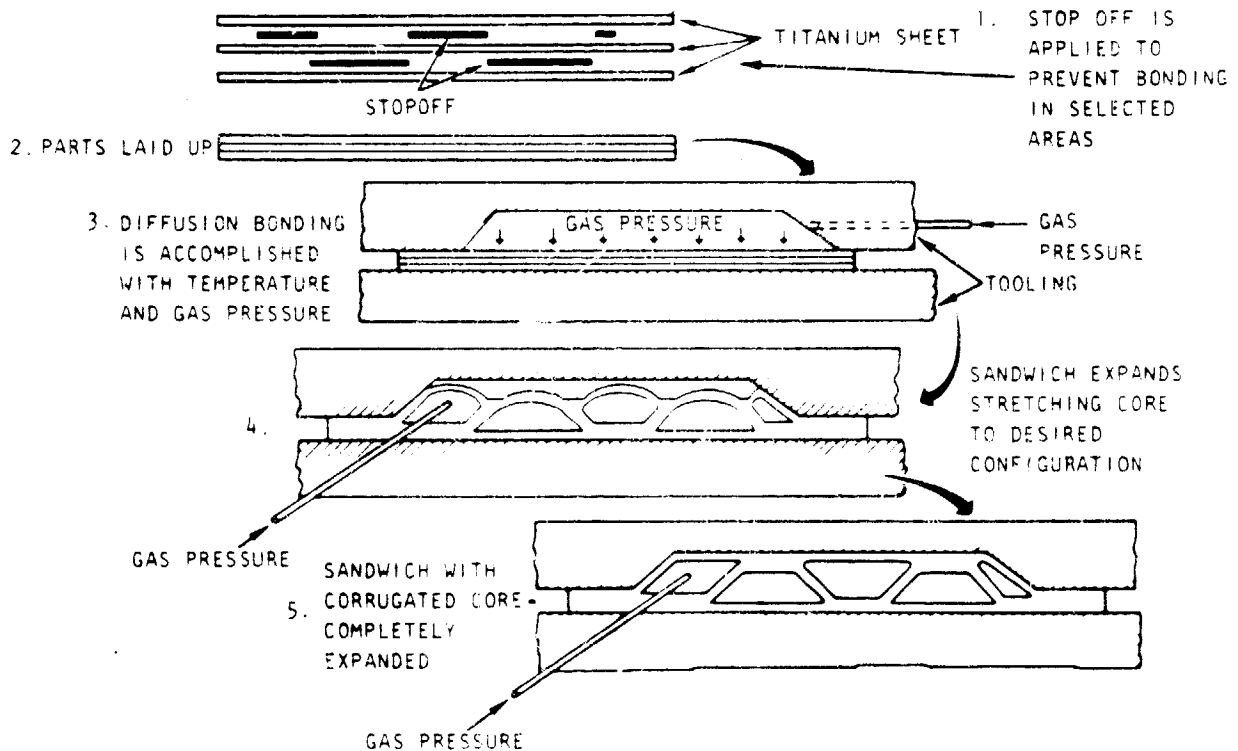
(b) EXPANDED SANDWICH PROCESS

Figure 1. SPF/DB Sandwich Evolution

39
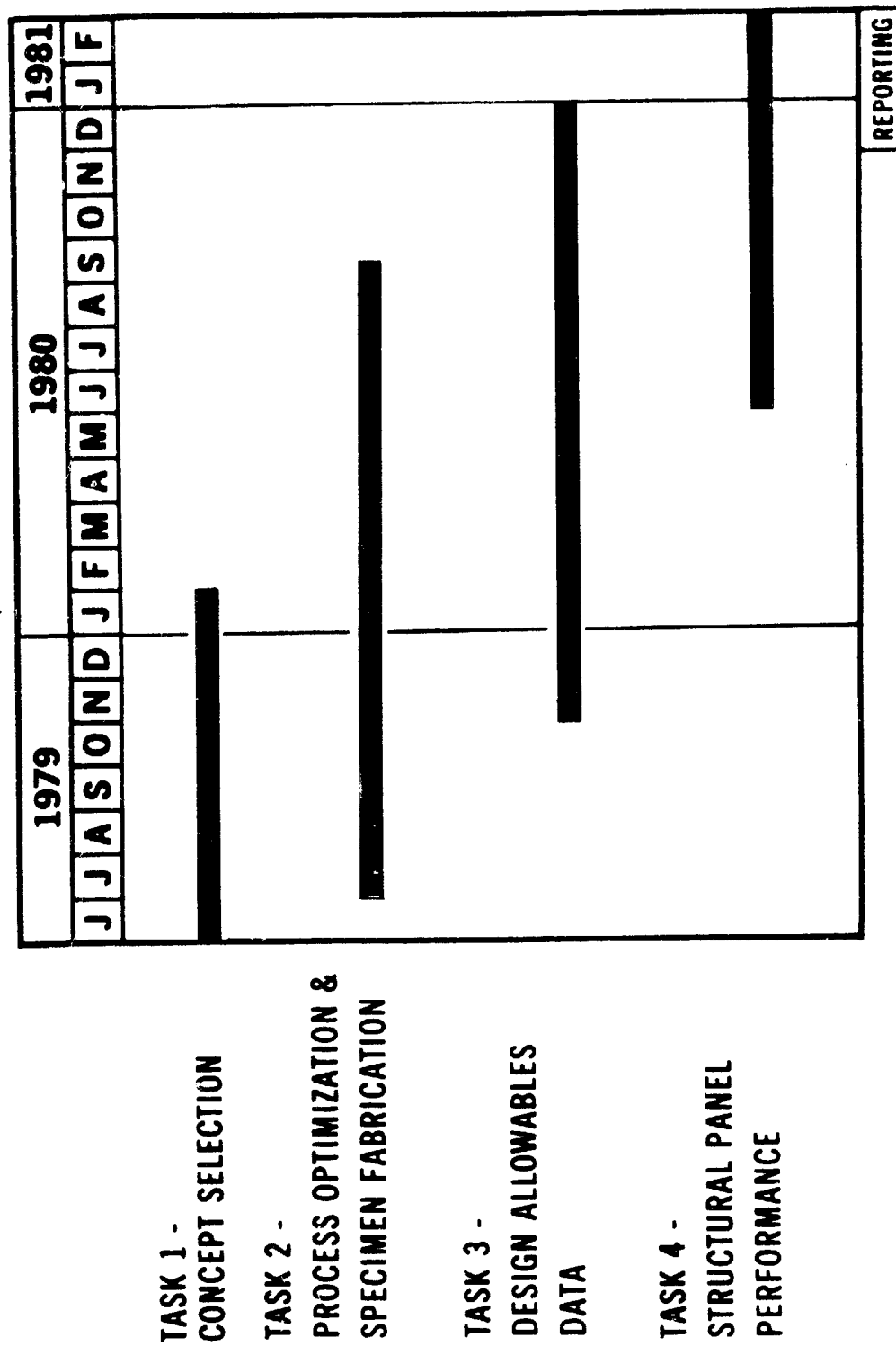
Figure 2. Program Schedule

CRITICAL PANEL LOCATION (UPPER & LOWER)
(POINT 4)
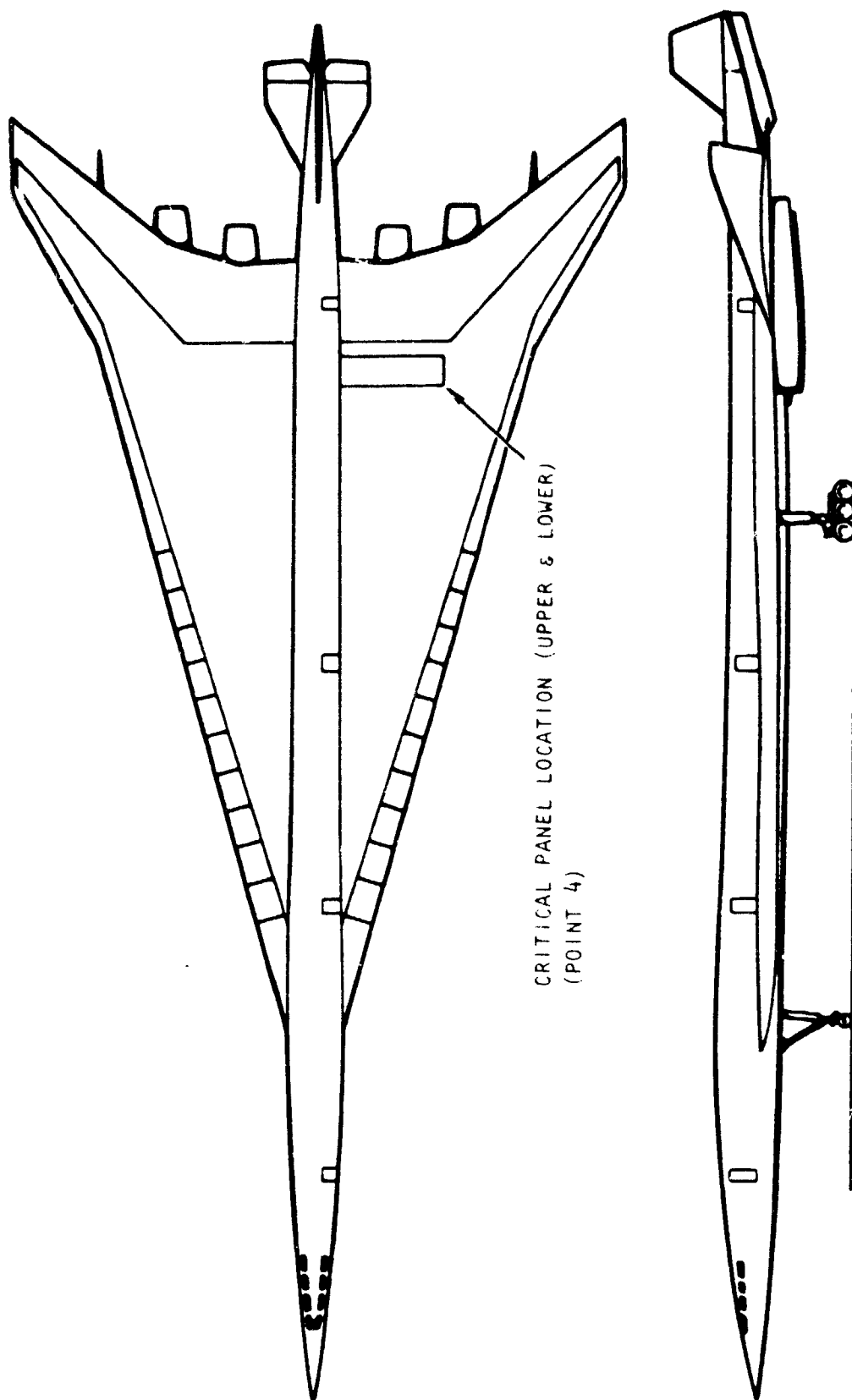
Figure 3. Selected Demonstration Panel - Boeing NASA SSI Study Aircraft
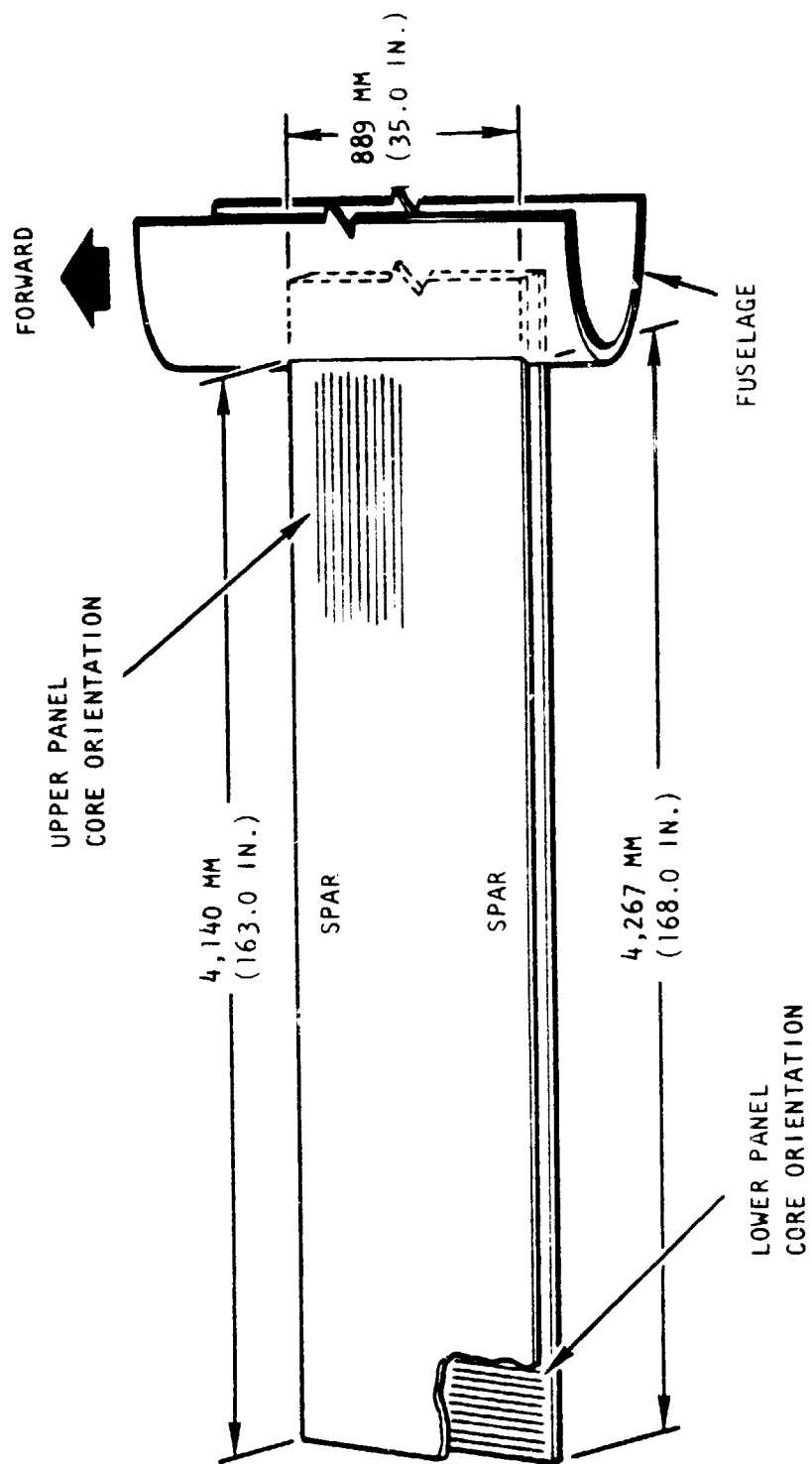
Figure 4. Design Wing Covers at Point 4
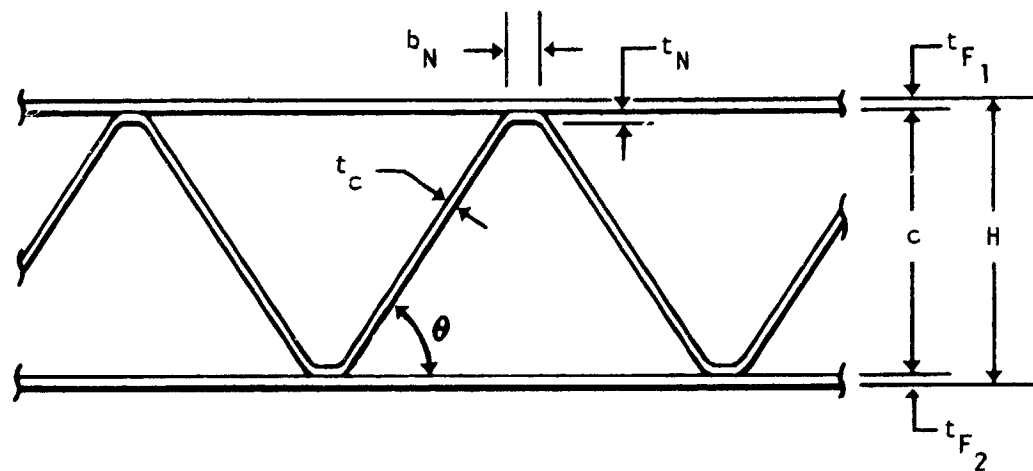
		c MM (IN.)	b_N MM (IN.)	t_{F_1} MM (IN.)	t_{F_2} MM (IN.)	t_N MM (IN.)	θ
PANEL	UPPER	23.67 (0.932)	3.81 (0.15)	1.04 (0.041)	1.04 (0.041)	1.37 (0.054)	60°
	LOWER	26.90 (1.059)	3.81 (0.15)	0.84 (0.033)	0.84 (0.033)	1.12 (0.044)	60°

Figure 5. Geometric Parameter. of Upper and Lower Wing Panels

CRACK-ARREST DEVICE
(CHEM-MILLING OMITTED)
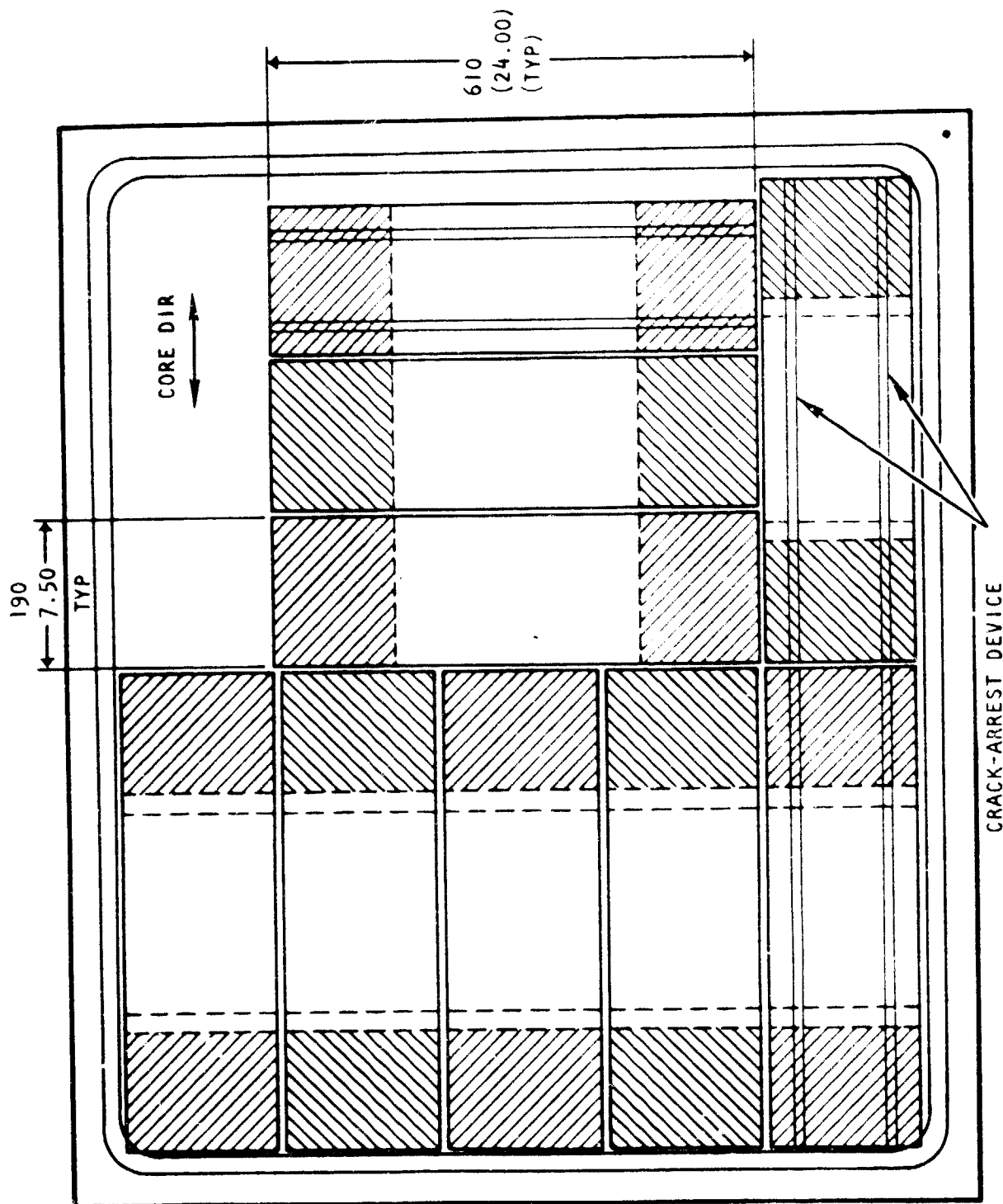
Figure 6. Typical Test Specimen Layout
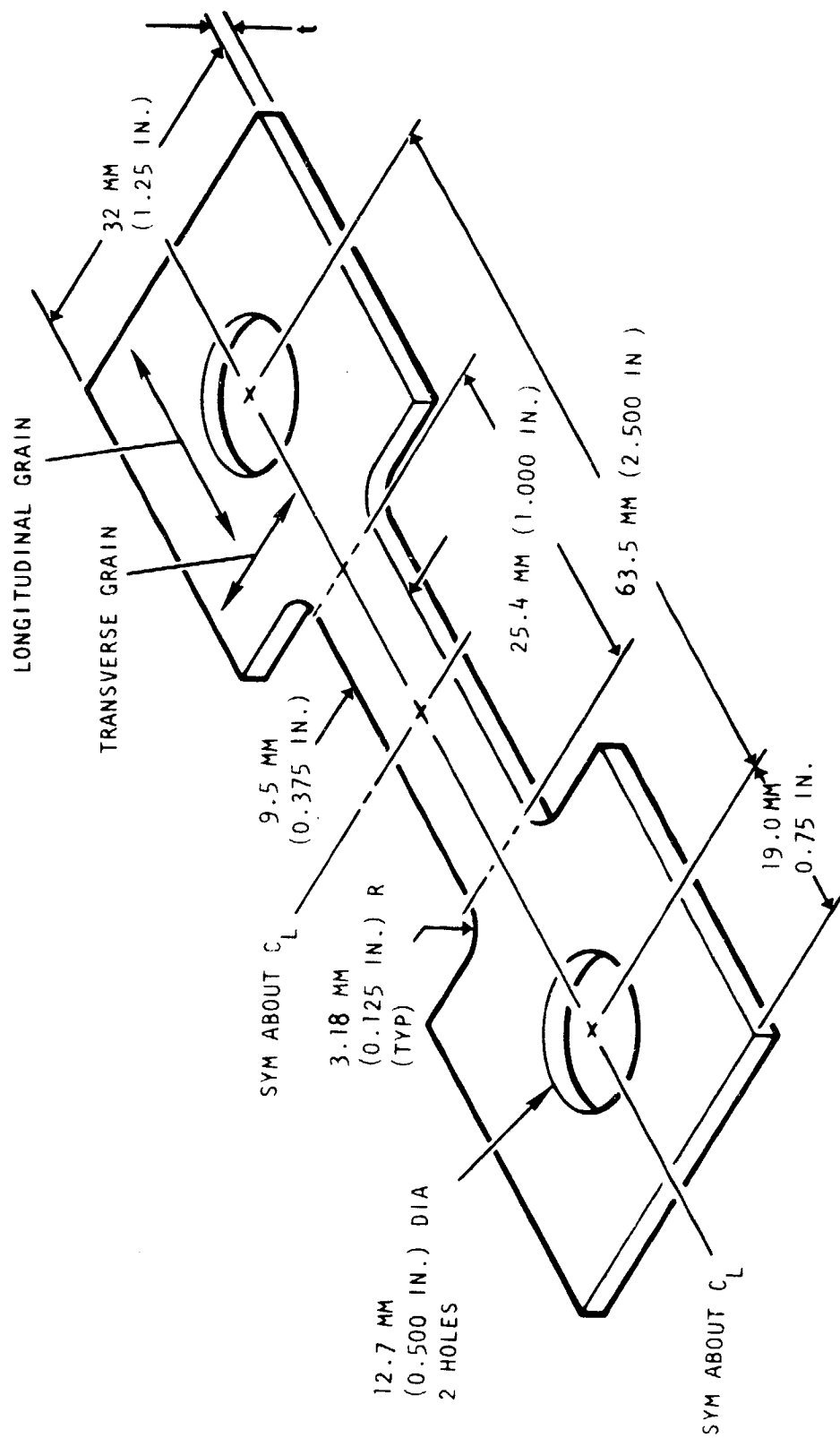
Figure 7. Tensile Specimen for SPF Parameter Determination

32 MM (1.25 IN.)

LONGITUDINAL GRAIN

TRANSVERSE GRAIN

SYM ABOUT C_L

9.5 MM (0.375 IN.)

3.18 MM (0.125 IN.) R (TYP)

25.4 MM (1.000 IN.)

63.5 MM (2.500 IN.)

19.0 MM 0.75 IN.

12.7 MM (0.500 IN.) DIA 2 HOLES

SYM ABOUT C_L

45
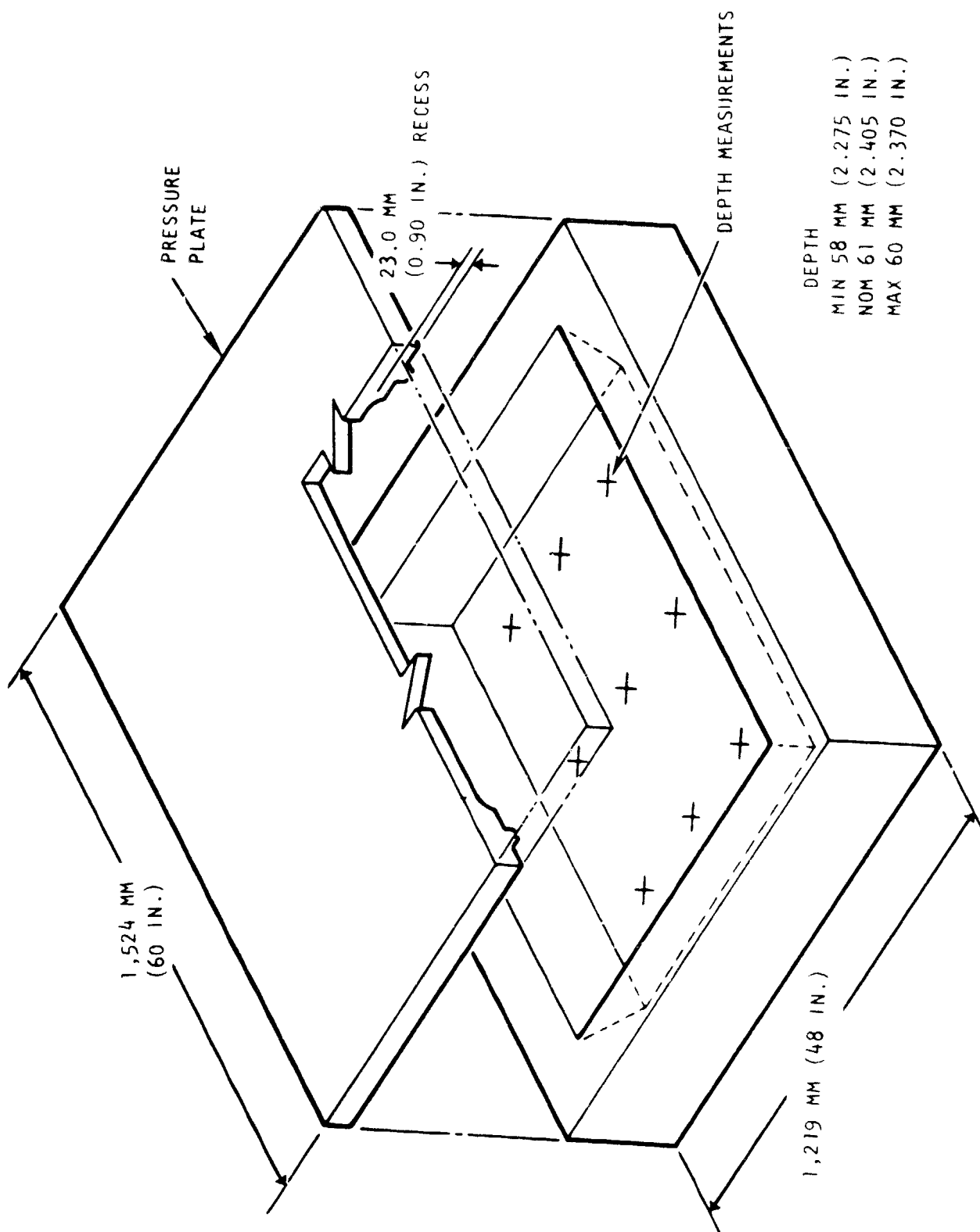
Figure 8. Container for SPF/DB Panel Fabrication

PRESSURE PLATE

23.0 MM (0.90 IN.) RECESS

DEPTH MEASUREMENTS

DEPTH
MIN 58 MM (2.275 IN.)
NOM 61 MM (2.405 IN.)
MAX 60 MM (2.370 IN.)

1,524 MM (60 IN.)

1,219 MM (48 IN.)
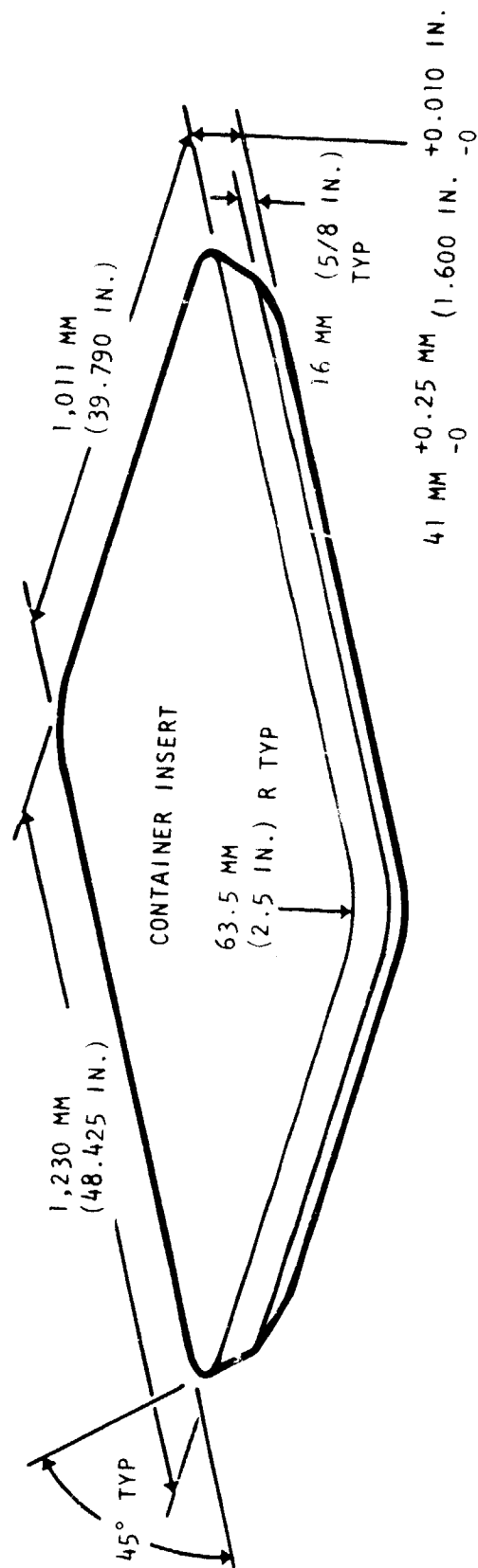
Figure 9. Insert Design

47

Figure 10. Argon Tubes Installation

Figure 11. Core Sheet Slots for Argon Tubes

49

Figure 12. Core Sheet Slot and Holes for Argon Circulation
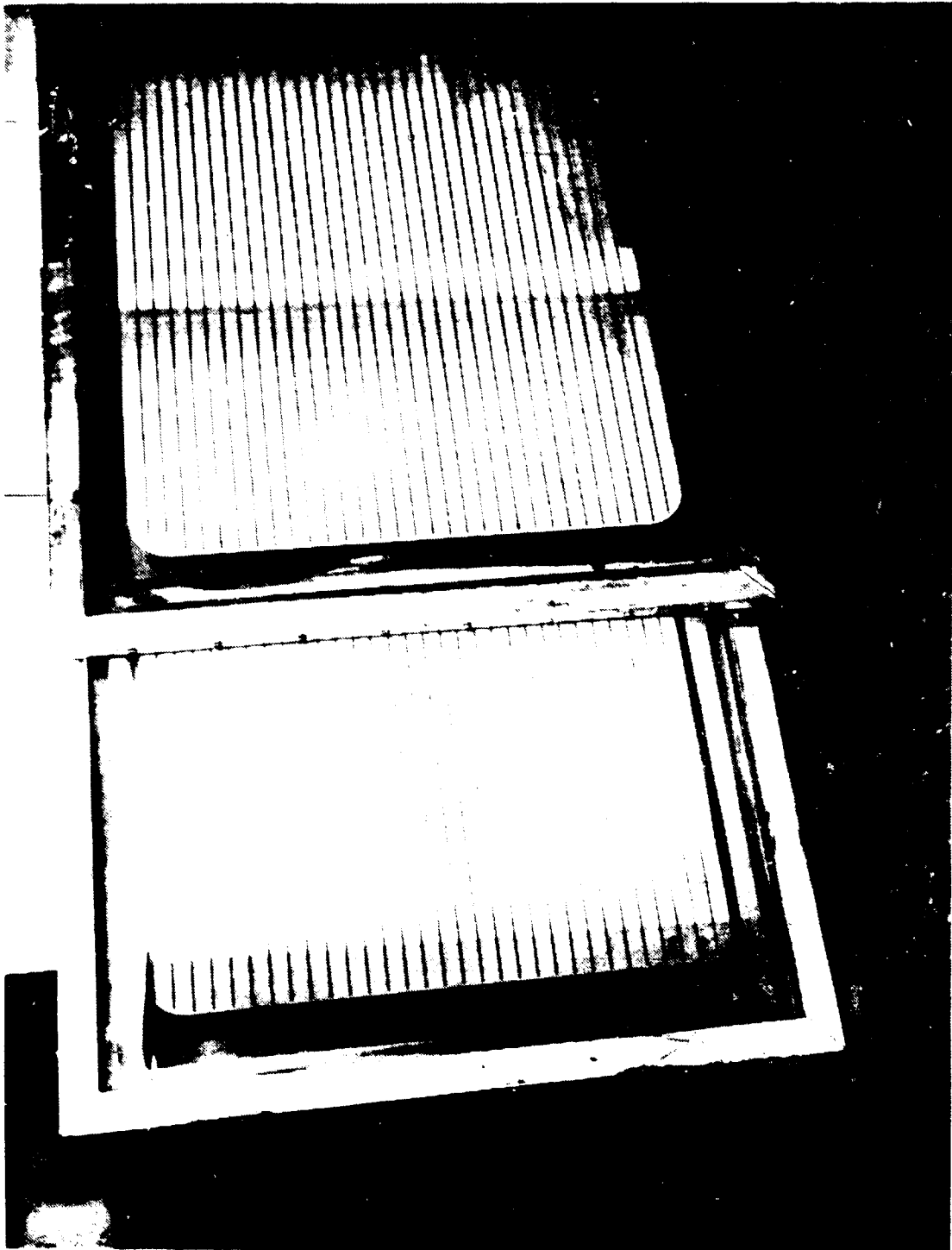
Figure 15. Core Pattern Silk Screens

51

Figure 11. Yttria Application

52

Figure 15. Core Site Alignment and Argon Tubes Installation
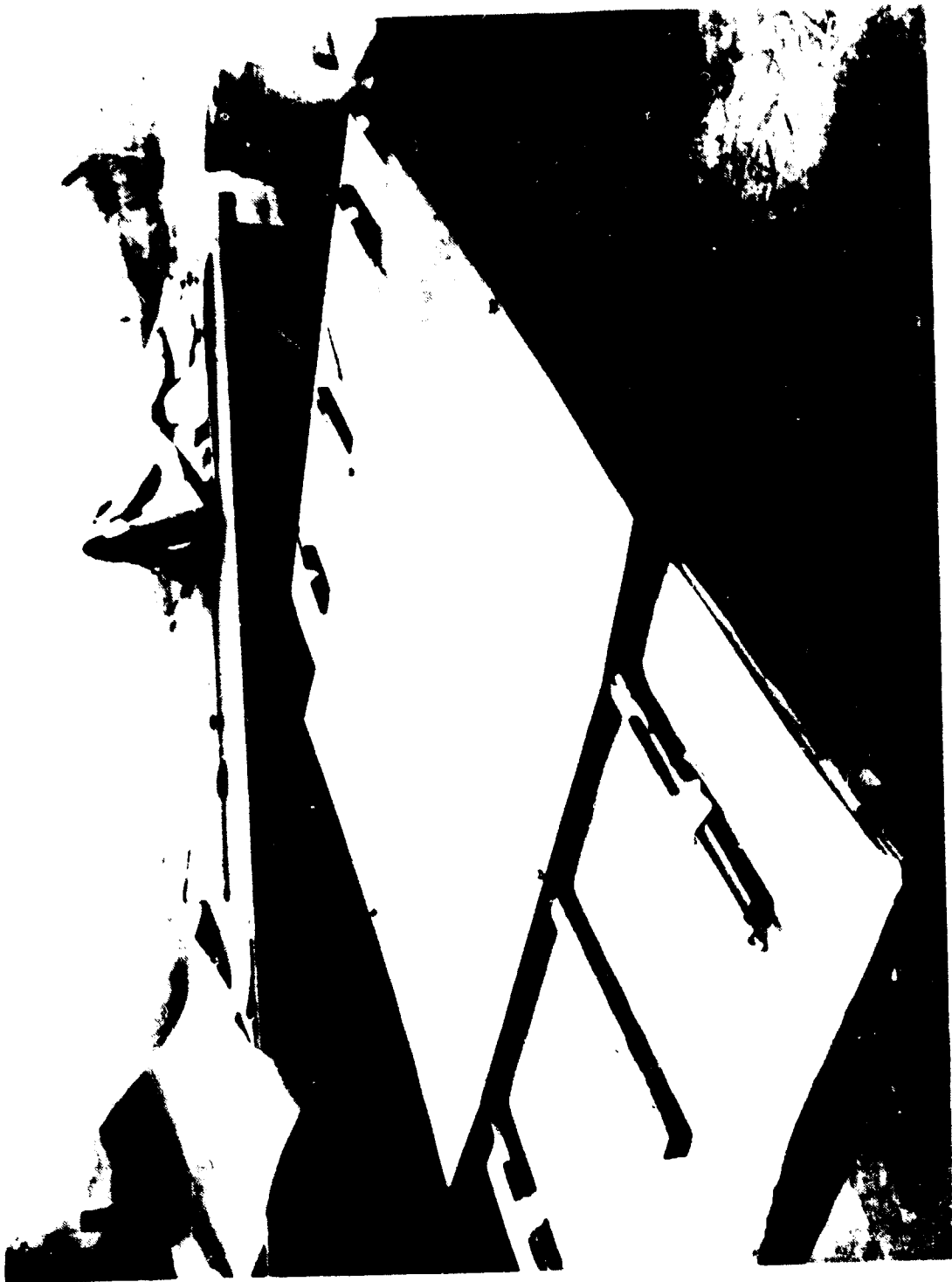
Figure 16. Pack Alignment

54

Figure 15. Pack Assembling
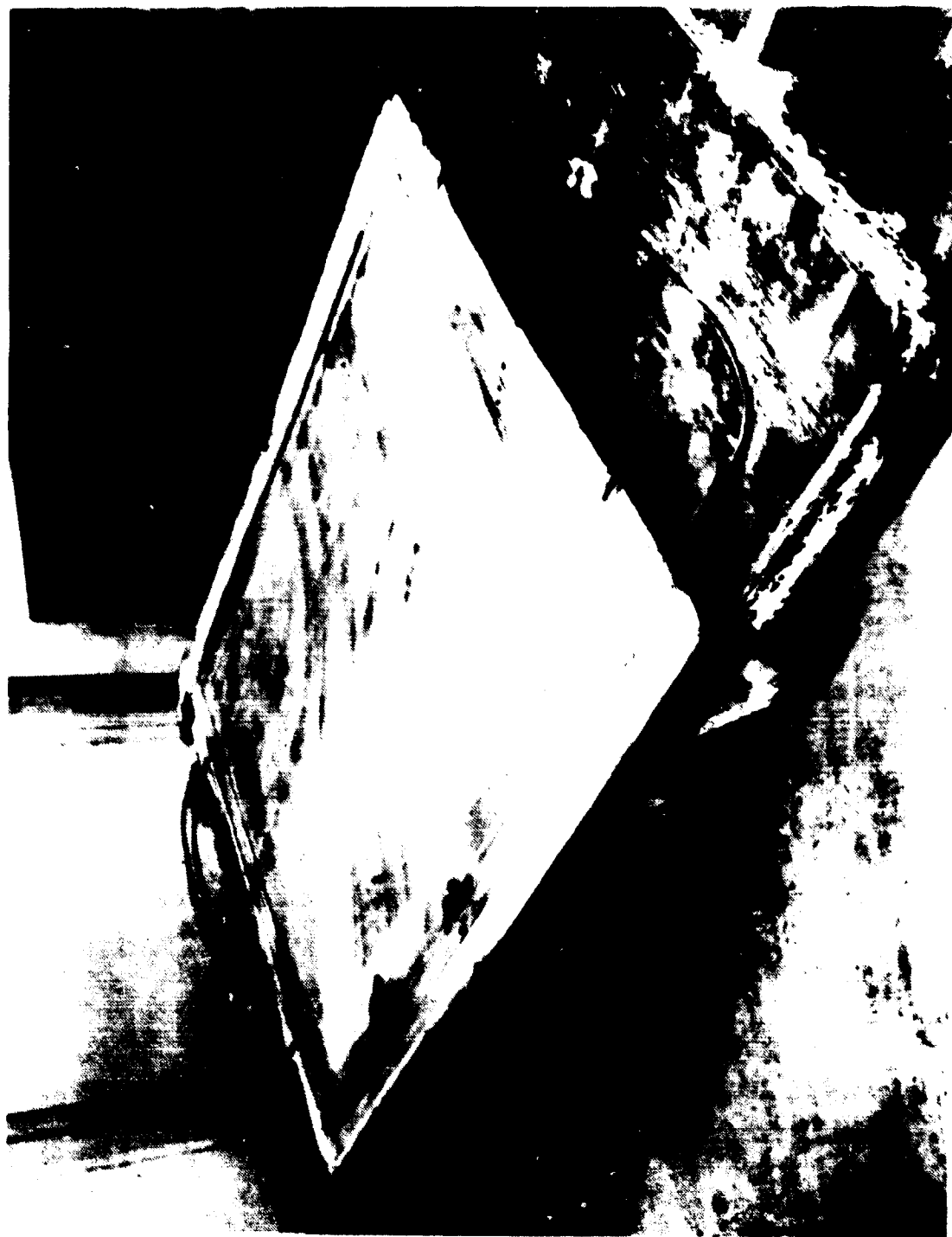
Figure 18. Pressure Plate

Figure 19. Container and Insert

57

Figure 20. Container on Heating Platen

Figure 21. Pack, Container, and Surrounding Installation

59
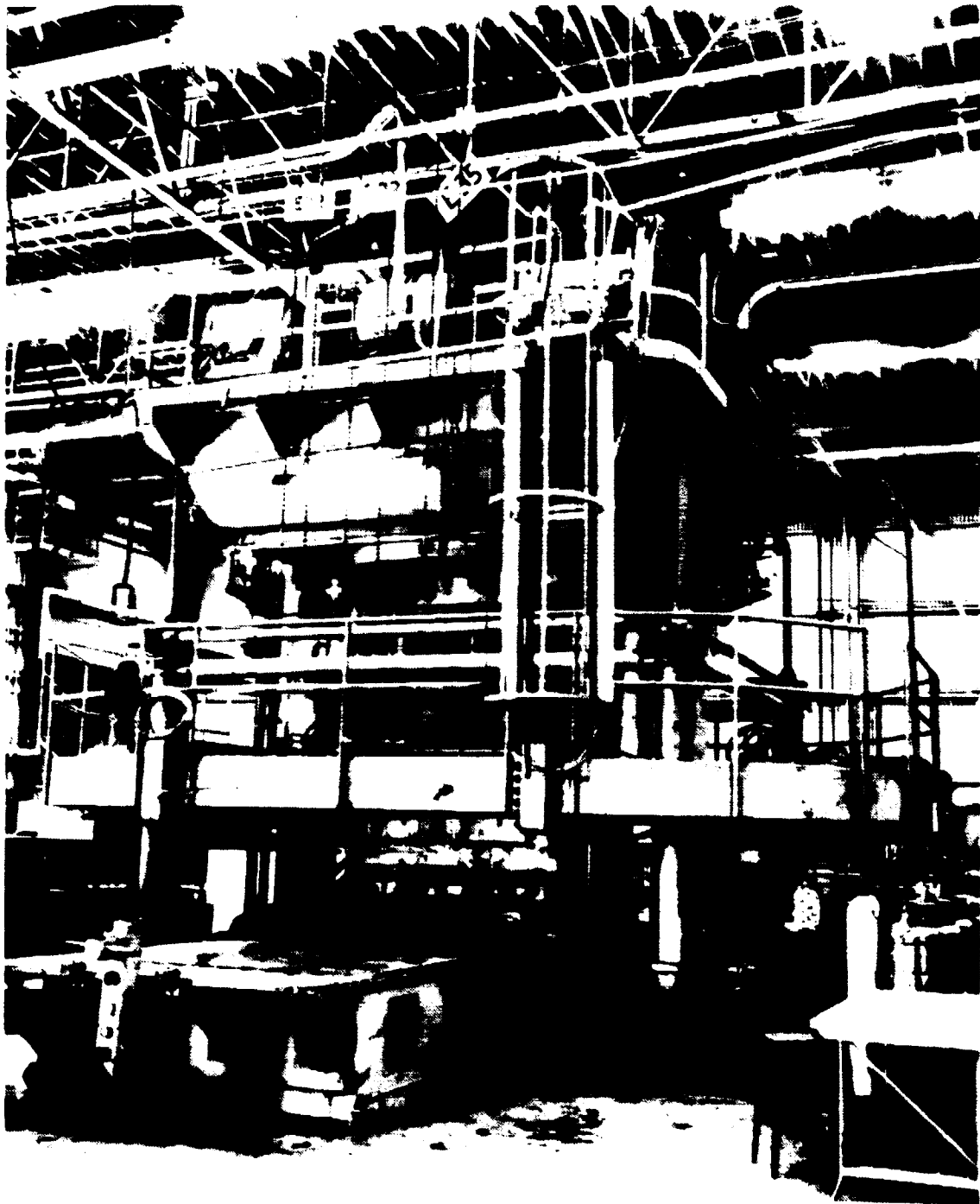
Figure 22. Entire System in 4,500 Ton Press, Ready for SPF DB Process
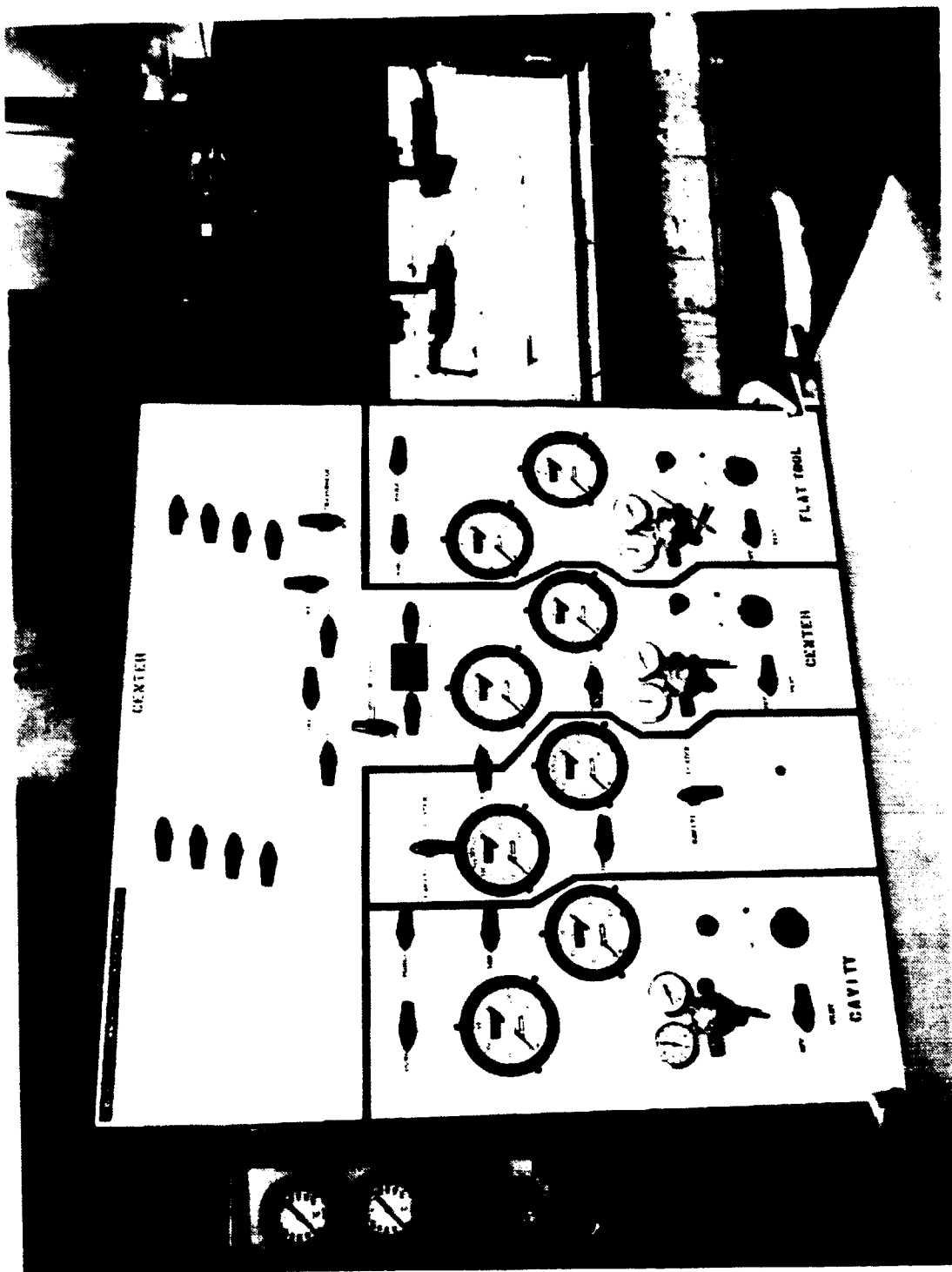
Figure 23.   Control Unit for SPF/DB Process

61
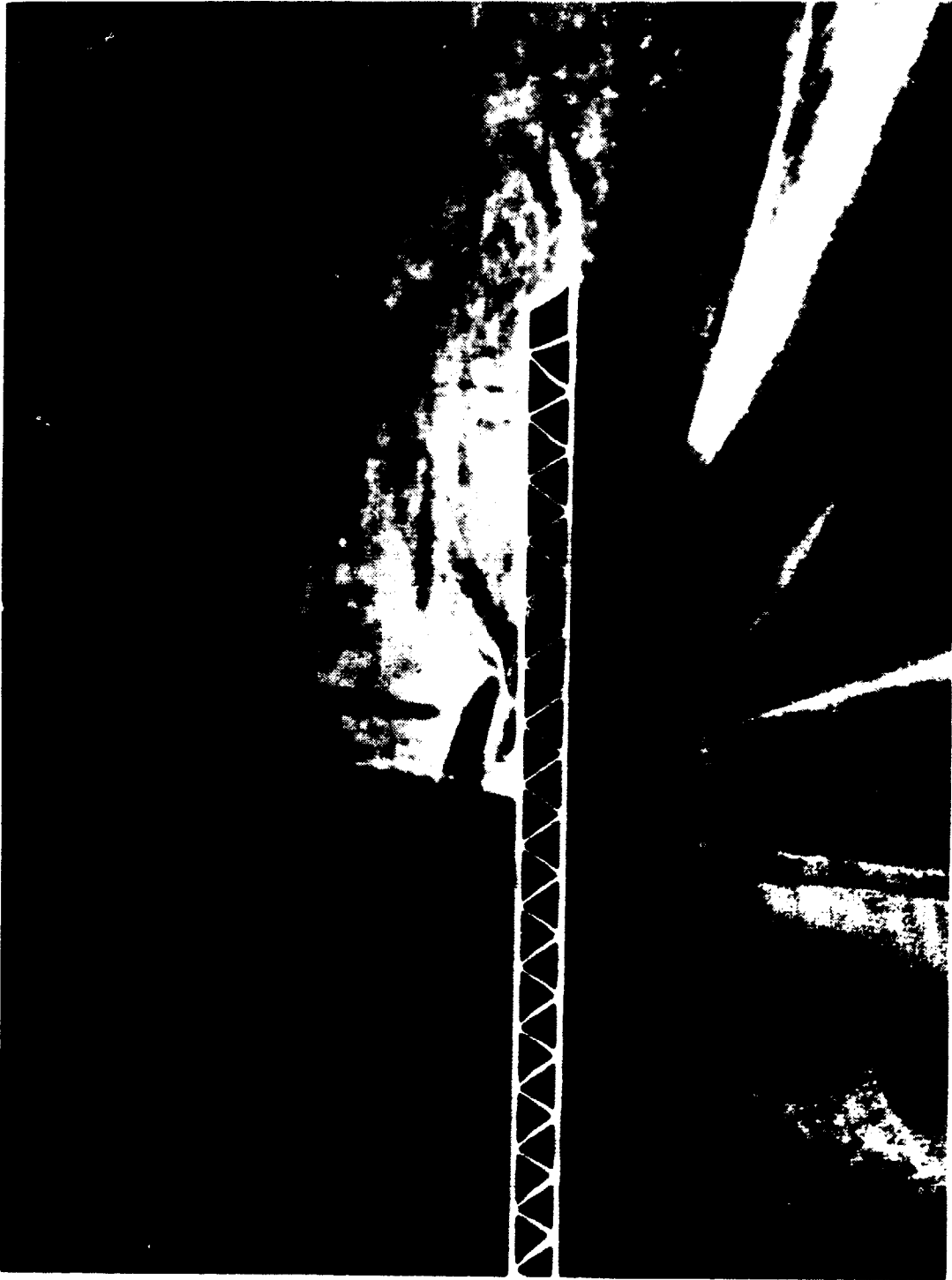
Figure 24. End Product - Truss Core Sandwich

Figure 25. Fatigue Panels
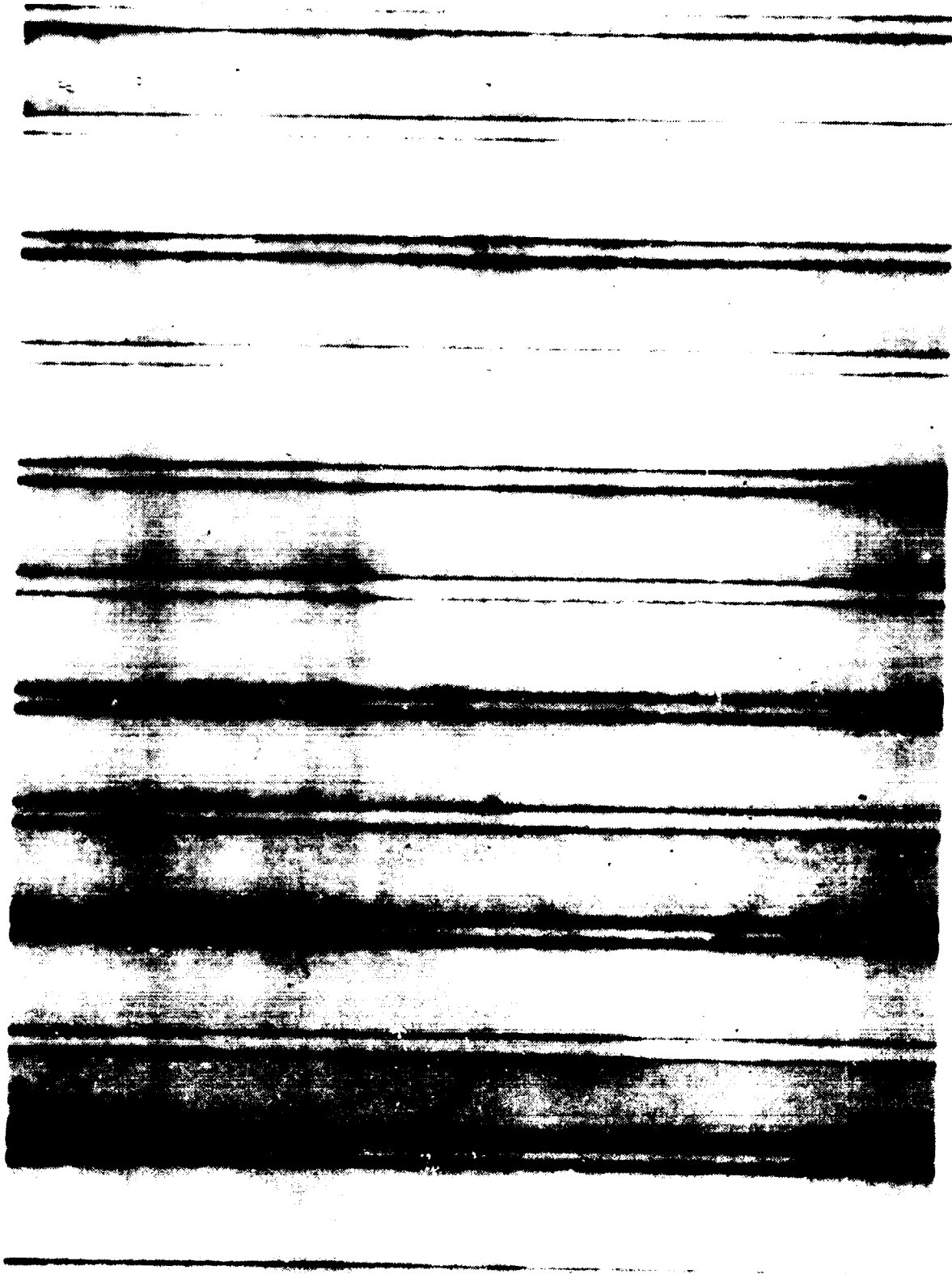
Figure 26. Typical Radiograph - Panel F 200

64
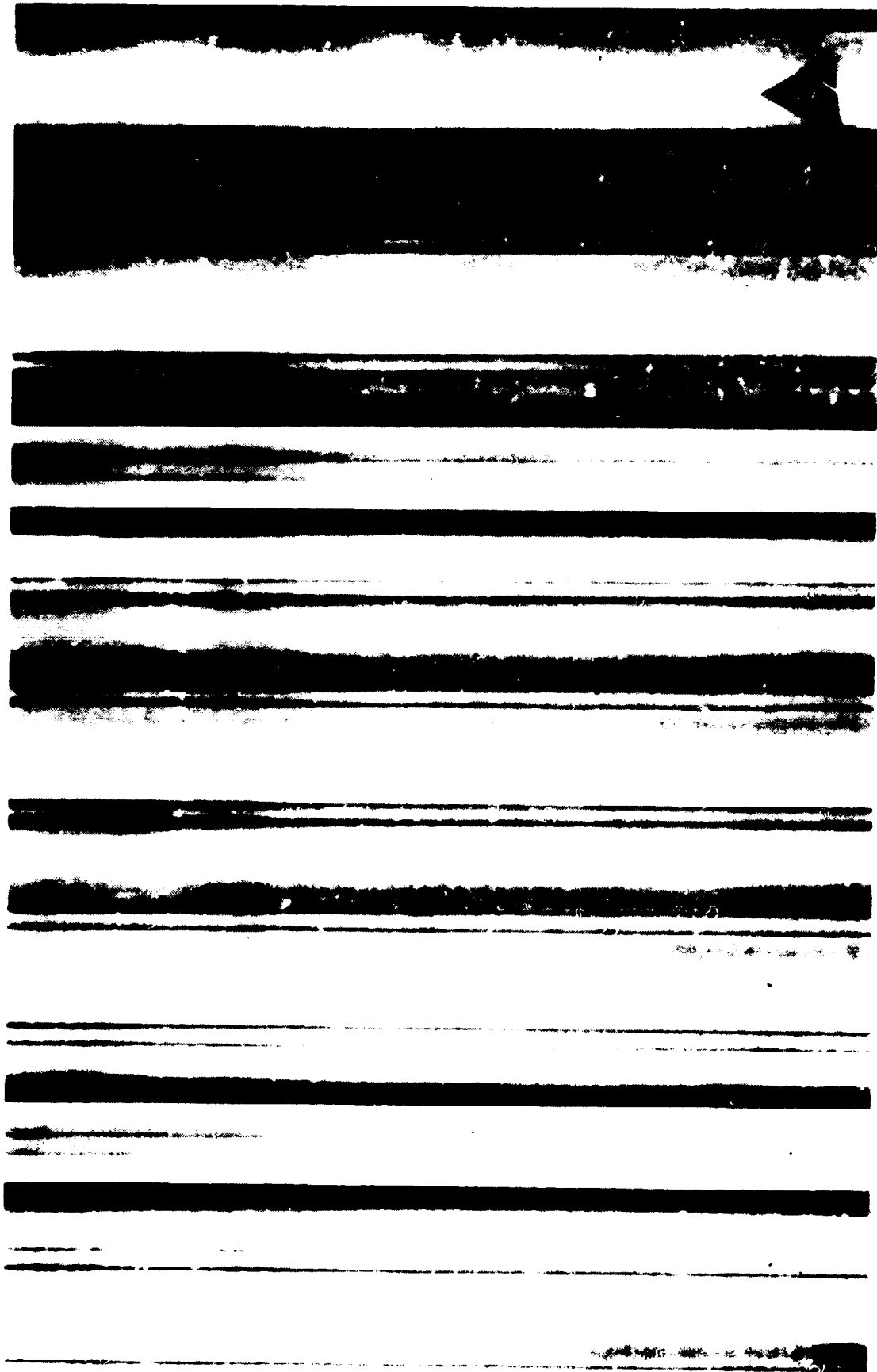
Figure 27. Typical Radiograph - Panel F 300 (With Crack-Arrest Strips)

65
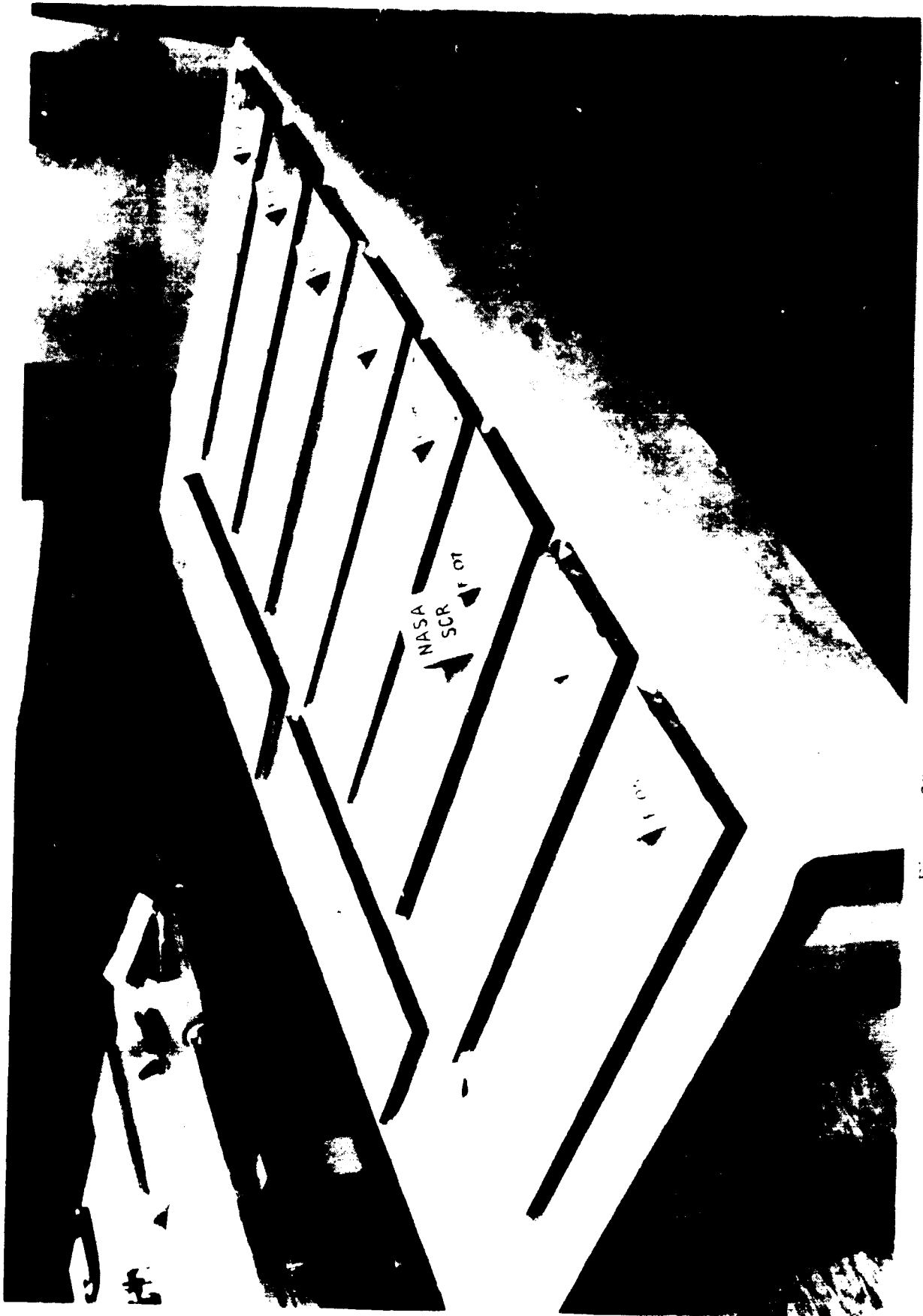
Figure 28. Fatigue Test Specimens

Figure 29. Fatigue Structural Performance Panel
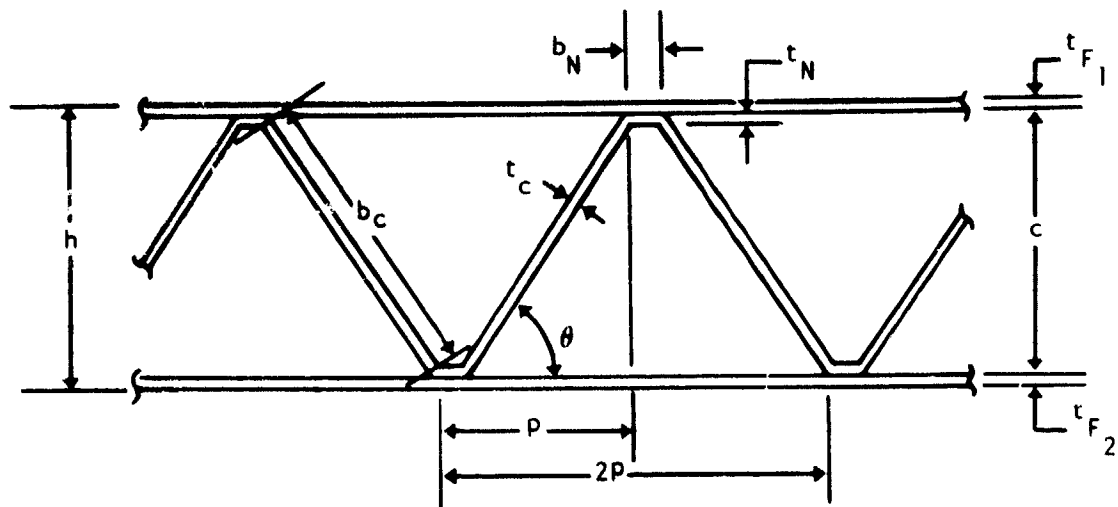
		c MM (IN.)	b_N MM (IN.)	t_{F_1} MM (IN.)	t_{F_2} MM (IN.)	t_N MM (IN.)	θ
PANEL	UPPER	23.67 (0.932)	3.81 (0.15)	1.04 (0.041)	1.04 (0.041)	1.37 (0.054)	60°
	LOWER	26.90 (1.059)	3.81 (0.15)	0.84 (0.033)	0.84 (0.033)	1.12 (0.044)	60°

Figure 30. Sandwich Geometry Nomenclature

CORE
DIRECTION

$\overline{LT}$

$\overline{LL}$

(a) LONGITUDIMAL SPECIMEN

$\overline{LL}$

$\overline{LT}$

(b) TRANSVERSE SPECIMEN
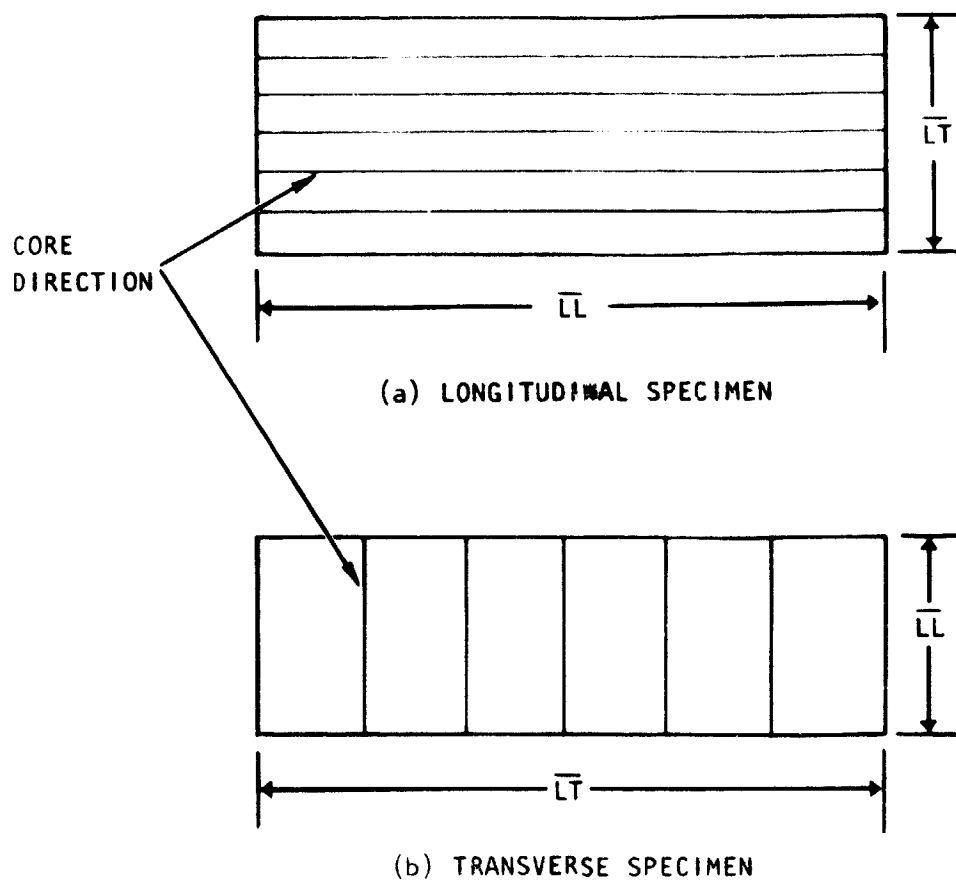
Figure 31.   Panel Dimensions Notation
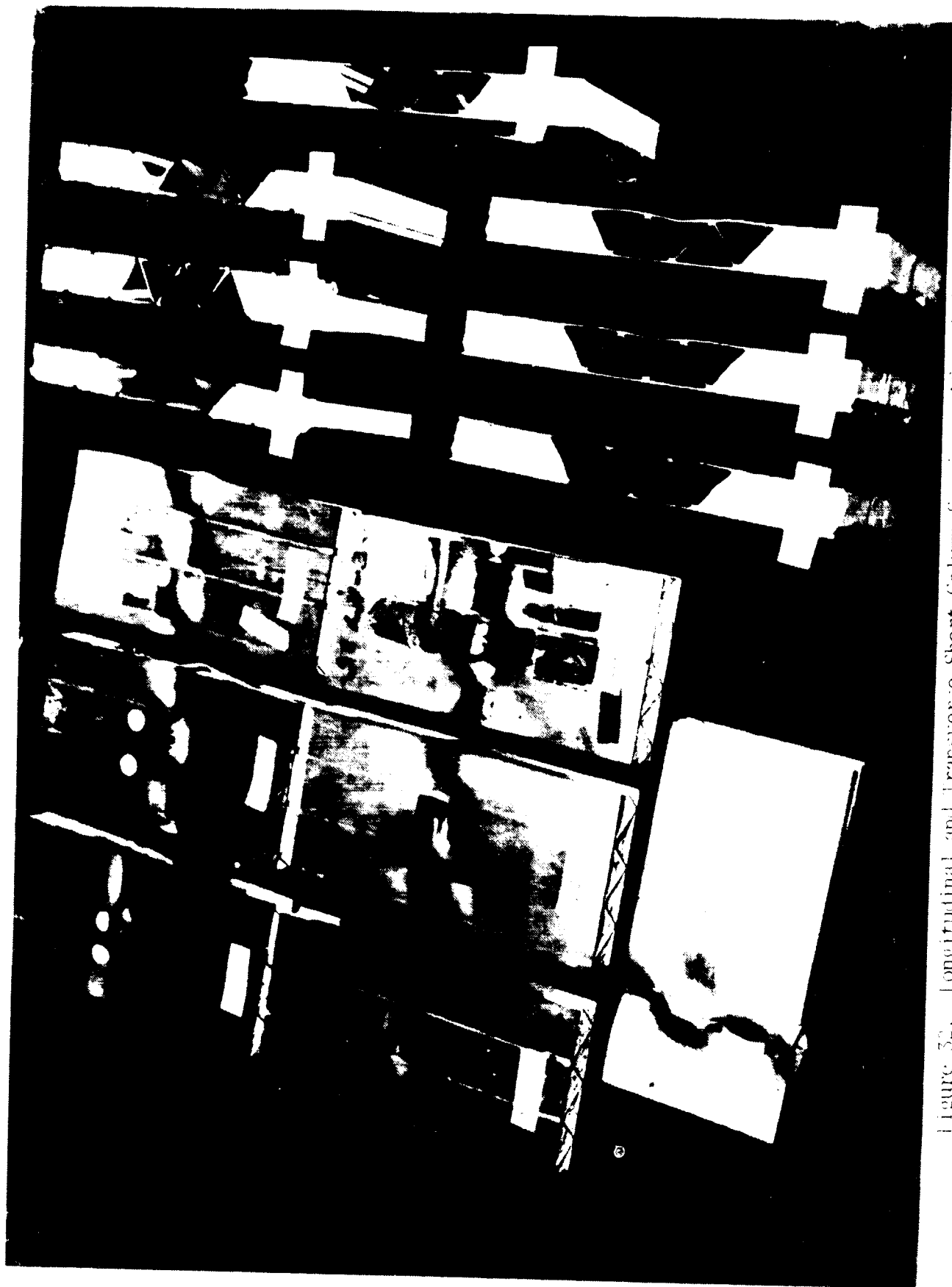
Figure 32. Longitudinal and Transverse Short Column Specimens After Failure
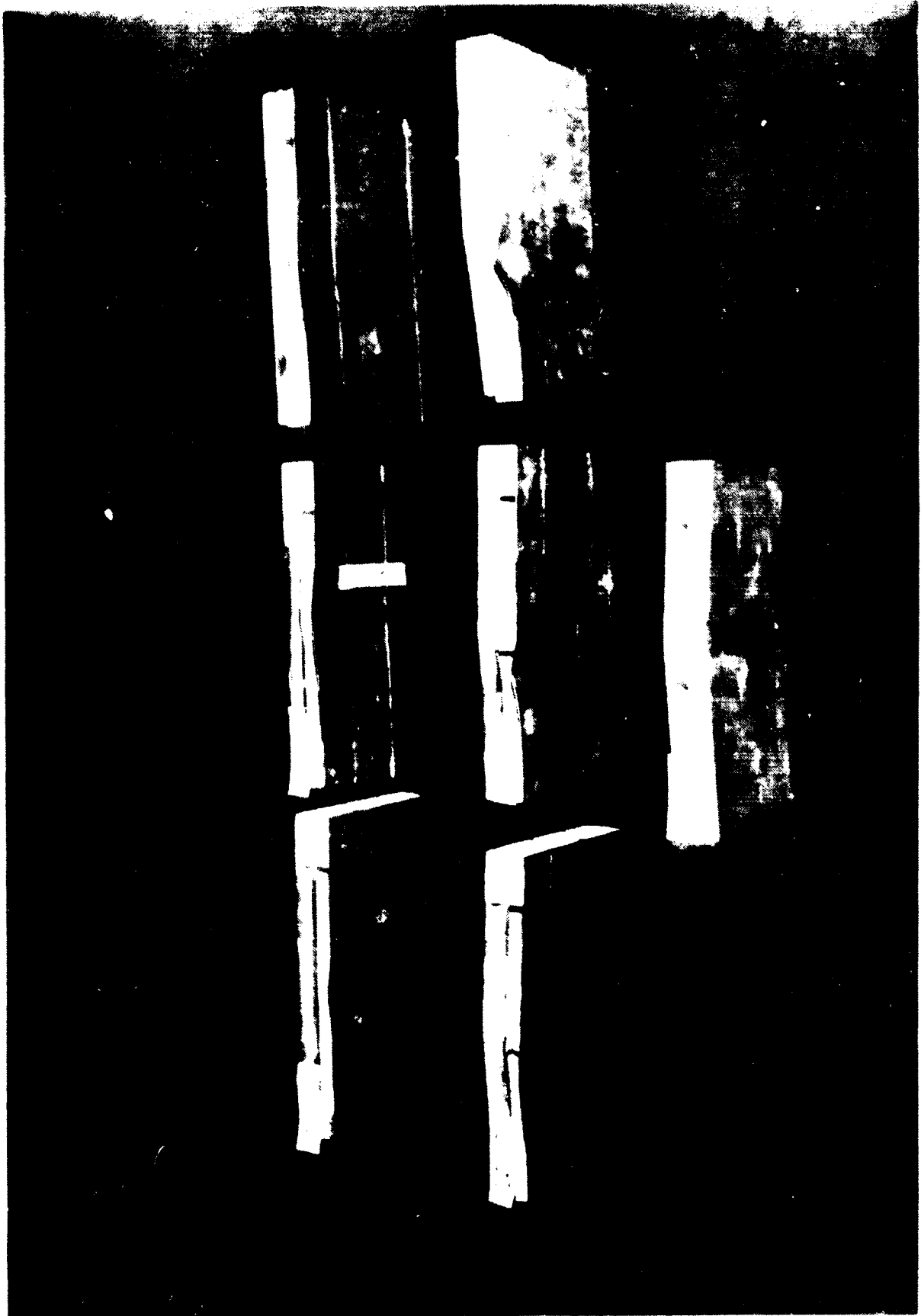
Figure 55. Longitudinal Core Shear Specimens

Figure 34. Longitudinal and Transverse Bending Beam Specimens
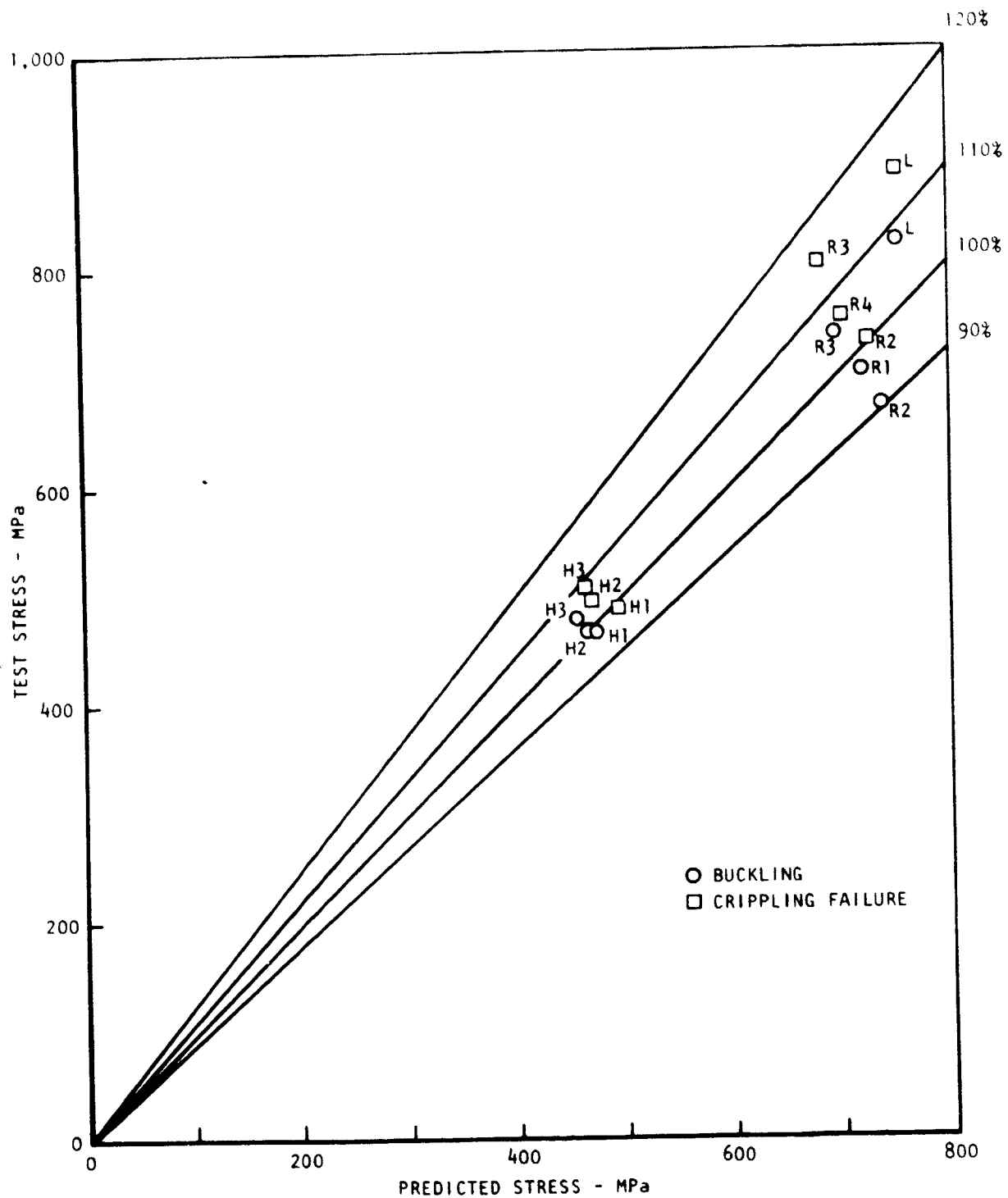
Figure 35. Longitudinal Short Column - Test Versus Predicted Stress
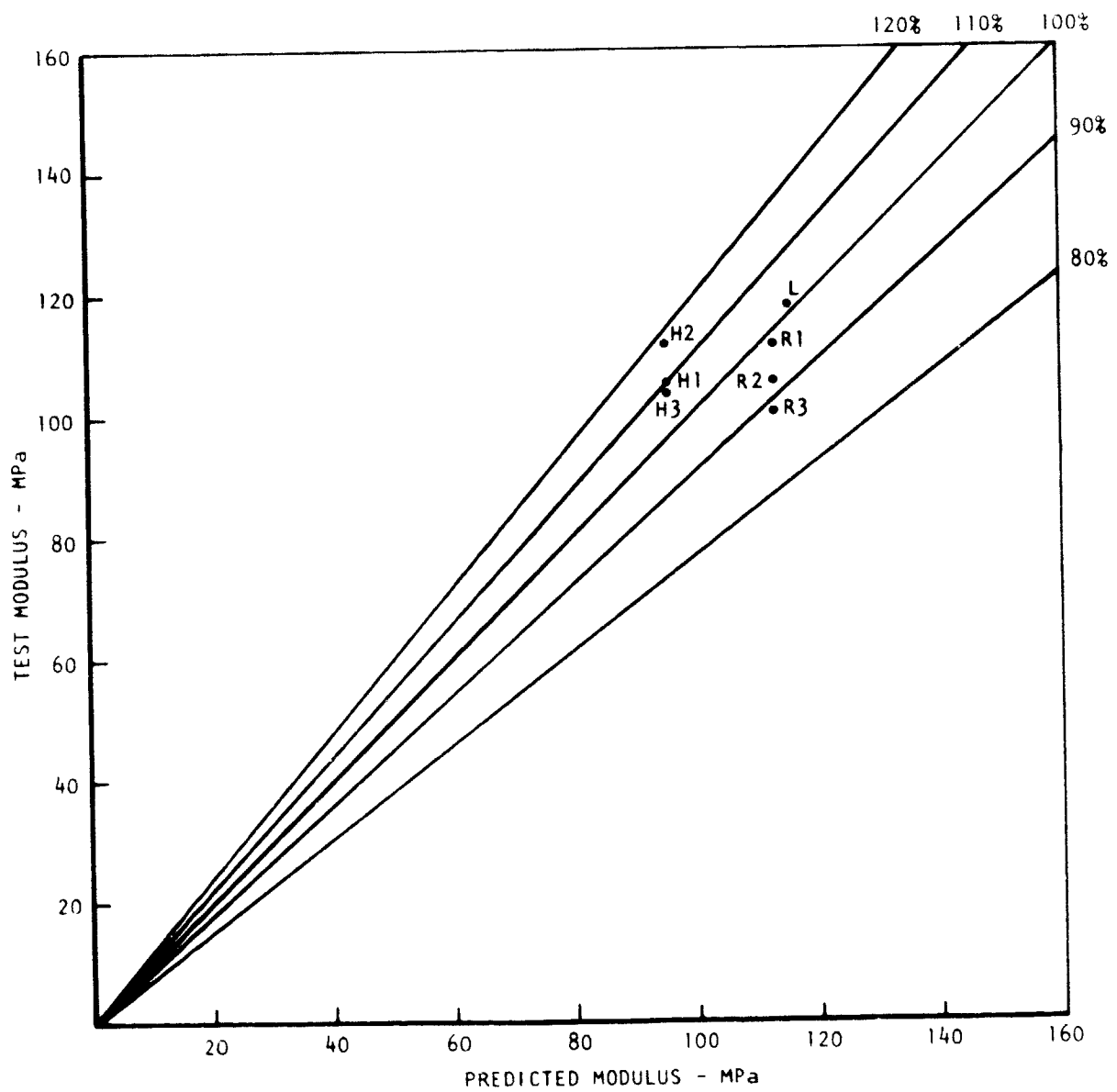
Figure 36. Longitudinal Short Column - Test Versus Predicted Modulus

Figure 57. Longitudinal Short Column Test Setup
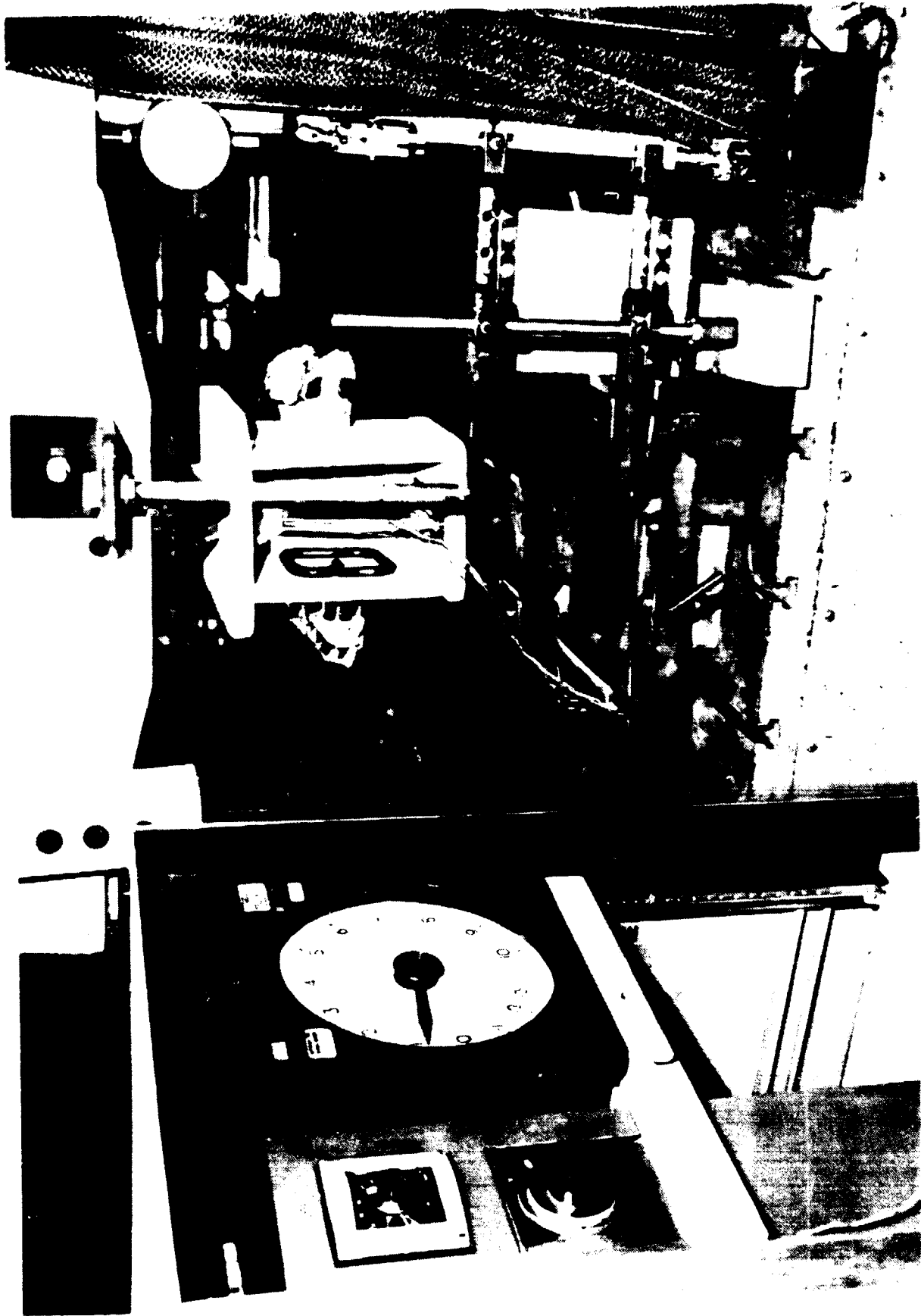
Figure 38. High-Temperature Longitduinal Short Column Test Setup

Figure 39. Longitudinal Short Column After Failure

Figure 40. Longitduinal Short Column - Closeup After Failure
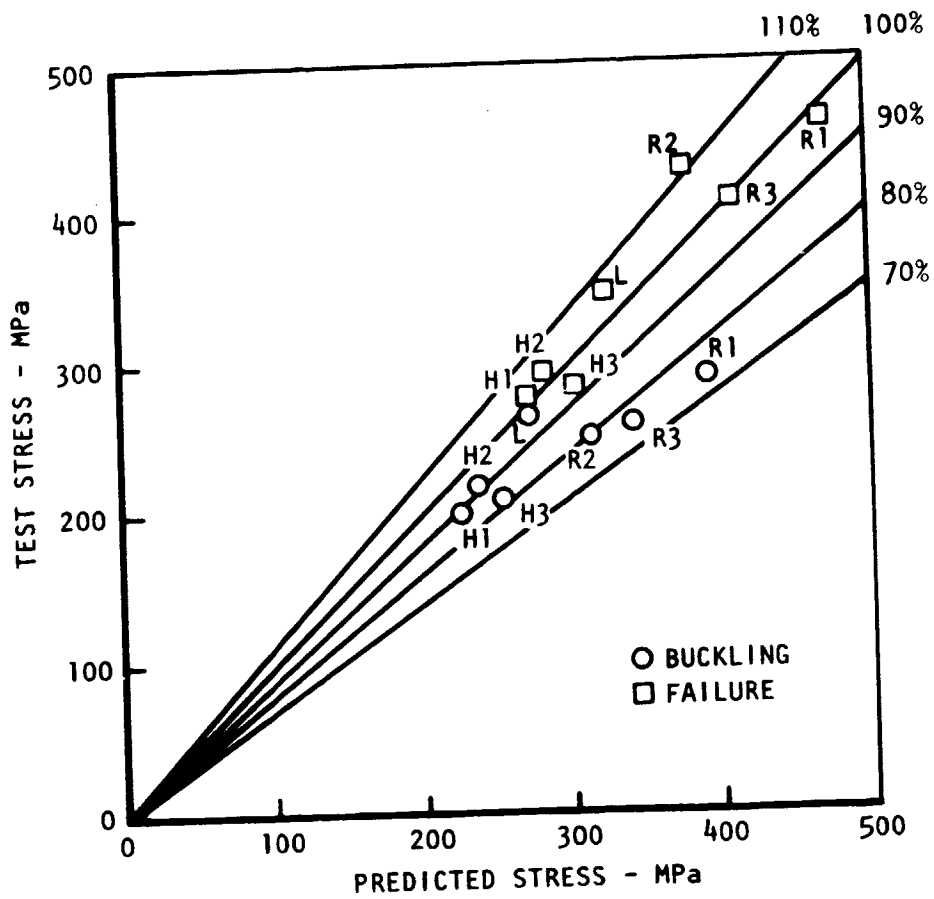
Figure 41. Transverse Short Column - Test Versus Predicted Stress
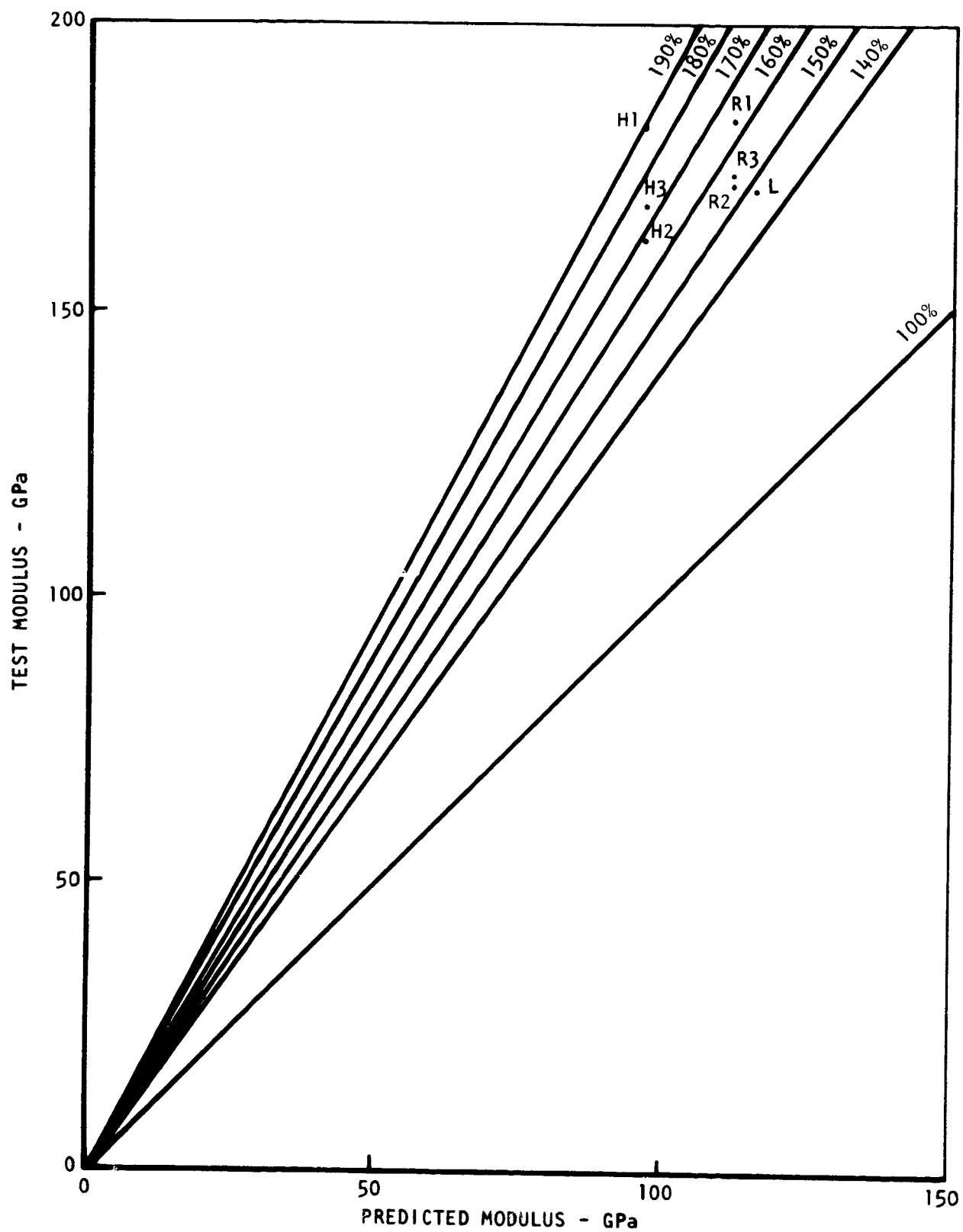
Figure 42. Transverse Short Column - Test Versus Predicted Modulus
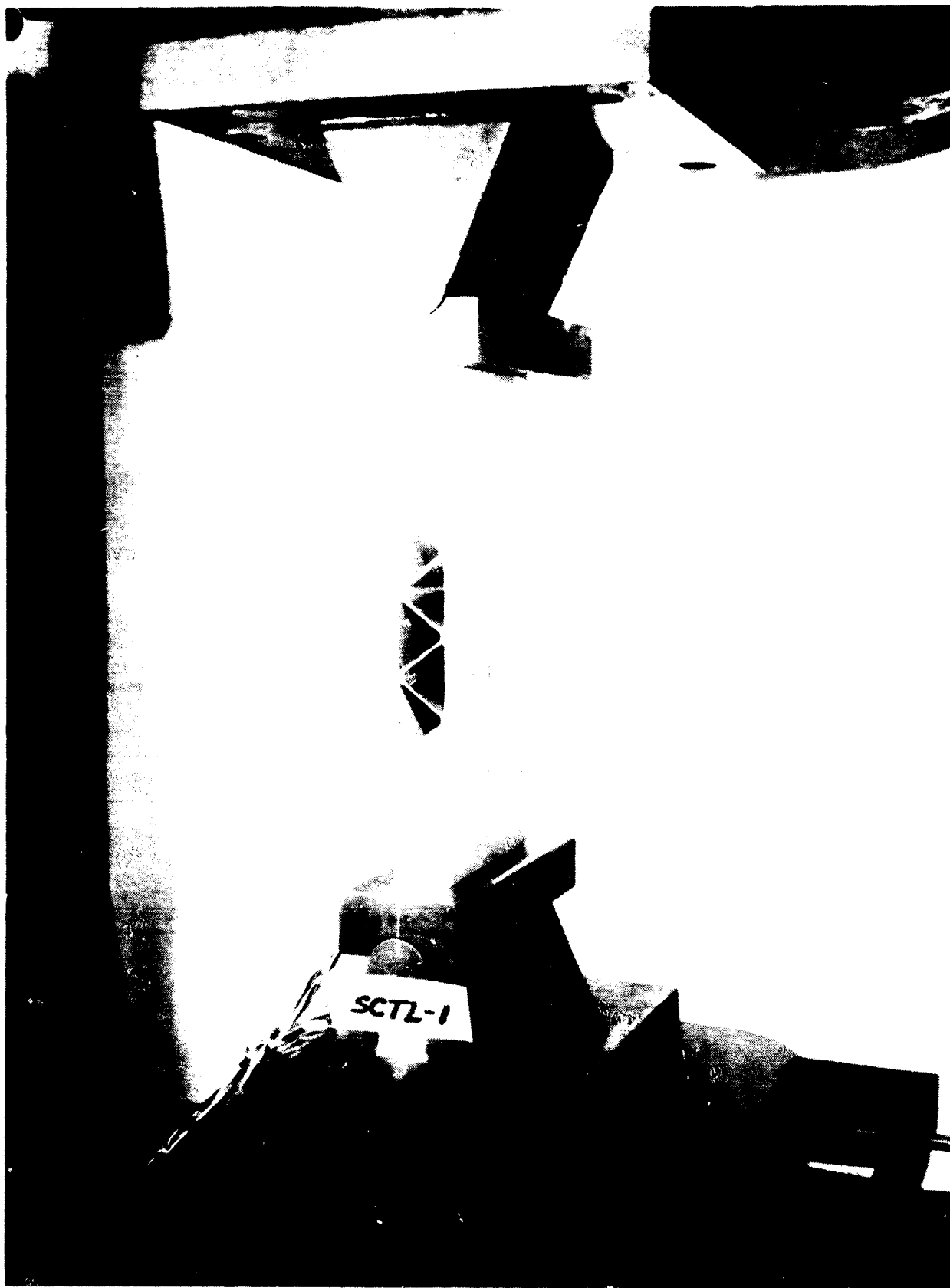
Figure 43. Transverse Short Column Test Setup
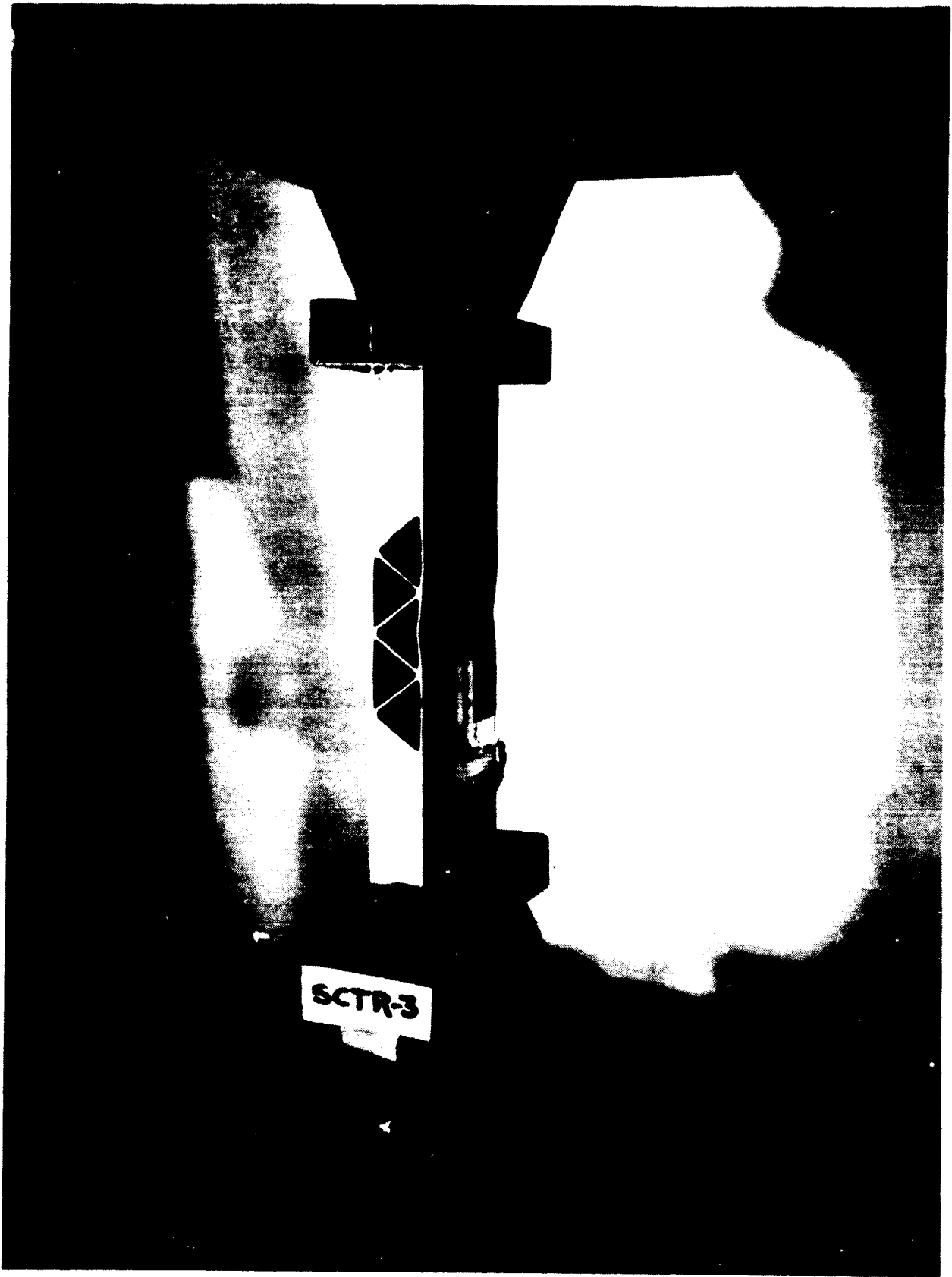
Figure 44.   Transverse Short Column in Test Machine After Failure
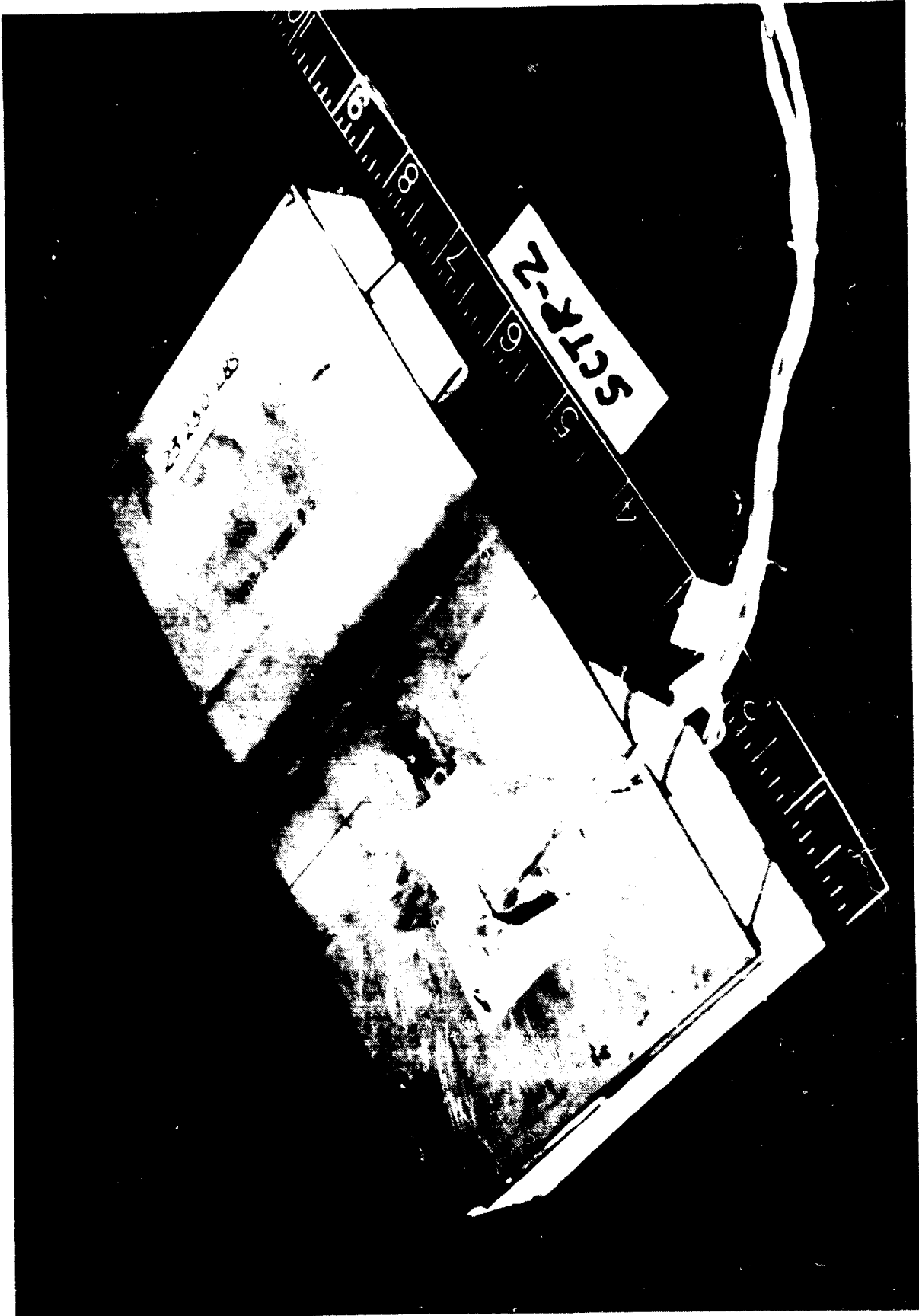
Figure 45. Transverse Short Column After Failure (Closeup)
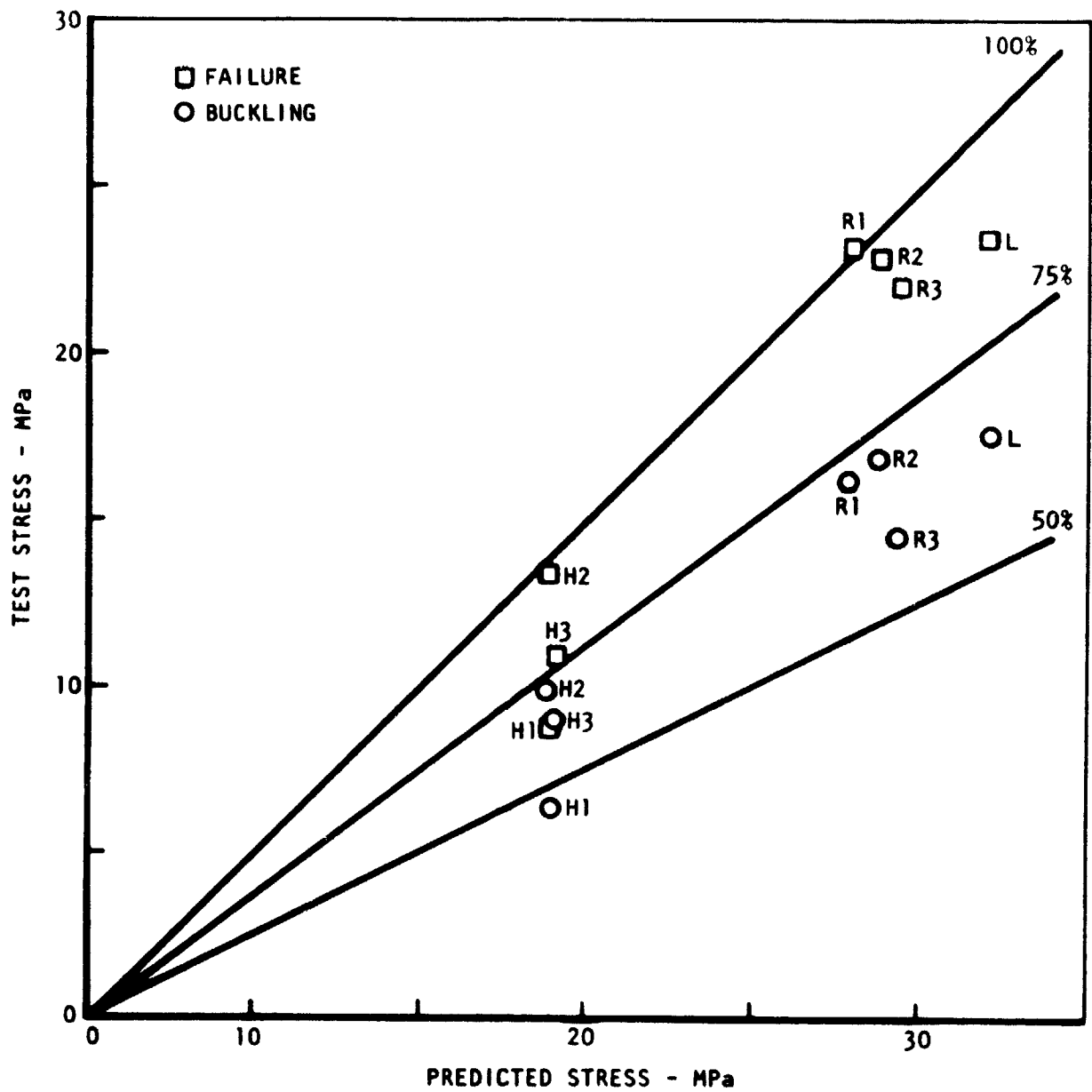
Figure 46.   Longitudinal Core Shear - Test Versus Predicted Stress
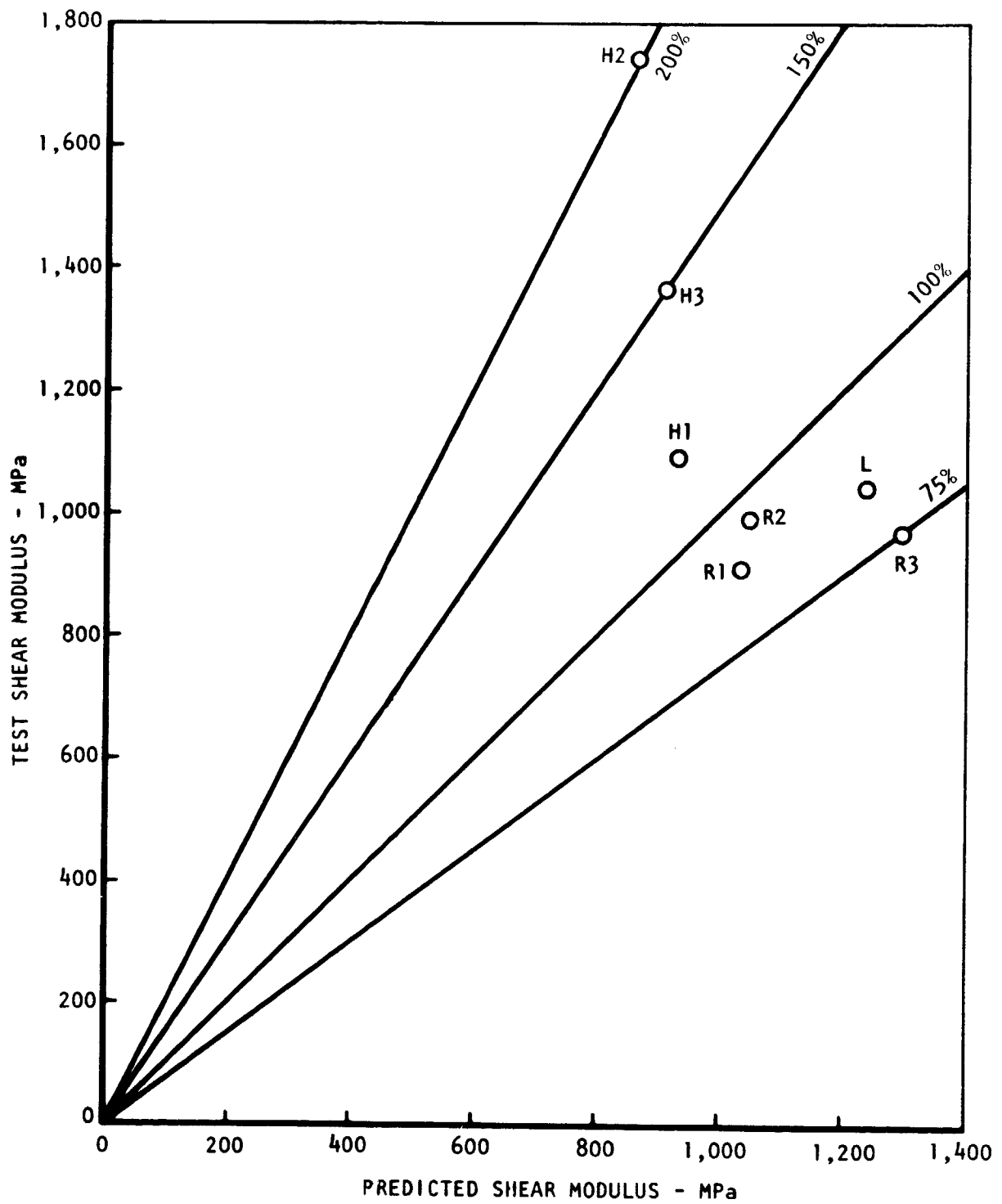
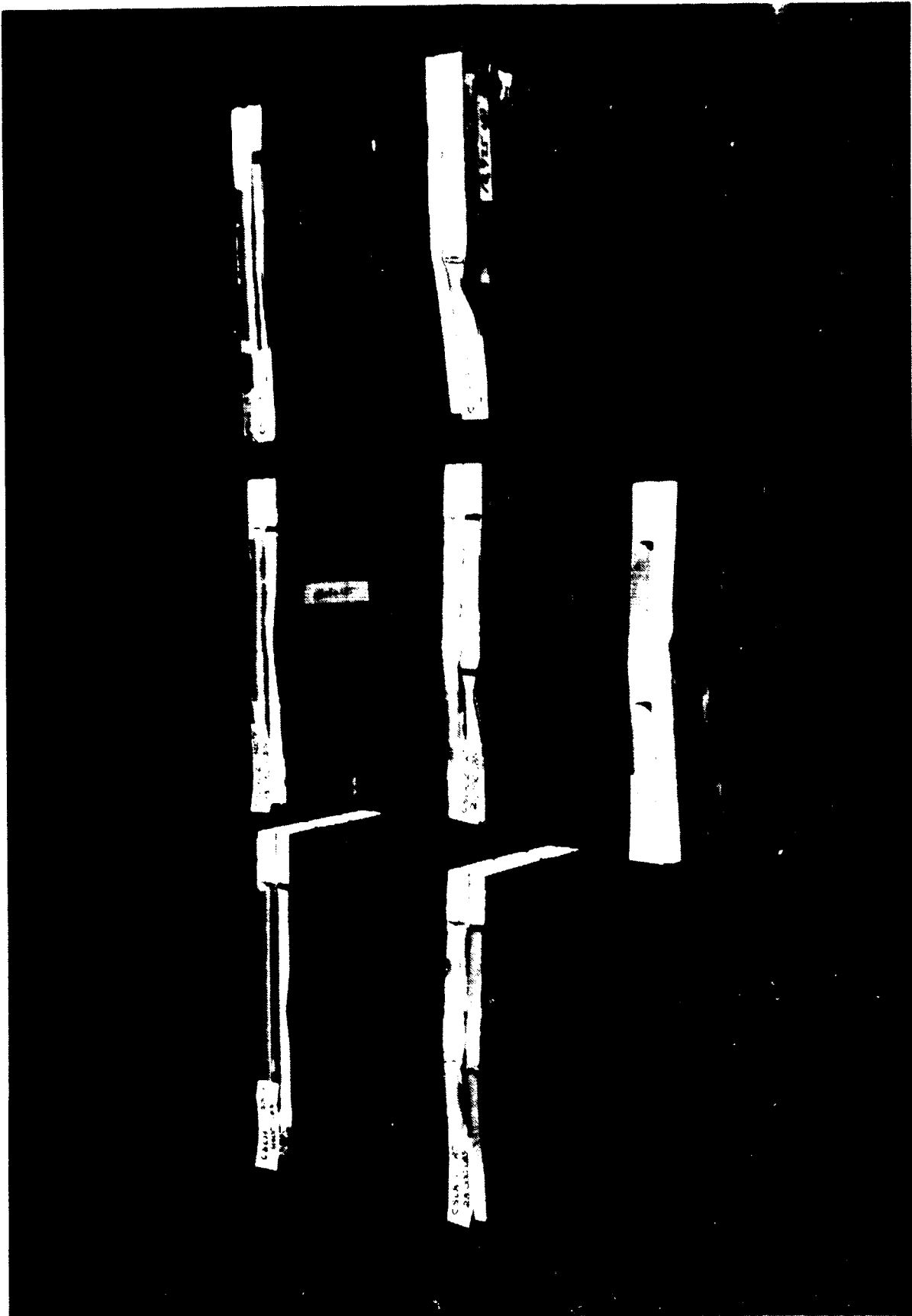Figure 47. Longitudinal Core Shear - Test Versus Predicted Modulus

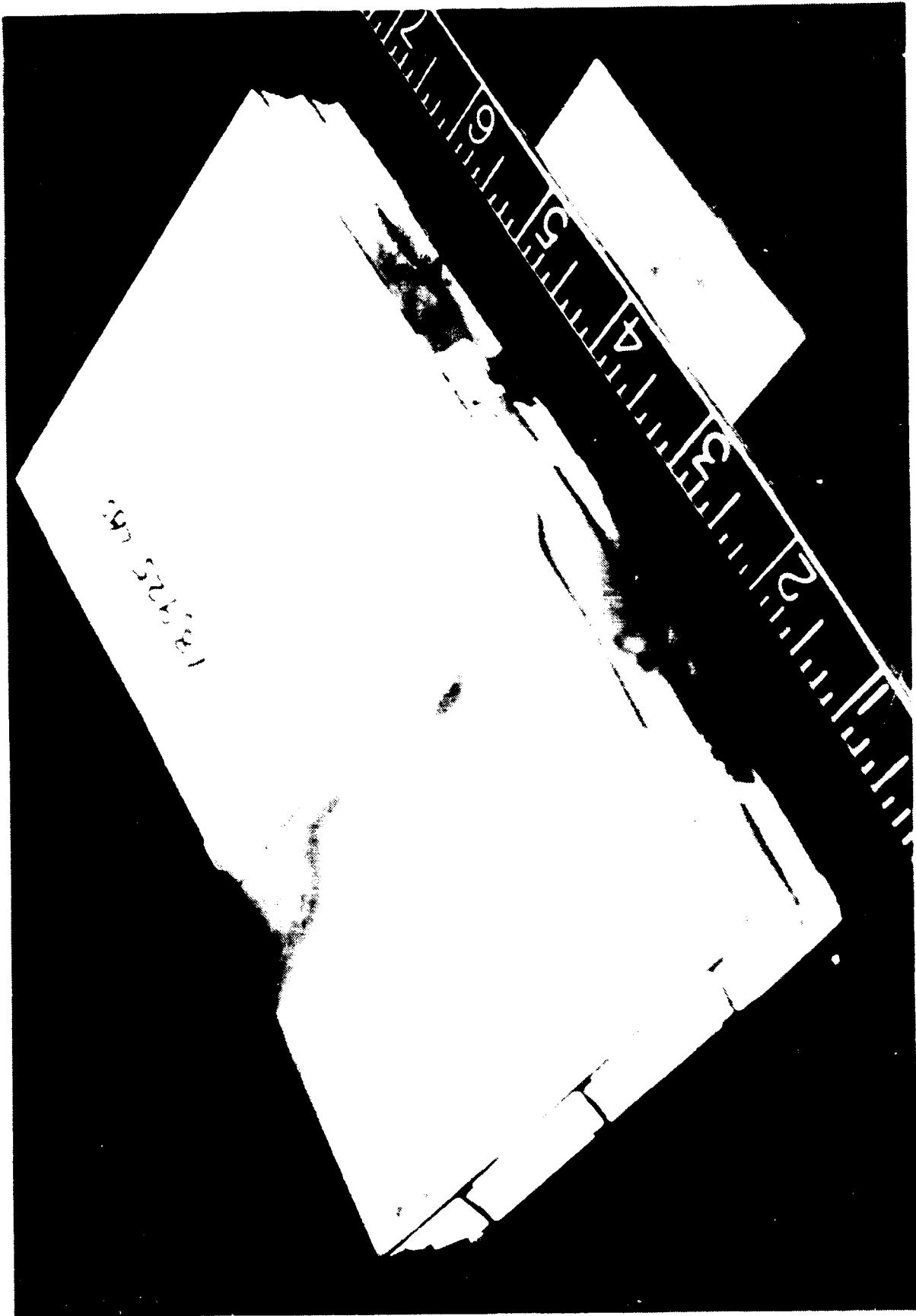Figure 48. Longitudinal Core Shear Specimens After Failure

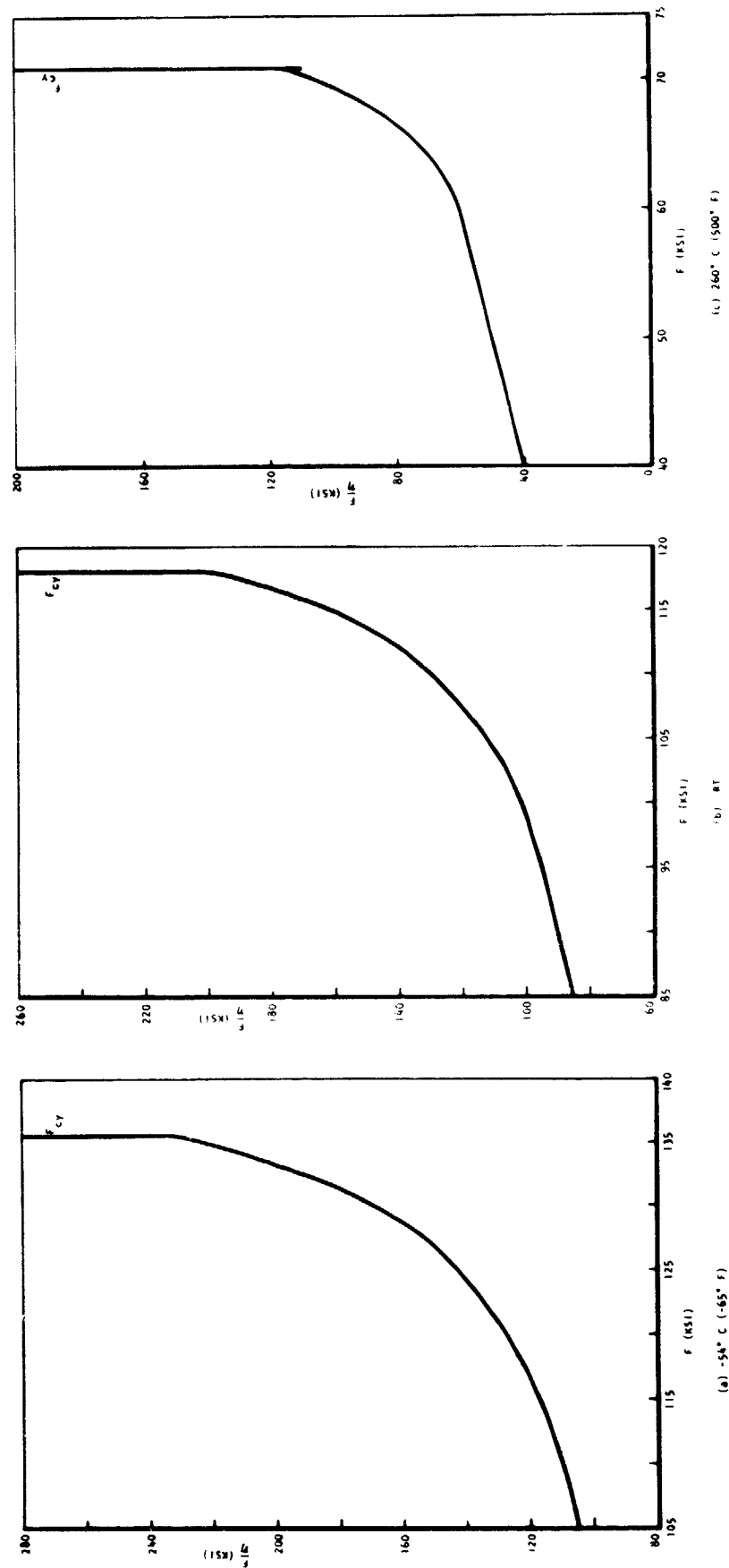Figure 49. Longitudinal Core Shear Specimen - Closeup After Failure

Figure 50. Plasticity Correction Factor in Compression
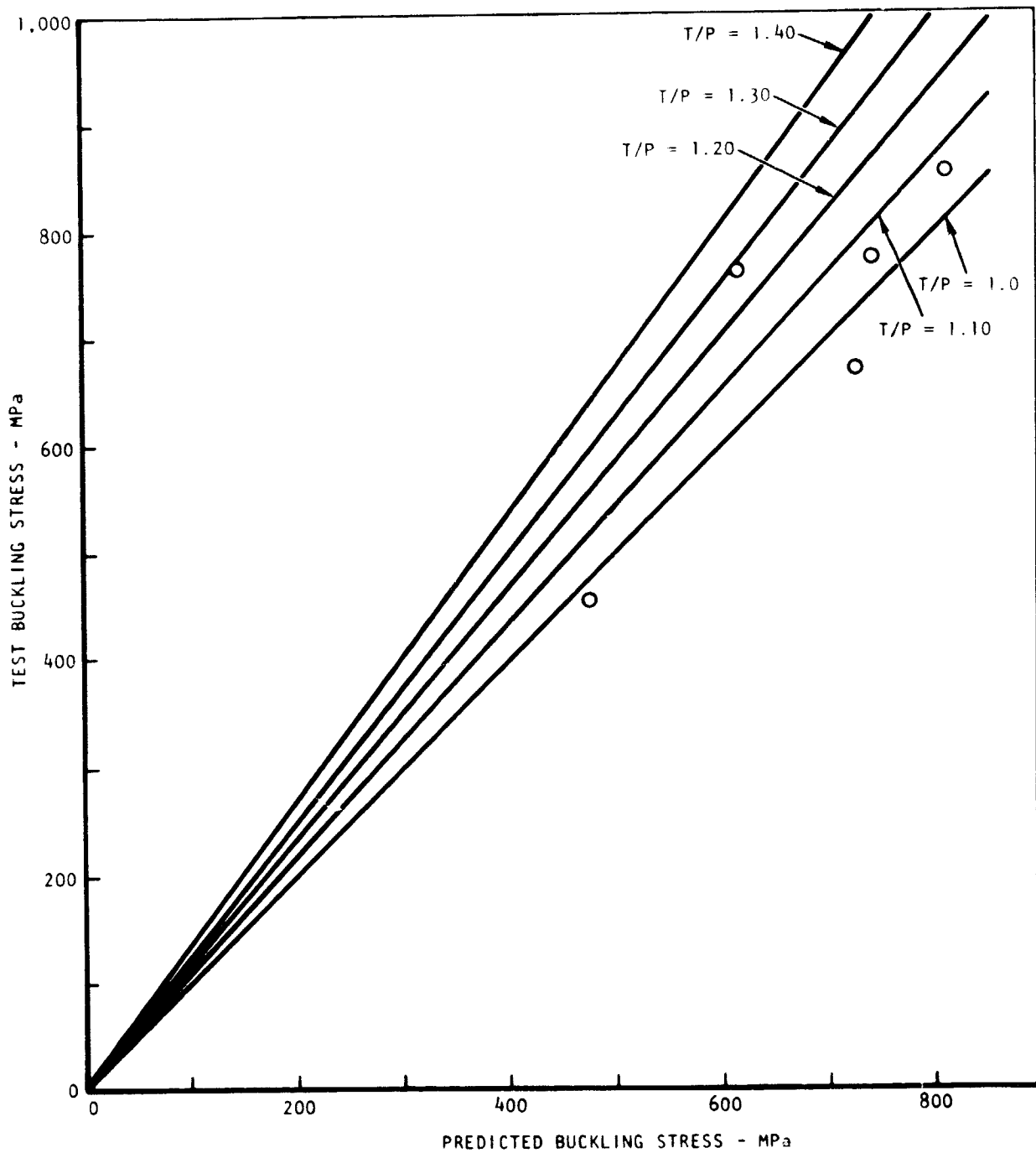for Ti-6Al-4V SPF/DB Processed Material

88

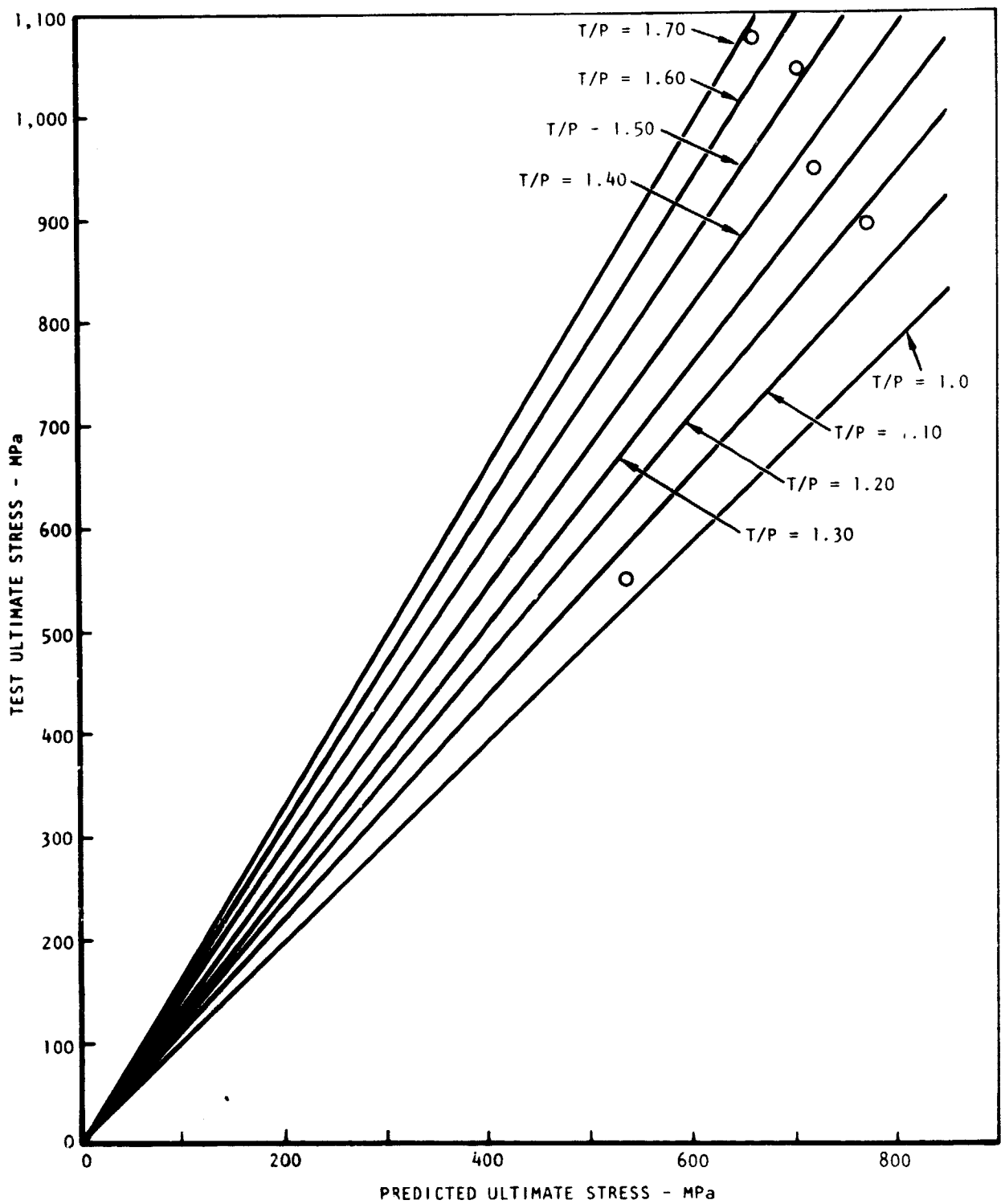Figure 51. Longitudinal Bending Beam - Test Versus Predicted Buckling Stress

Figure 52.   Longitudinal Bending Beam - Test Versus Predicted Ultimate Stress
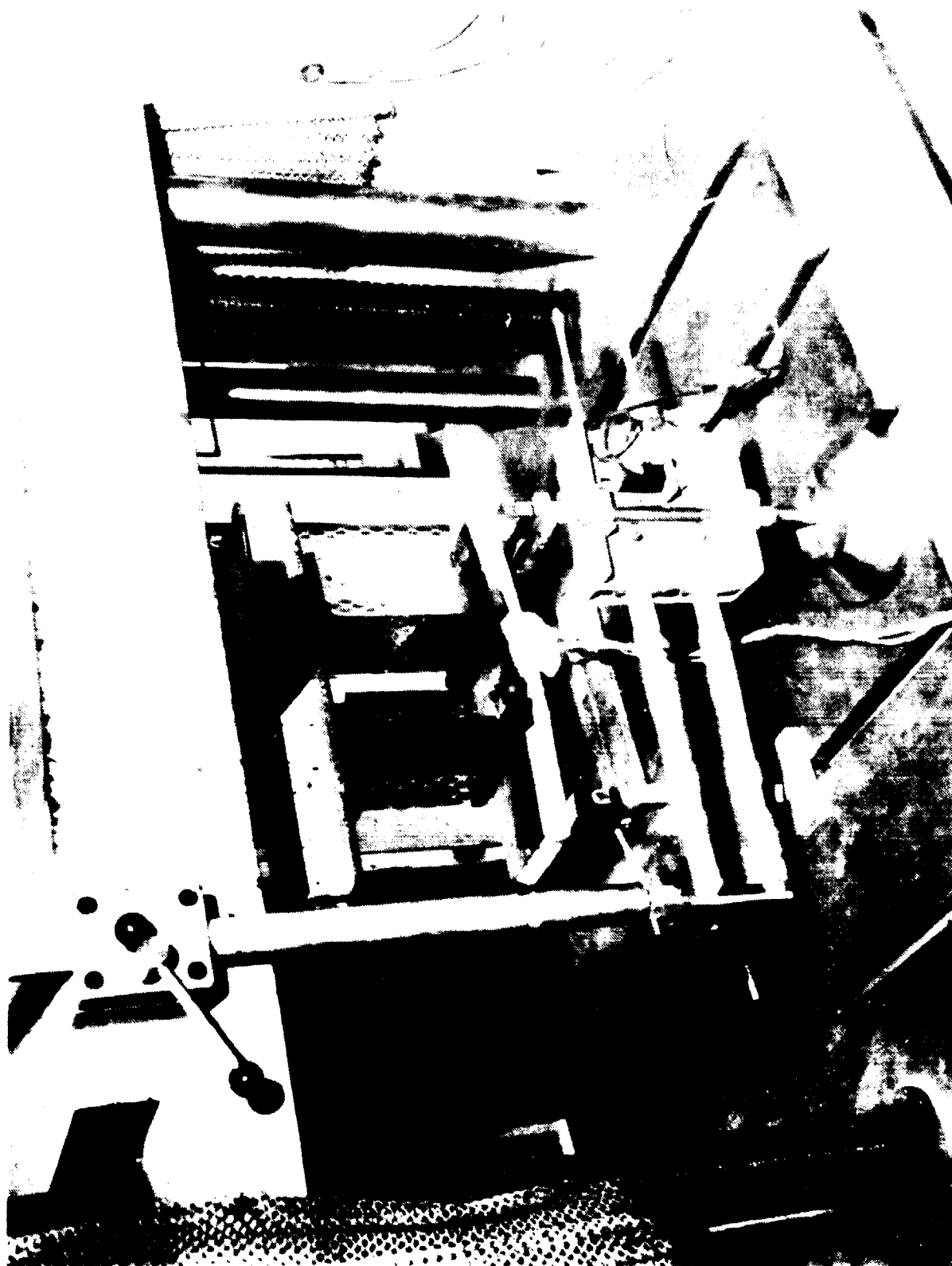
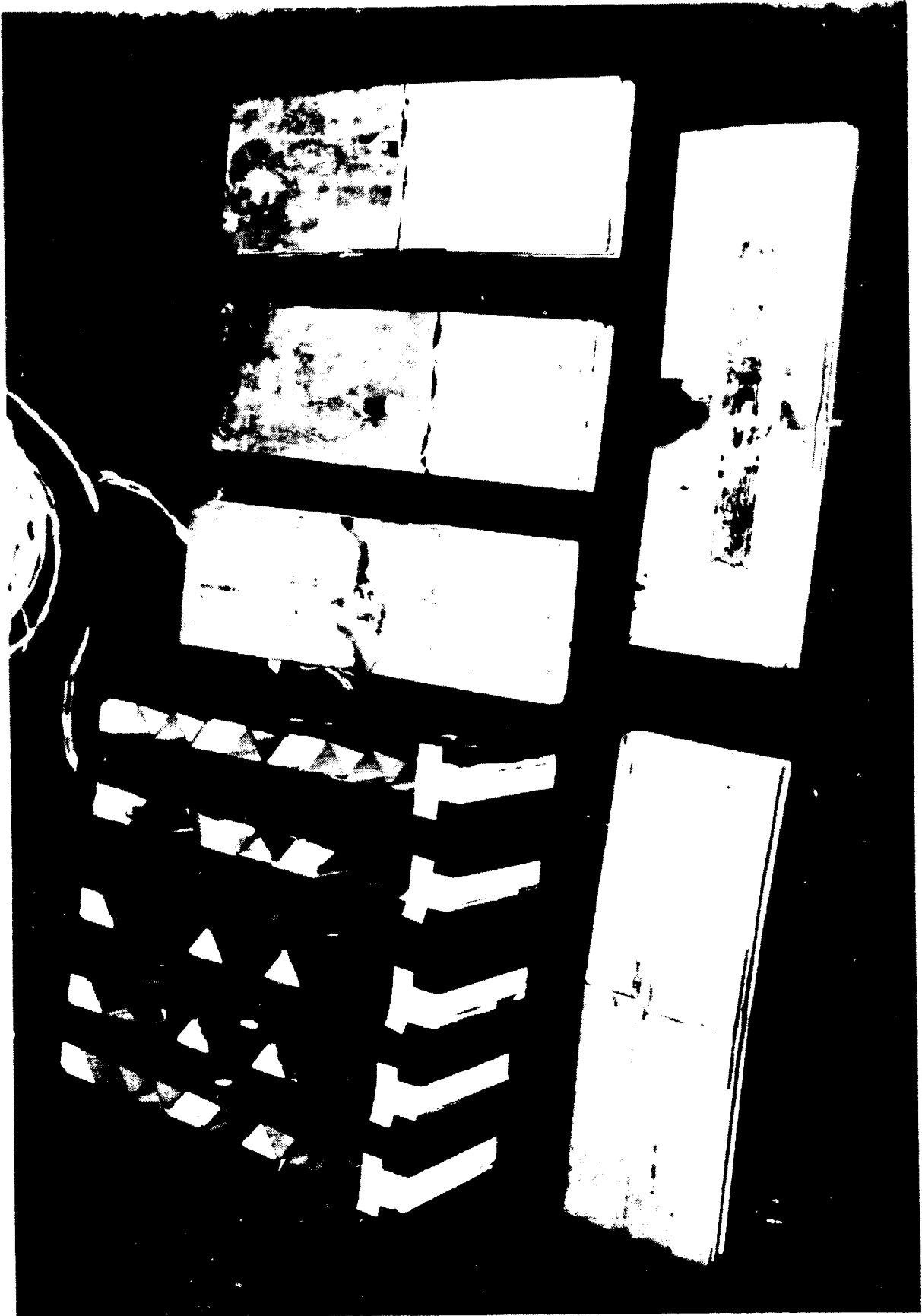Figure 53. Longitudinal Bending Beam in Test Machine After Failure

Figure 54. Longitudinal and Transverse Bending Beams After Failure
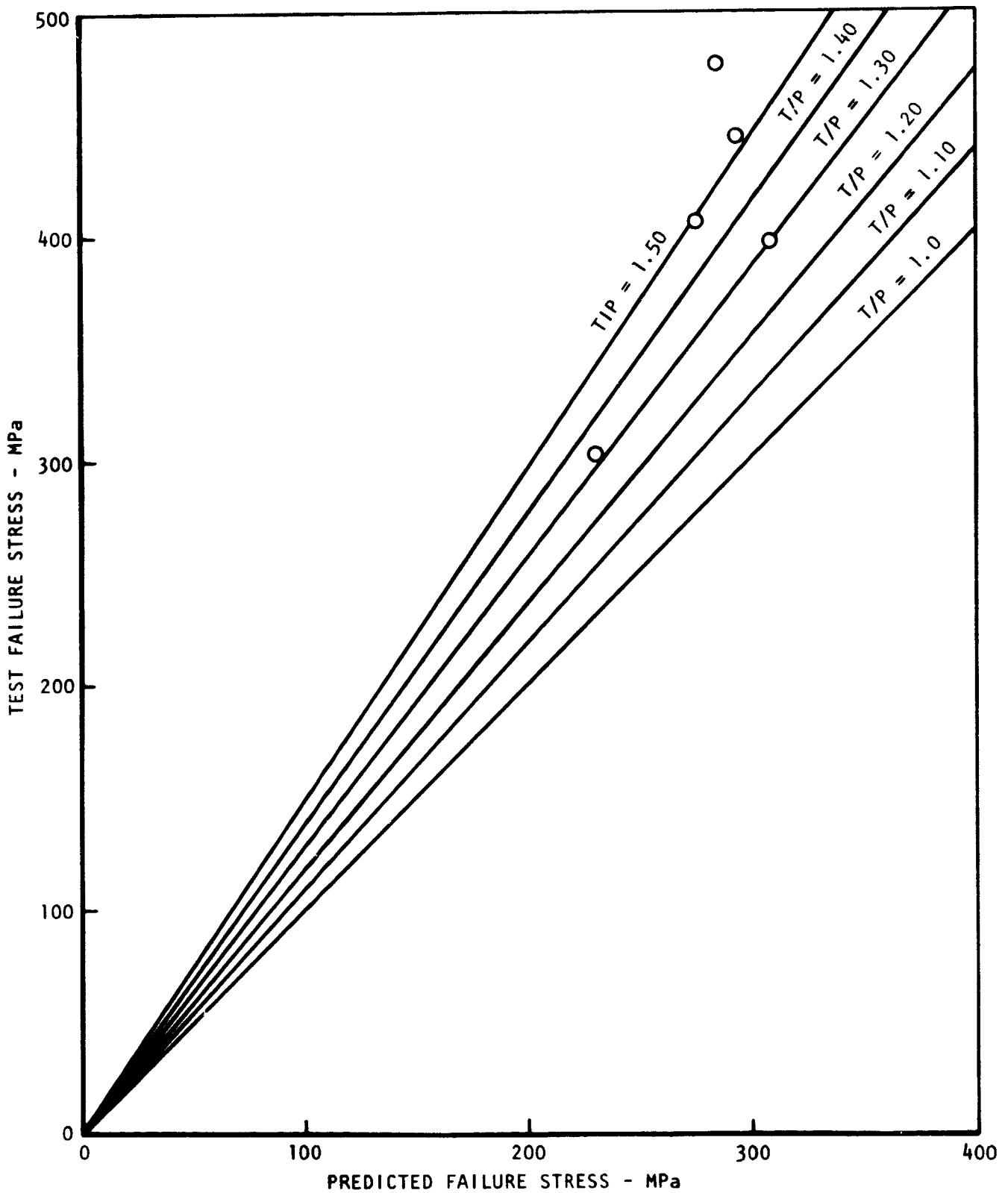
Figure 55. Transverse Bending Beam - Test Versus Predicted Stress

Figure 56. Transverse Bending Beam in Test Machine After Failure
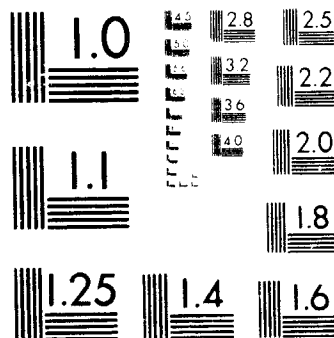
SPECIMENS F-07, F-09, F-10

t_{F_1}

25.1
(0.988)

t_{F_2}

2.54
(0.10) EDM FLAW (TYP)

190.5 (7.50) (TYP.)

SPECIMENS F-05, F-06

r_{F_1}

12.7
(0.50)

18.5
(0.73)

55.4 (2.18)

t_3

t_{F_2}

SPECIMENS F-12, F-13, F-14

t_{F_1}

TRANSVERSE CORE

t_{F_2}

190.5 (7.50) (TYP)

SPECIMEN F-11

t_{F_1}

TRANSVERSE CORE

12.7
(0.50)

57.1 (2.25)

t_3

T_{F_2}
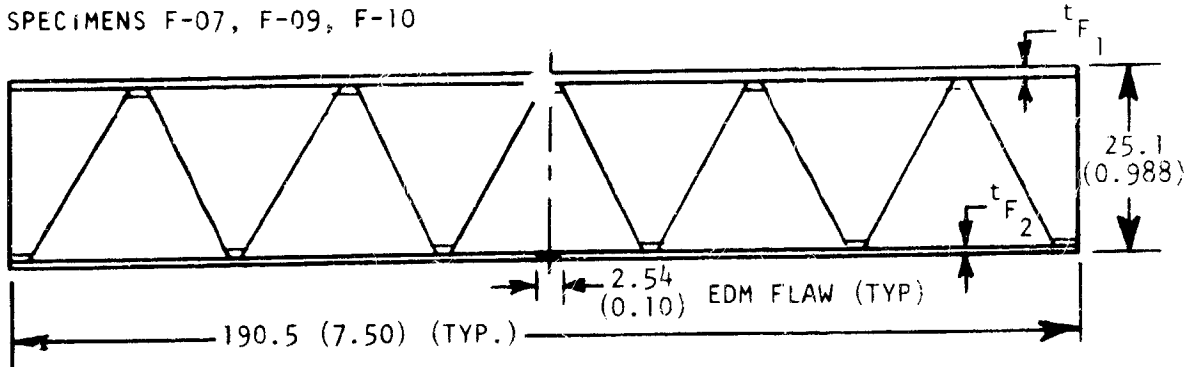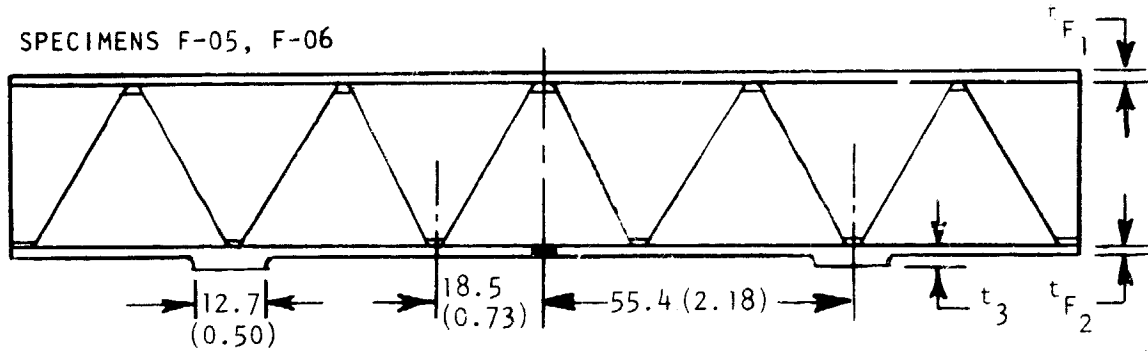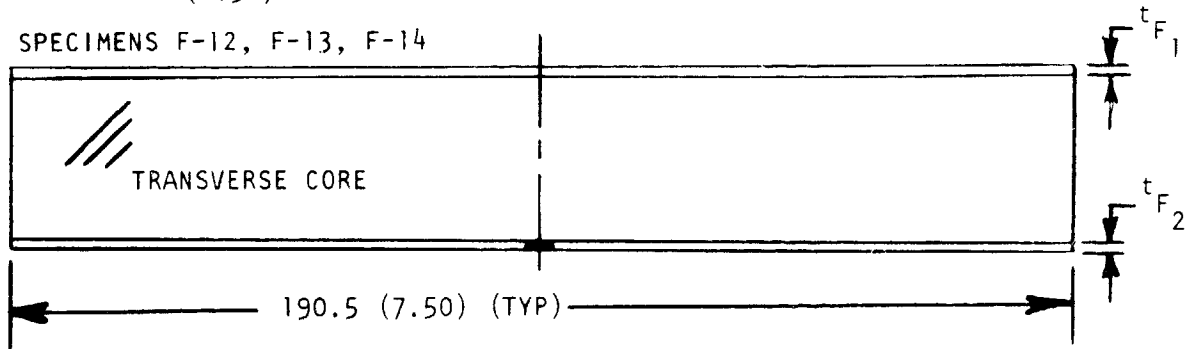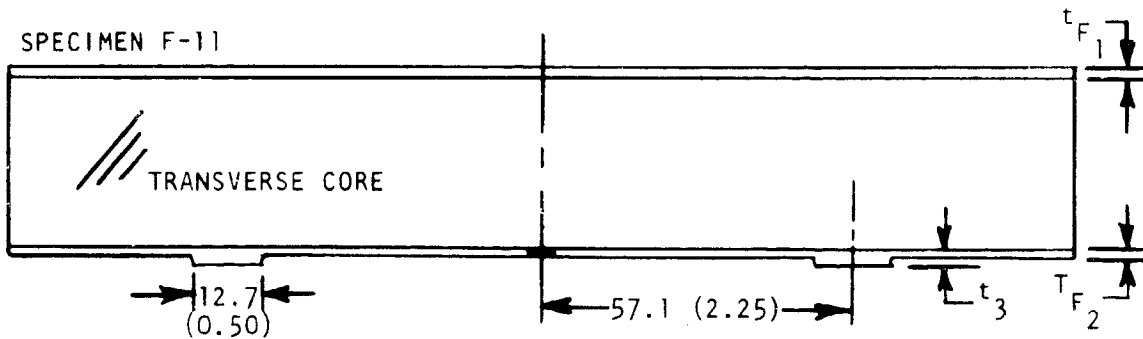
DIMENSIONS IN MM (IN.)

Figure 57.   Cross Sections of Crack Growth Test Specimens
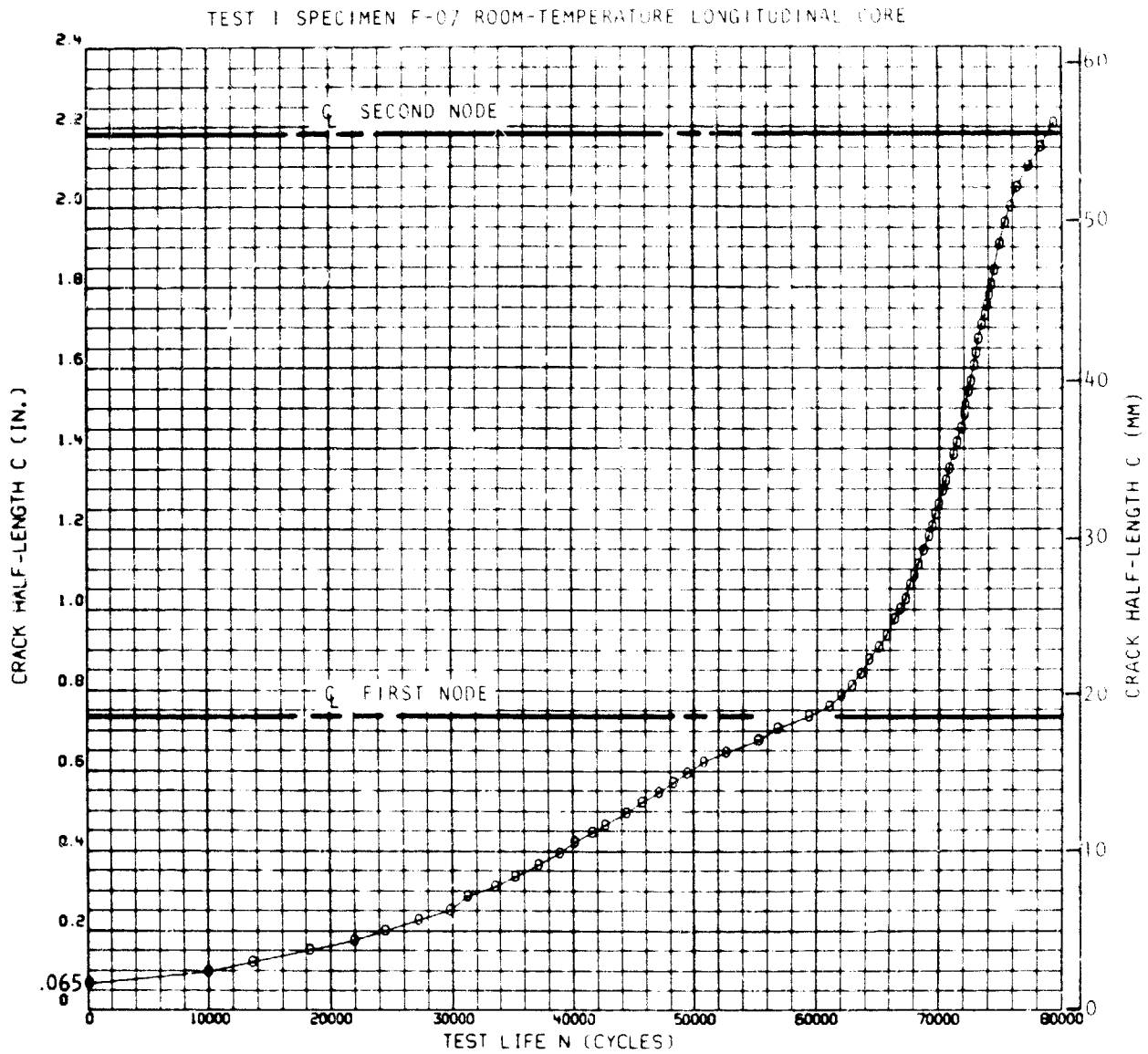
Figure 58. Crack Growth Curve for Test Specimen F-07 at 21° C (70° F)
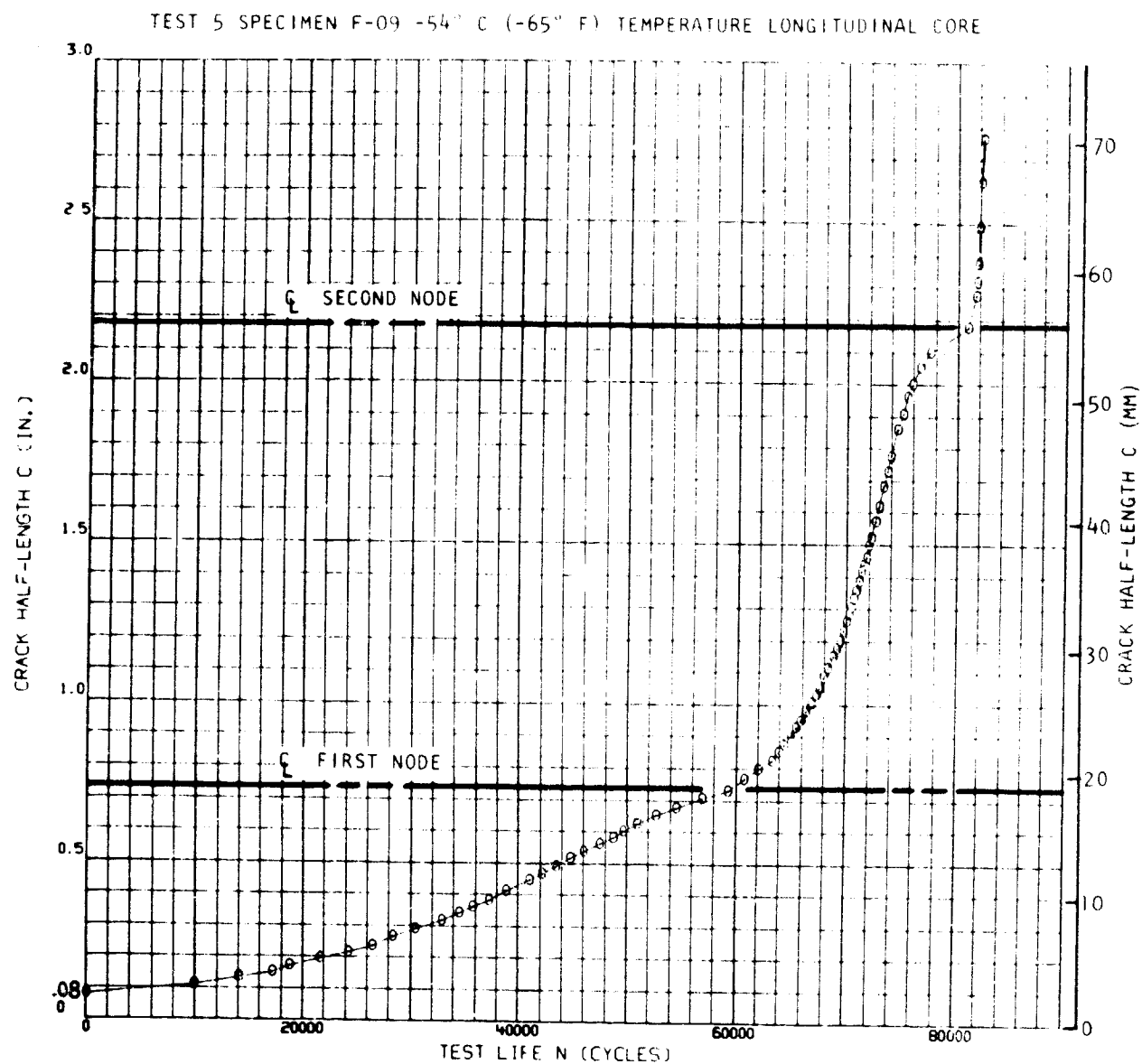
Figure 59.   Crack Growth Curve for Test Specimen F-09 at -54° C (-65° F)
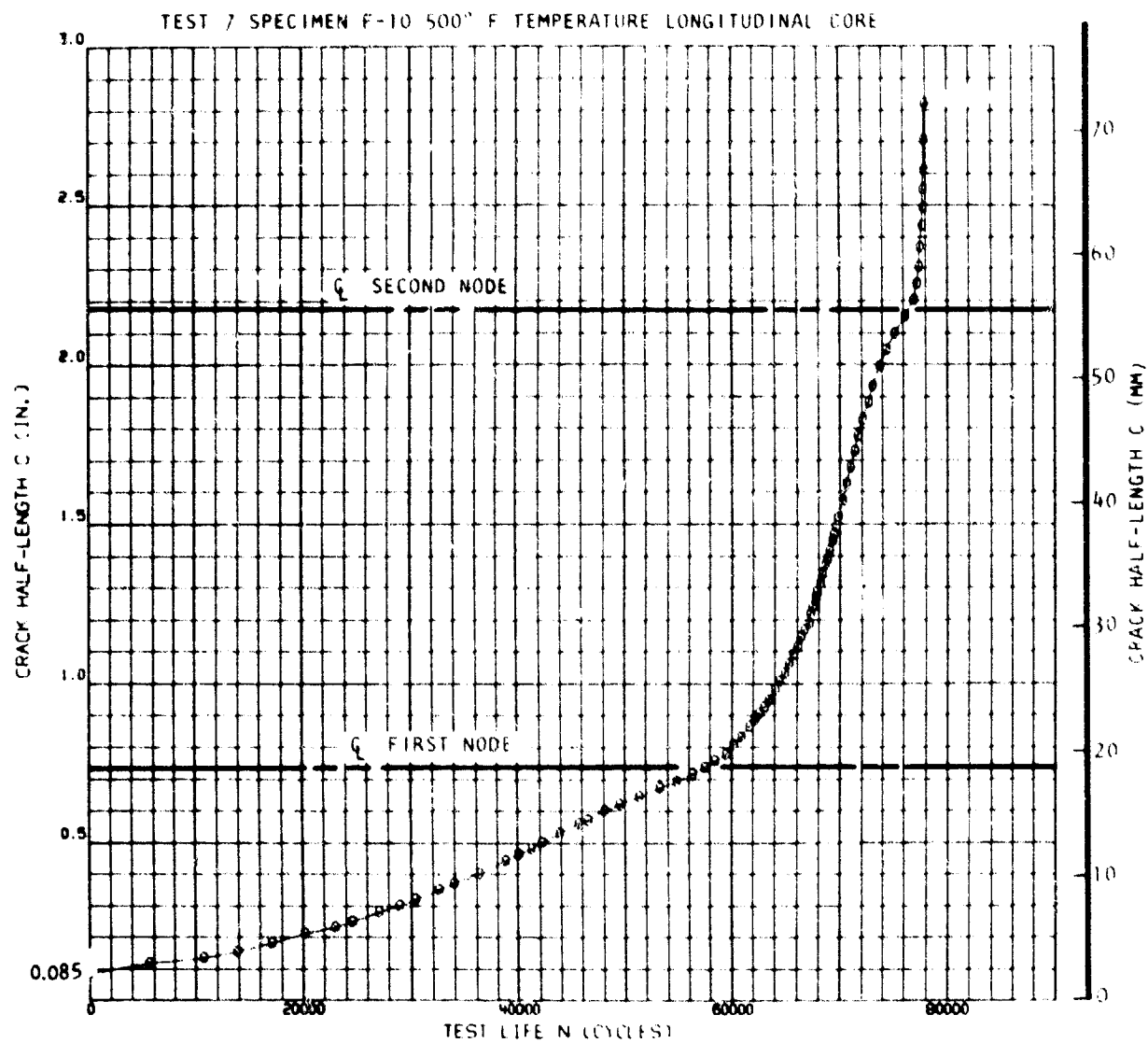
Figure 60. Crack Growth Curve for Test Specimen F-10 at 260° C (500° F)
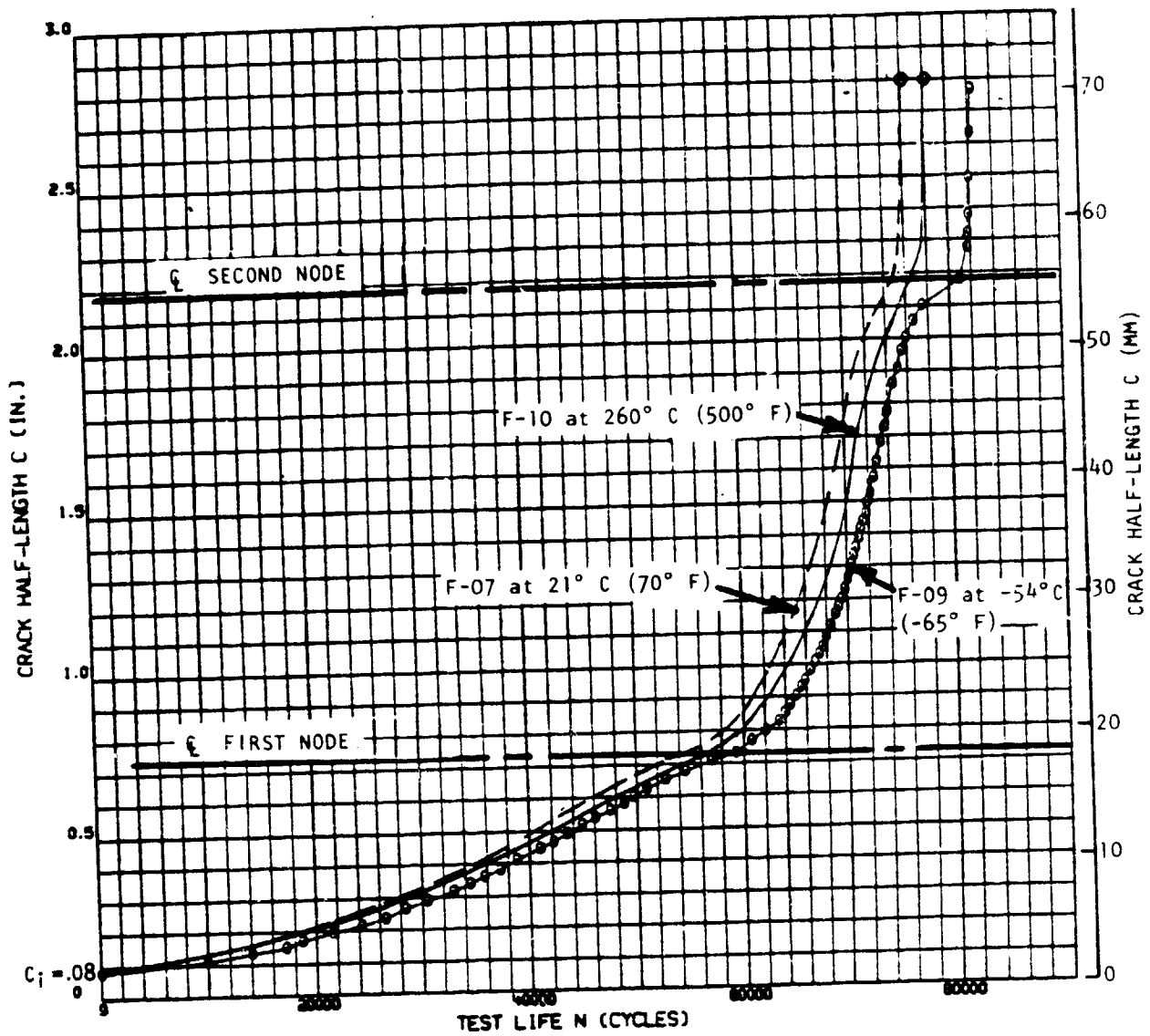
Figure 61.   Crack Growth Curves for Longitudinal Core Tests
at Three Temperatures

TEST 3 SPECIMEN F-05 ROOM-TEMPERATURE LONGITUDINAL CORE

OUTER EDGE OF CRACK-ARREST STRIP

CENTERLINE OF CRACK-ARREST STRIP

INNER EDGE OF CRACK-ARREST STRIP

CENTERLINE OF FIRST NODE

CRACK HALF-LENGTH C (IN.)

CRACK HALF-LENGTH C (MM)

TEST LIFE N (CYCLES)
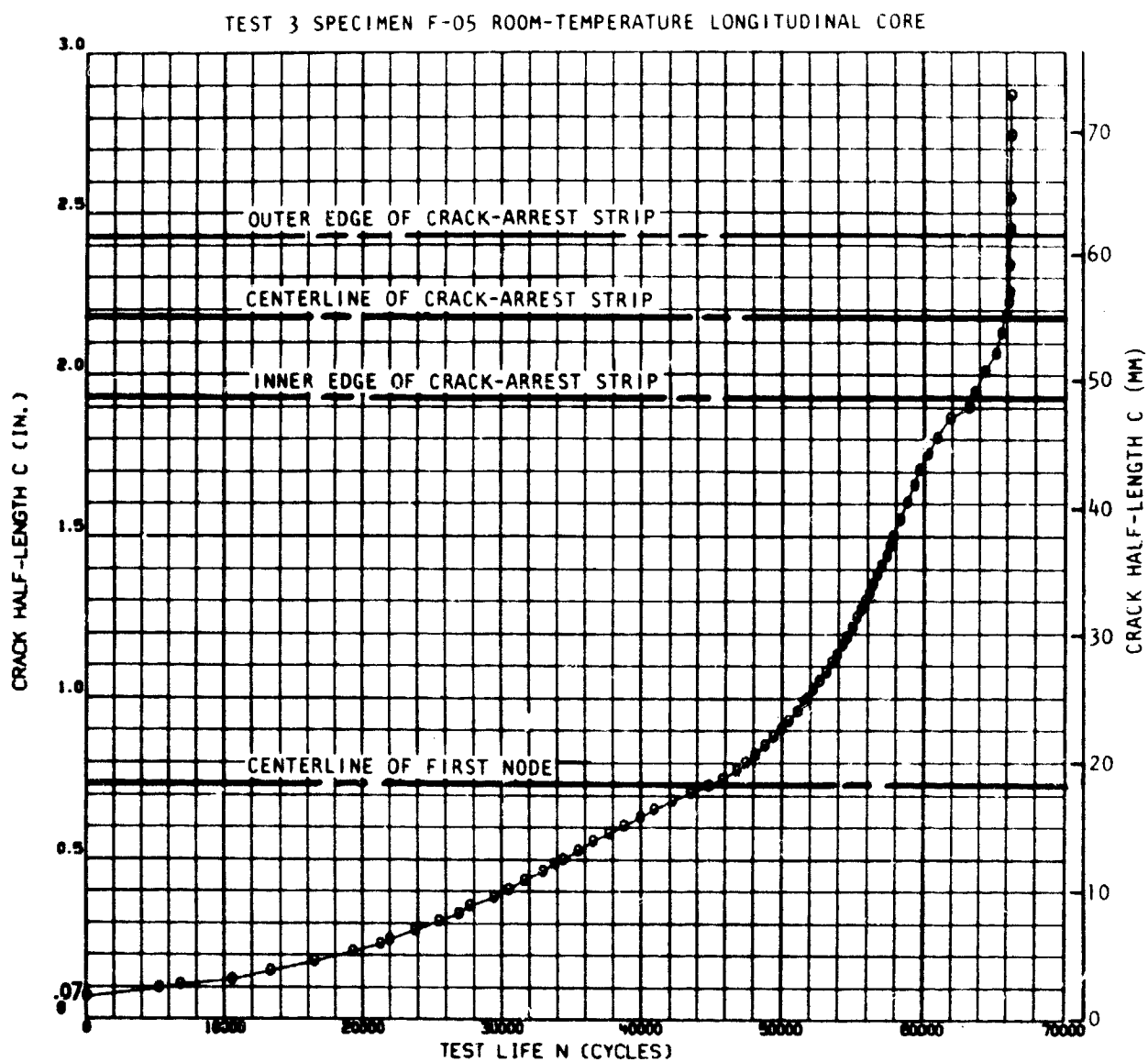
Figure 62. Crack Growth Curve for Test Specimen F-05 at 21° C (70° F)
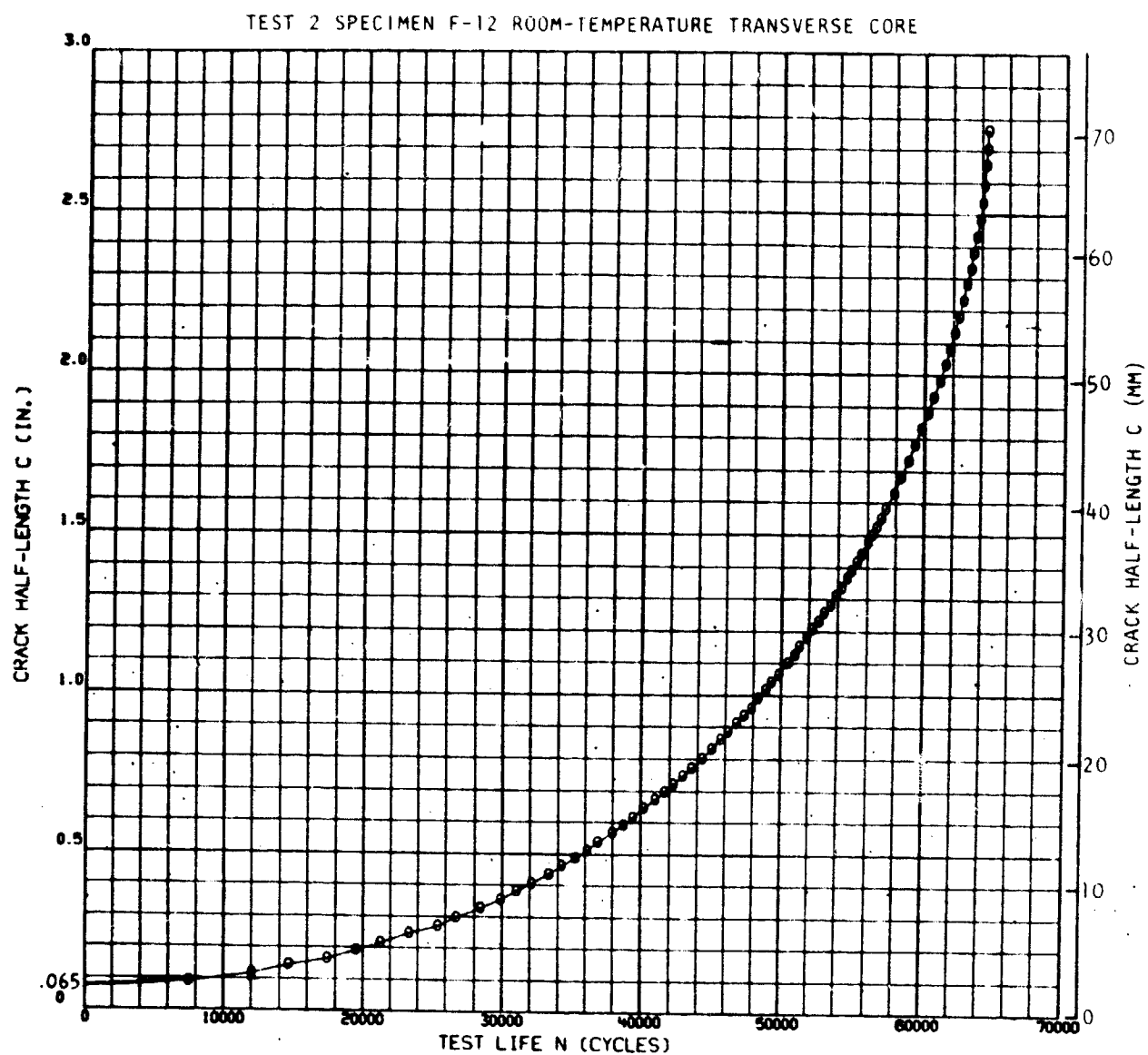
Figure 65. Crack Growth Curve for Test Specimen F-12 at 21° C (70° F)
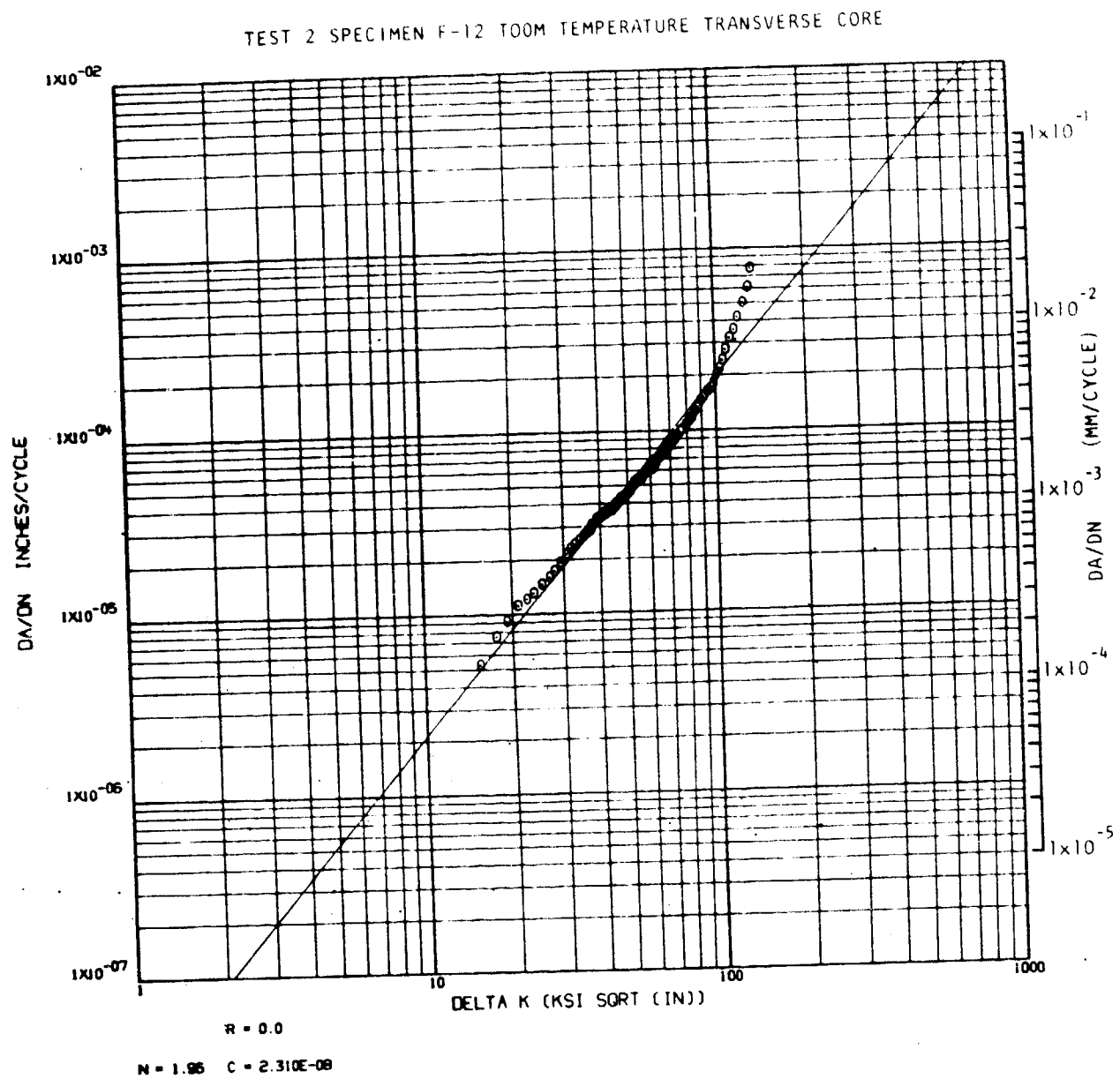
Figure 64. Crack Growth Rate Plot for Test Specimen F-12 at 21° C (70° F)

TEST 6 SPECIMEN F-13 -54° C (-65° F) TEMPERATURE TRANSVERSE CORE

Figure 65.   Crack Growth Curve for Test Specimen F-13 at -54° C (-65° F)

TEST 6 SPECIMEN F-13 -54° C (-65° F) TEMPERATURE TRANSVERSE CORE

R = 0.0

N = 2.05   C = 1.365E-08
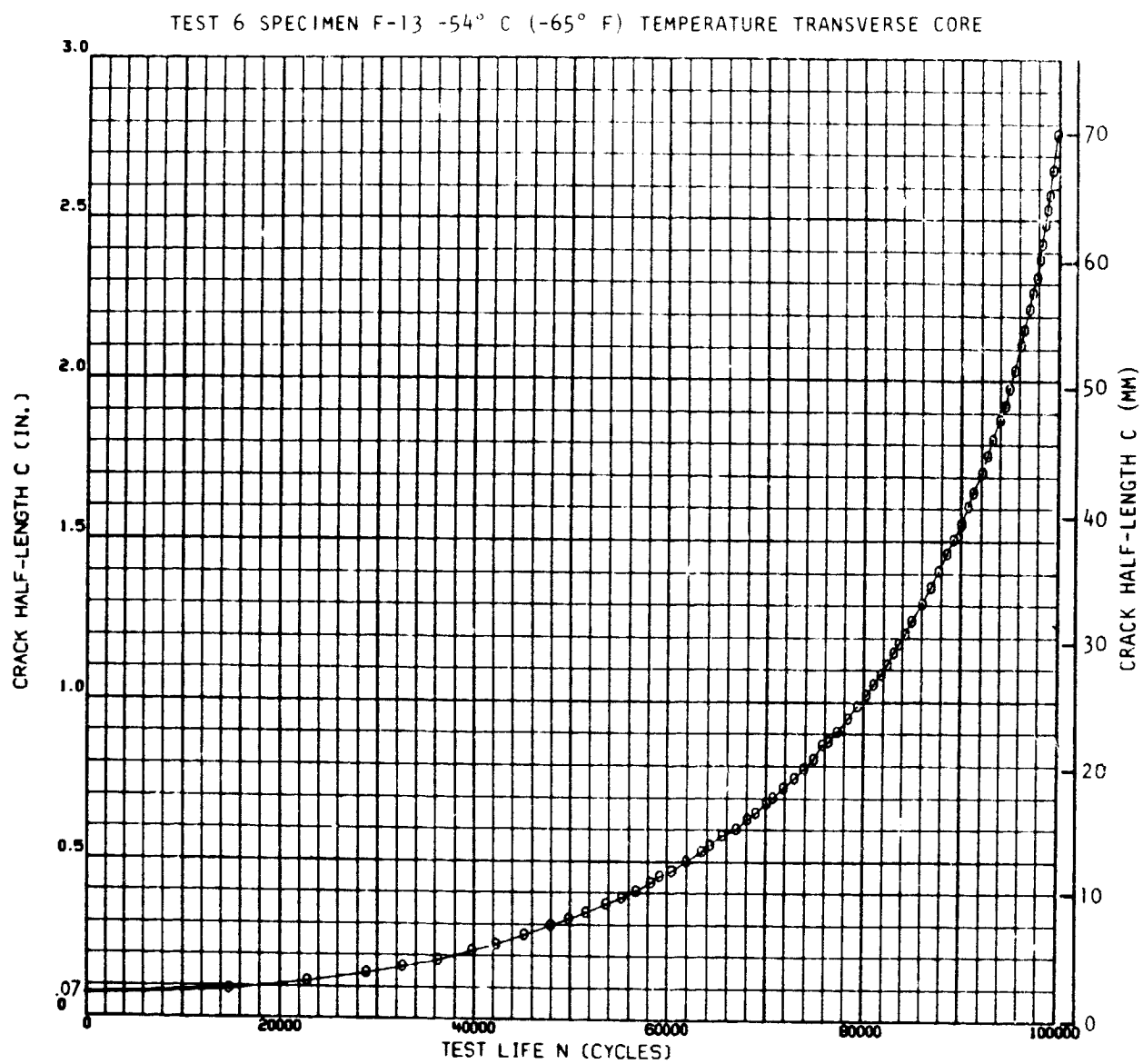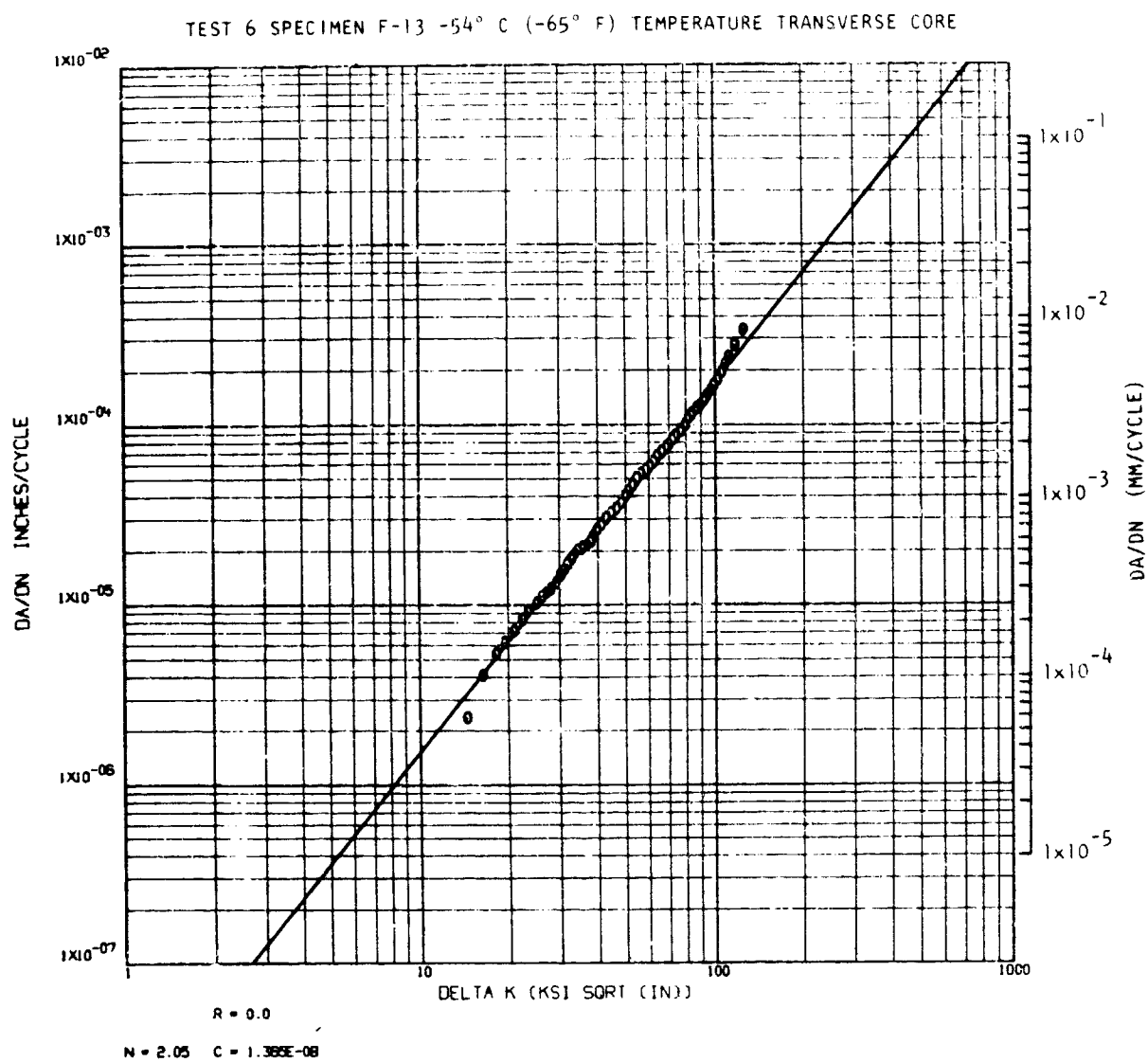
Figure 66.   Crack Growth Rate Plot for Test Specimen F-13 at -54° C (-65° F)
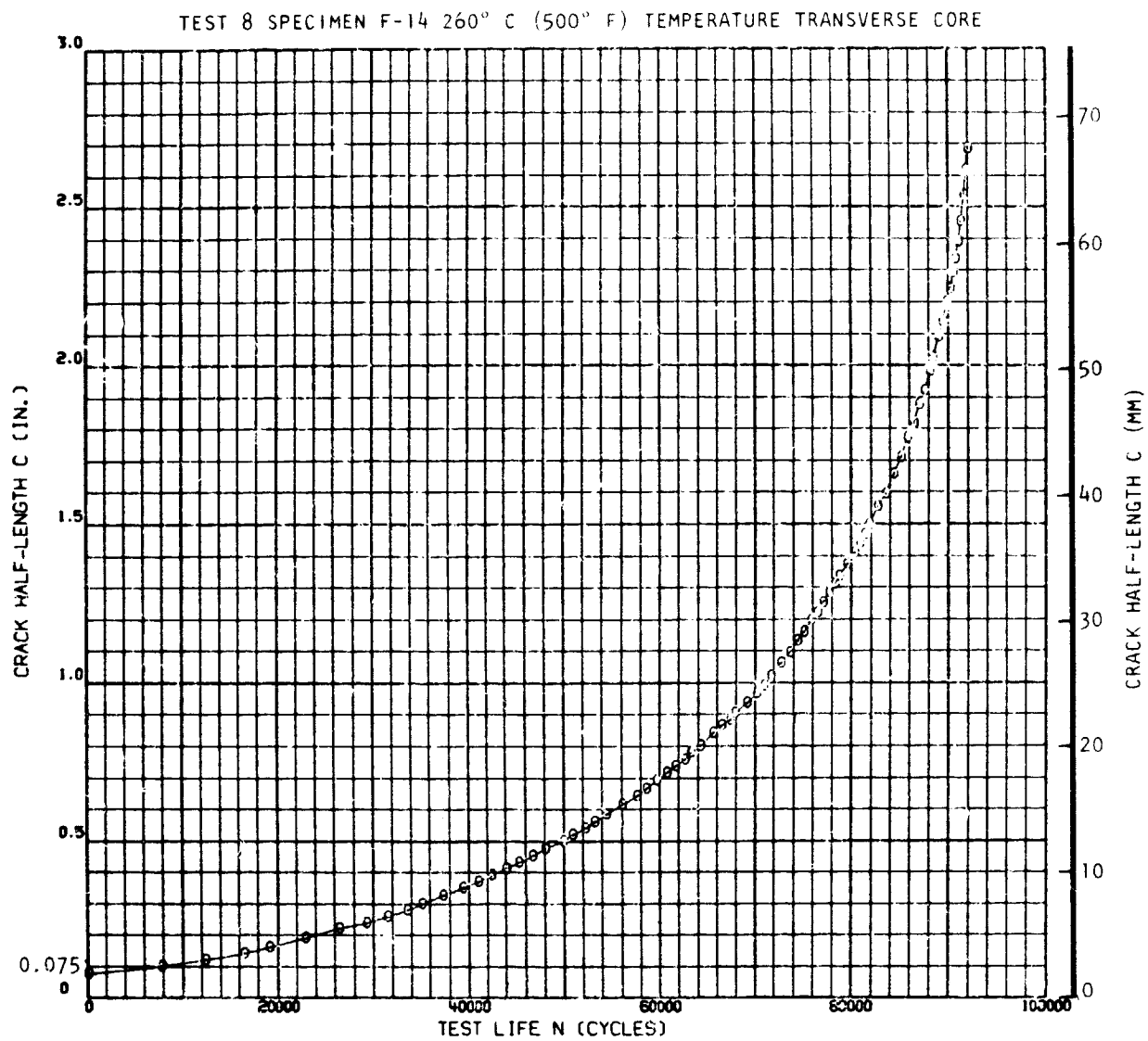
Figure 67. Crack Growth Curve for Test Specimen F-14 at 260° C (500° F)
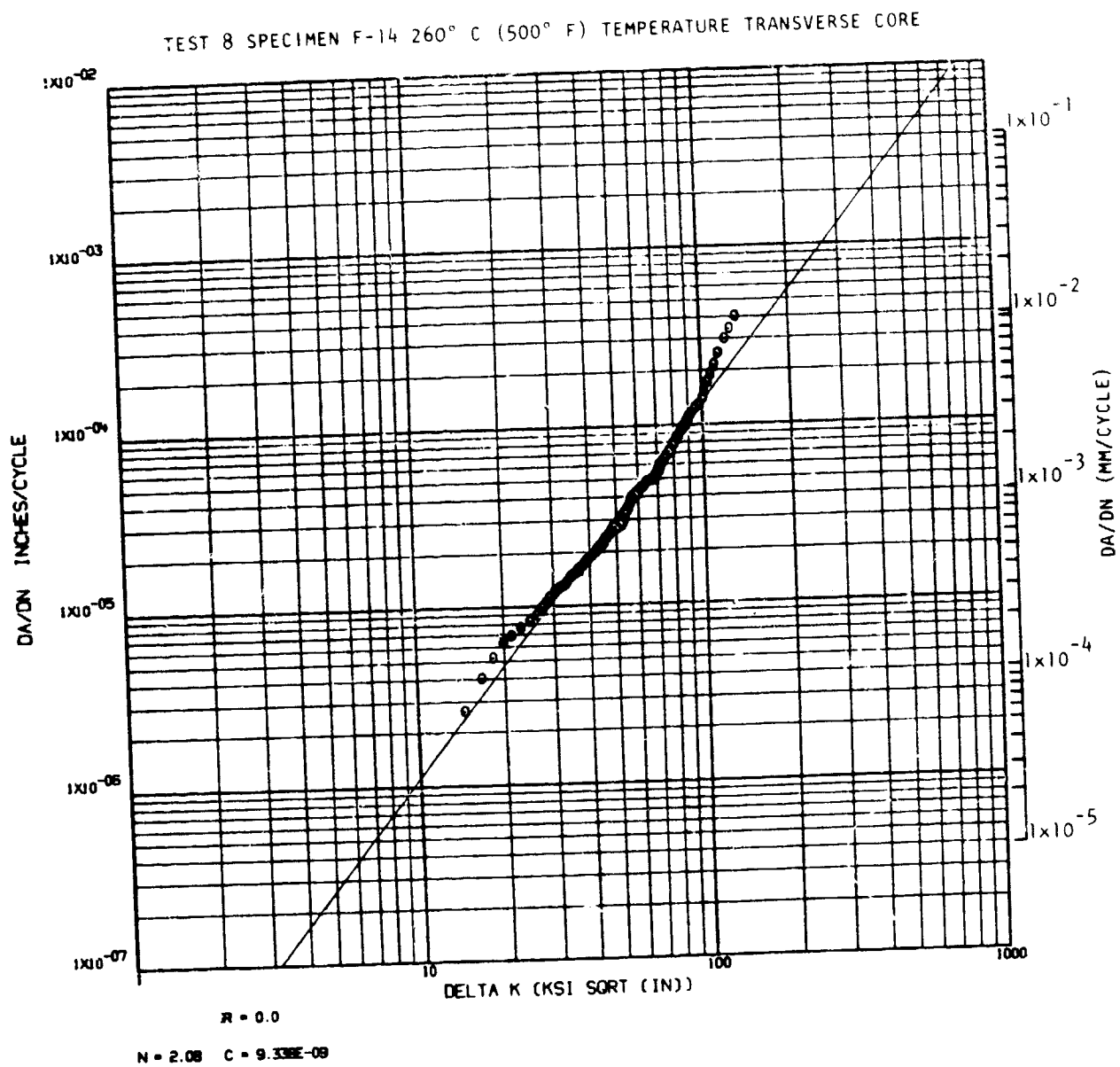
Figure 68. Crack Growth Rate Plot for Test Specimen F-14 at 260° C (500° F)
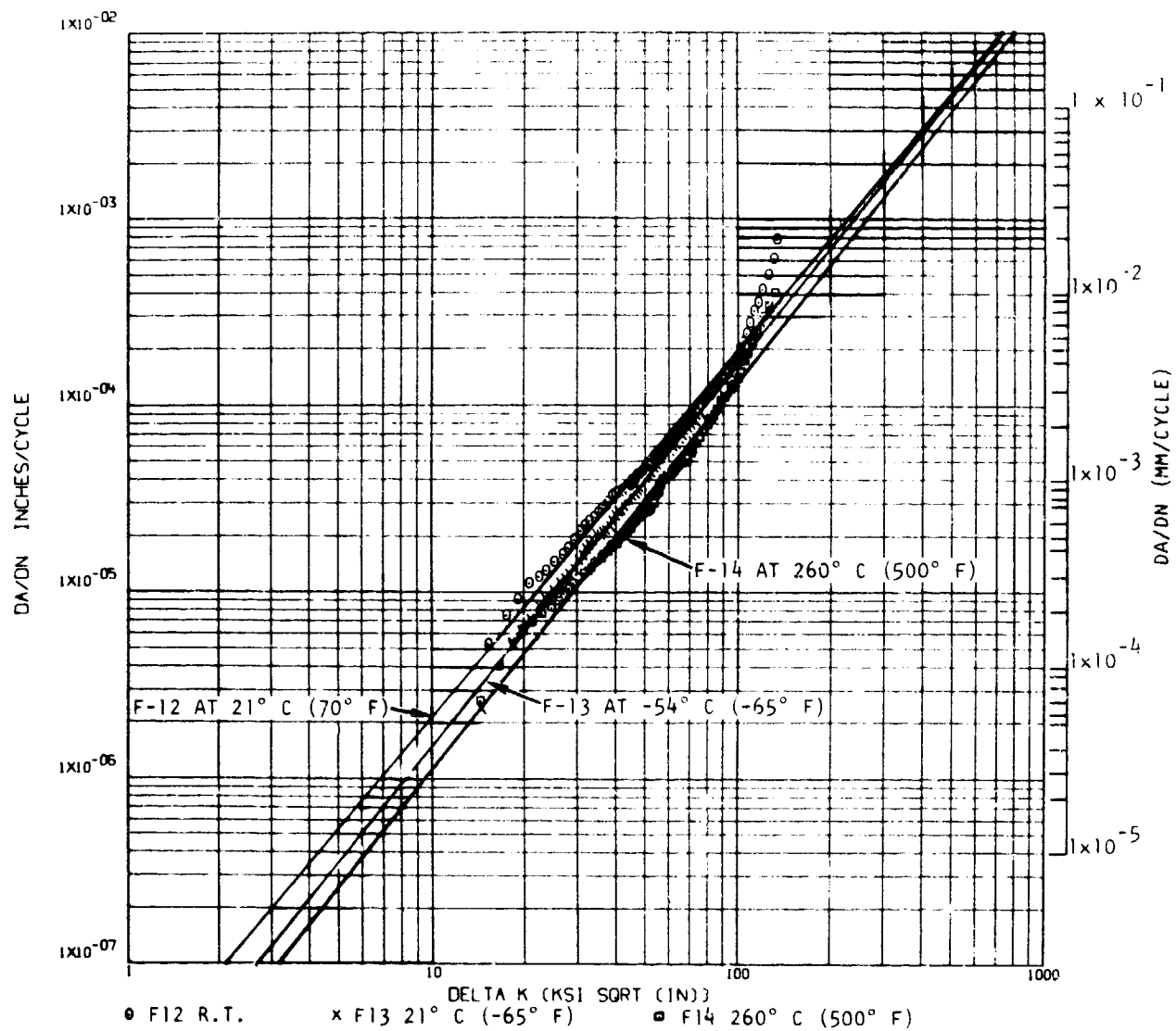
Figure 69.   Crack Growth Rates for Transverse
Core Tests at Three Temperatures
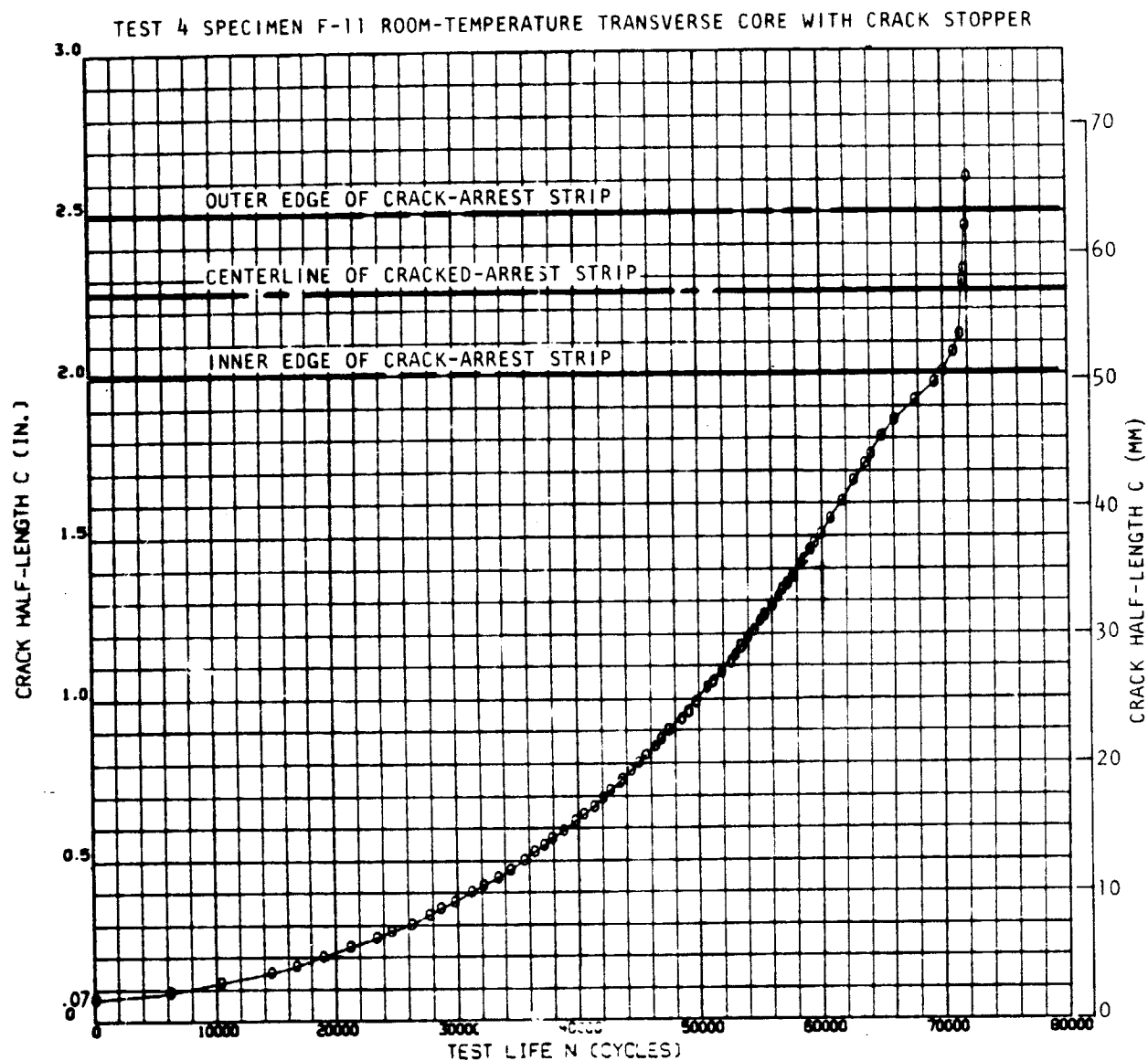
Figure 70. Crack Growth Curve for Test Specimen F-11 at 21° C (70° F)
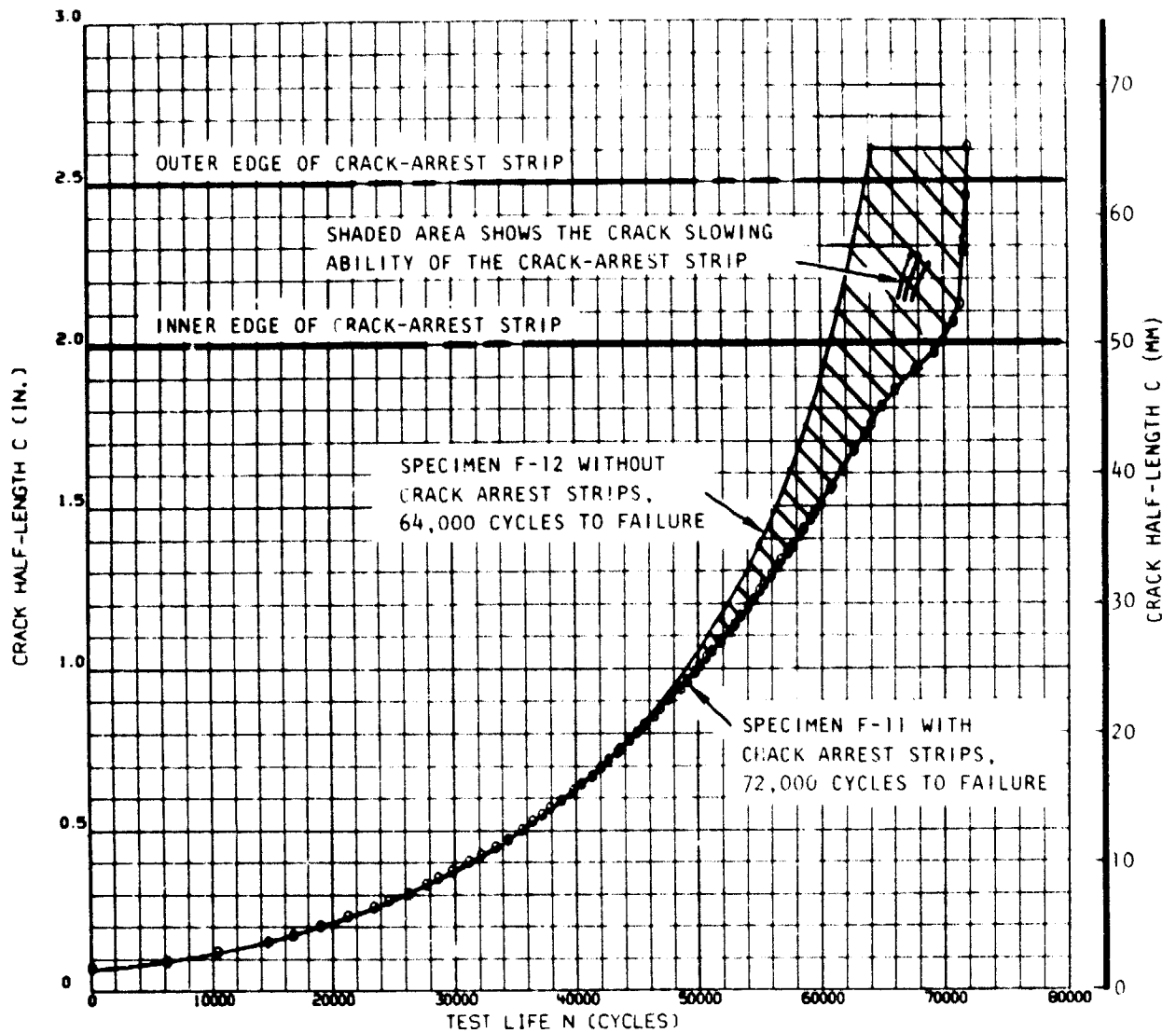
Figure 71. Comparison of Crack Growth Curves in Transverse
Core Specimens With and Without Crack Arrest Strips
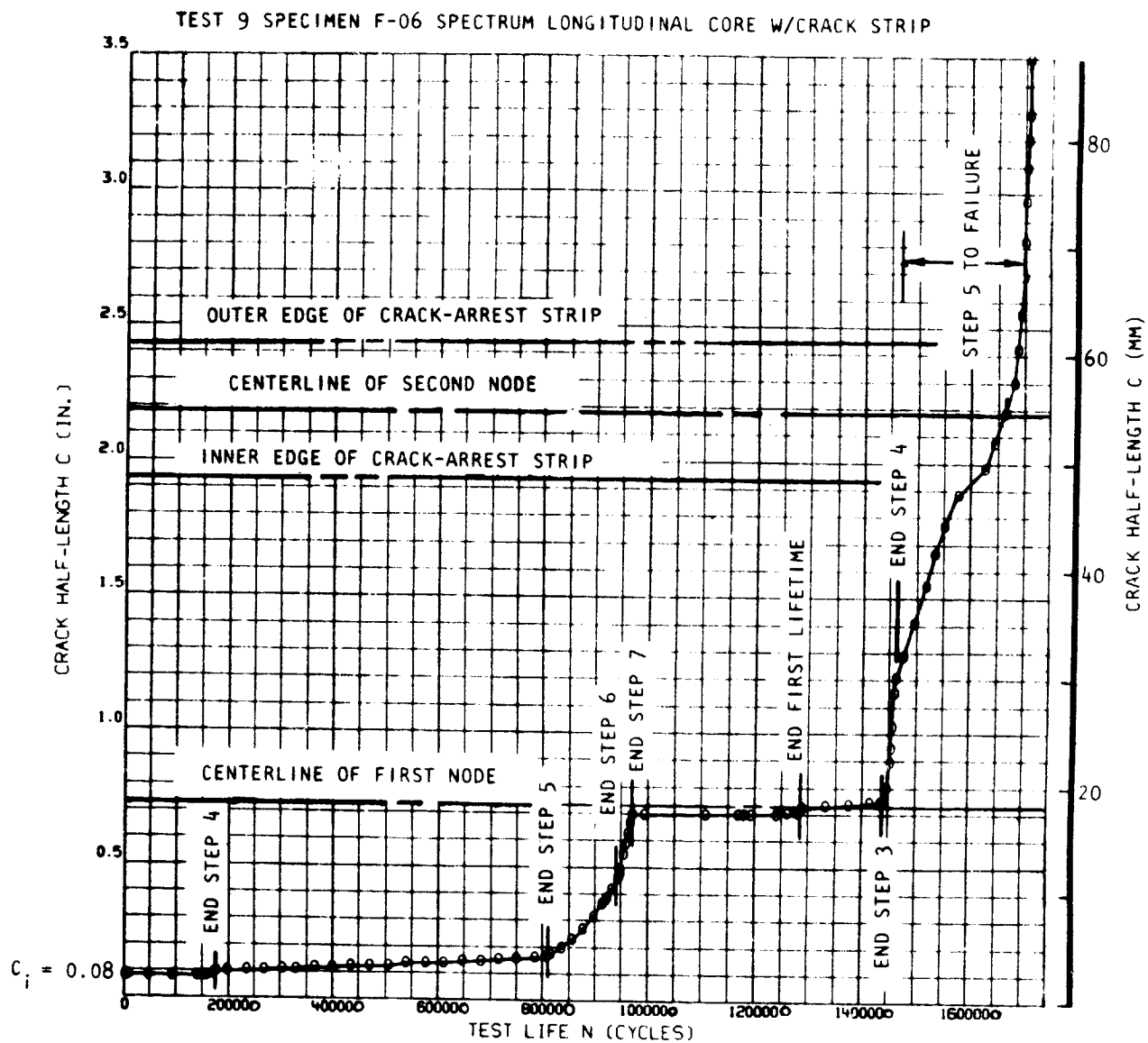
Figure 72. Crack Growth Curve for Spectrum Test Specimen F-06
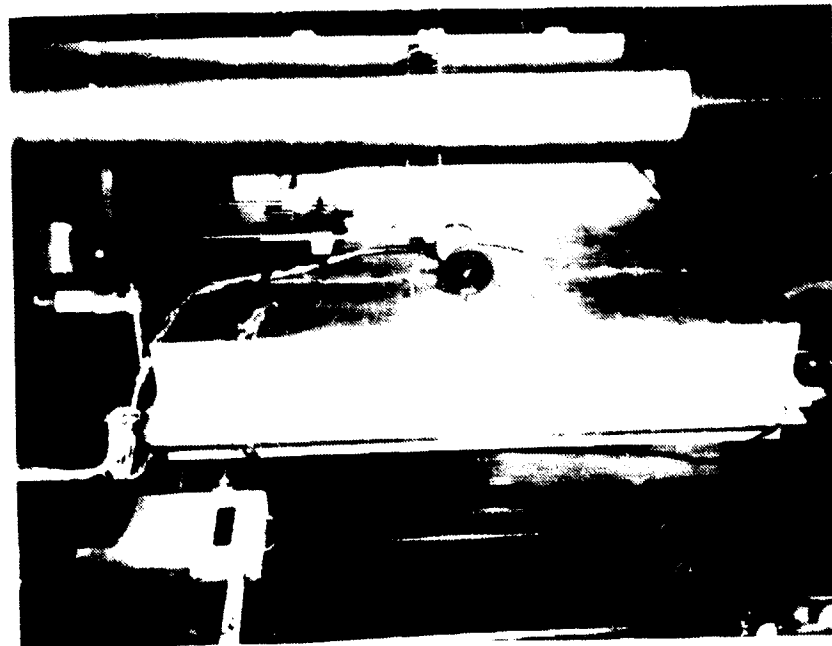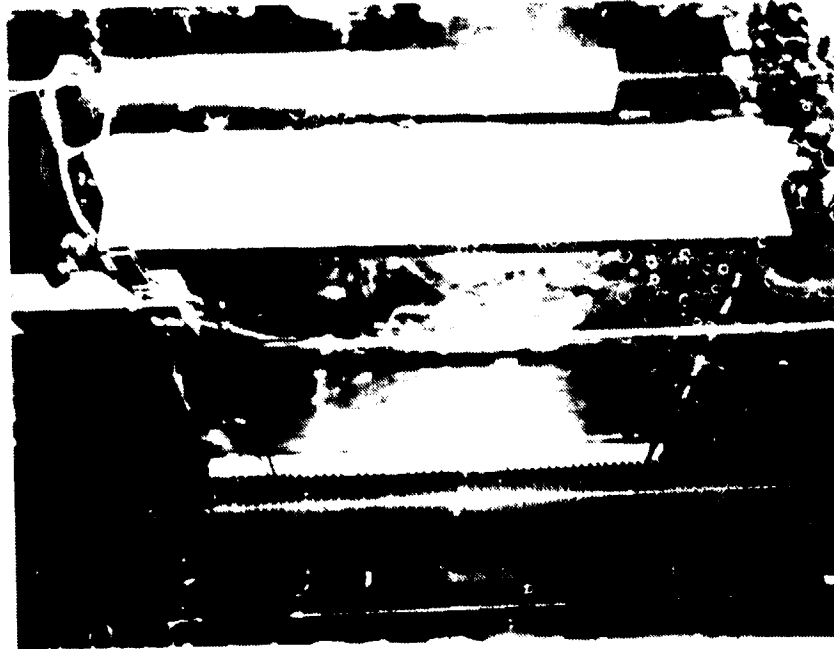
Figure 73. Compression Panel Test Setup

111
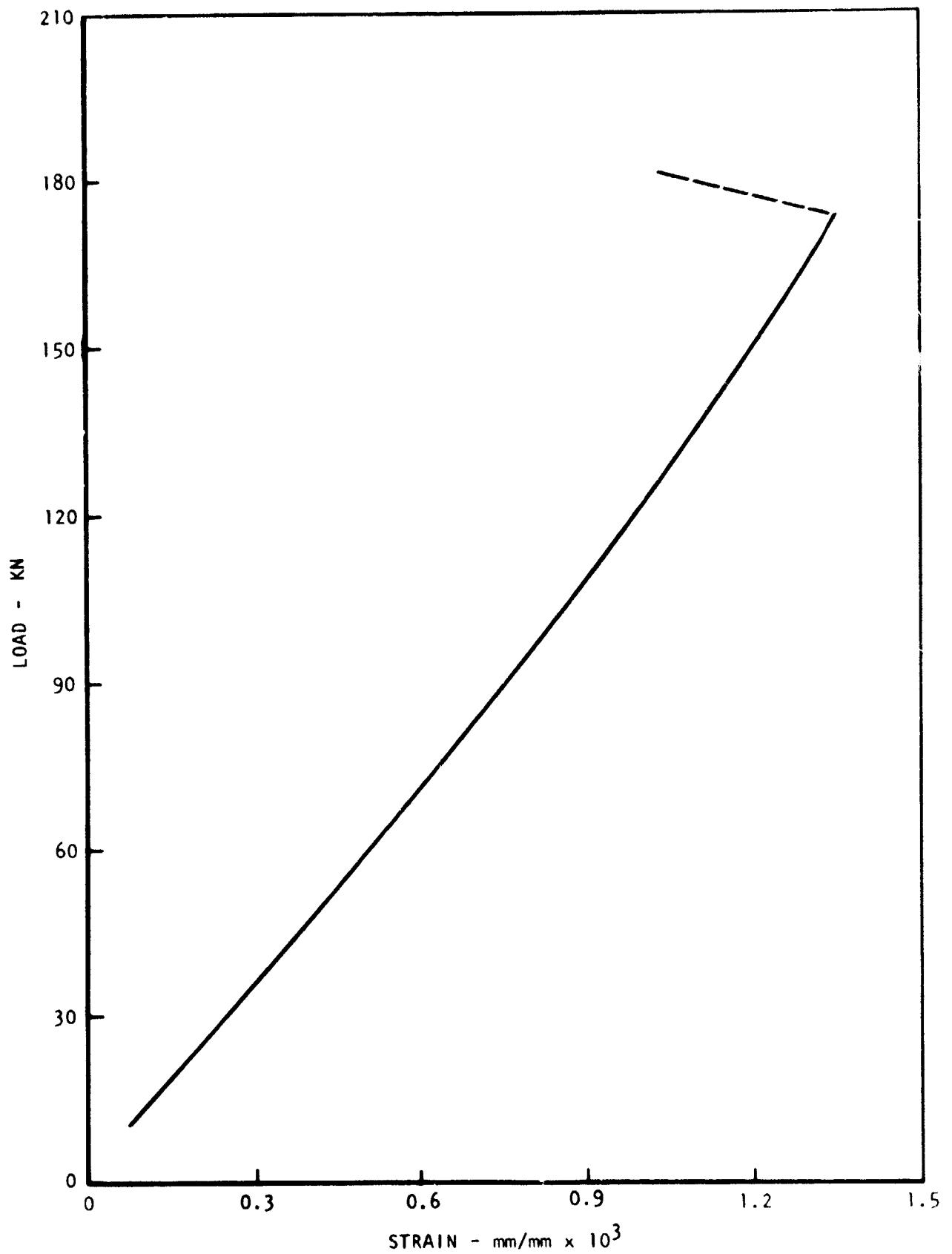
Figure 74. Transverse Long Column - Load Versus Strain (Strain Gage 7)
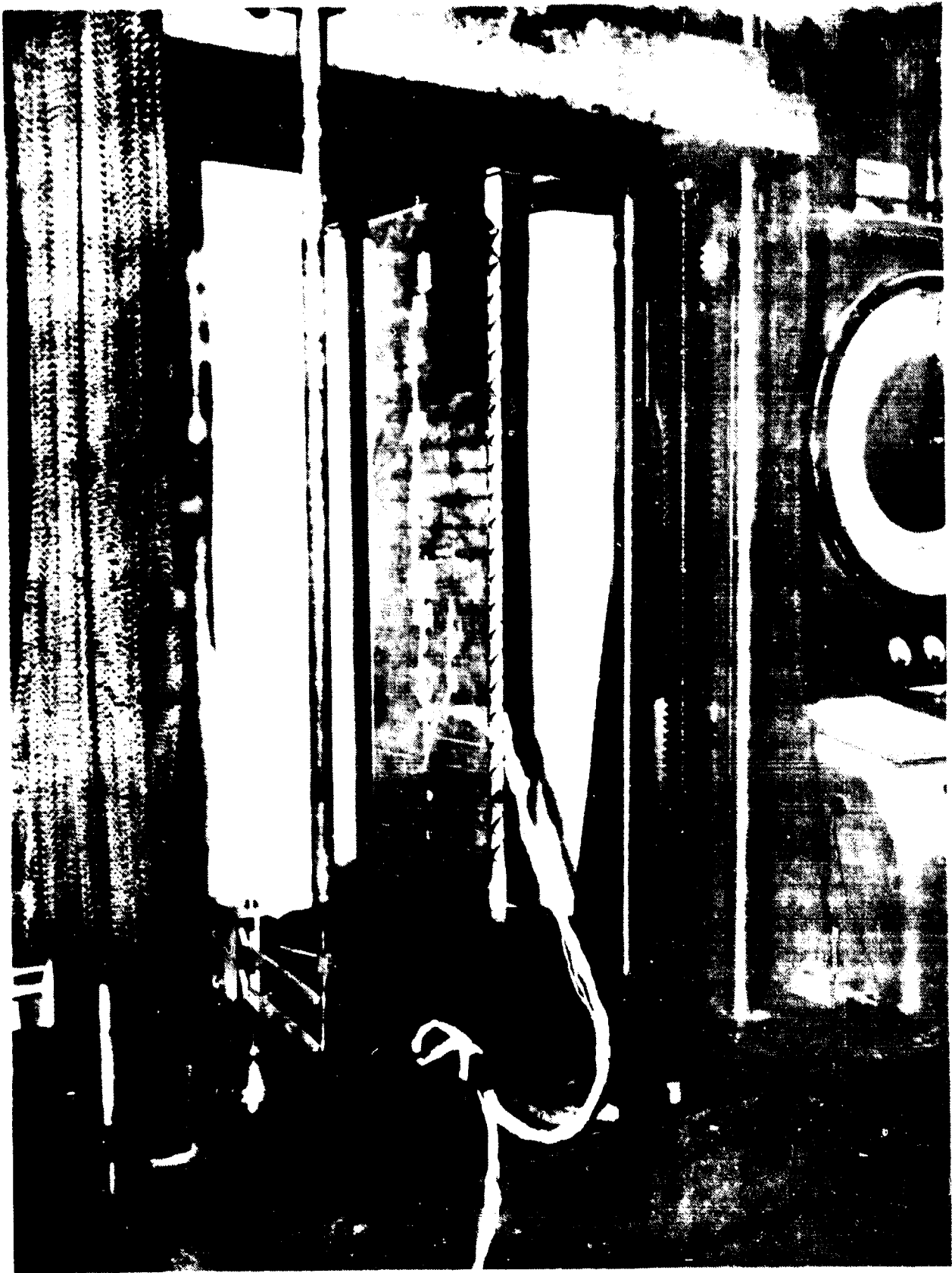
Figure 75. Transverse Long Column Test Section

Figure 7b. Transverse Long Column - Local Failure

Figure 77. Transverse Long Column - Local Failure - Closeup

115

CORE

610(24)

25.35
(0.988)

711
(28)

1219
(48)

914
(36)

LOAD PLATE

0.89
(0.035)

EDM Flaw
2nd Lifetime

55.4
(2.18)

166.1
(6.54)

.038
(.038)

12.7
.50
TYP

3.0(.120)
TYP

SECTION A-A

ALL DIMENSIONS ARE IN MM(IN.)
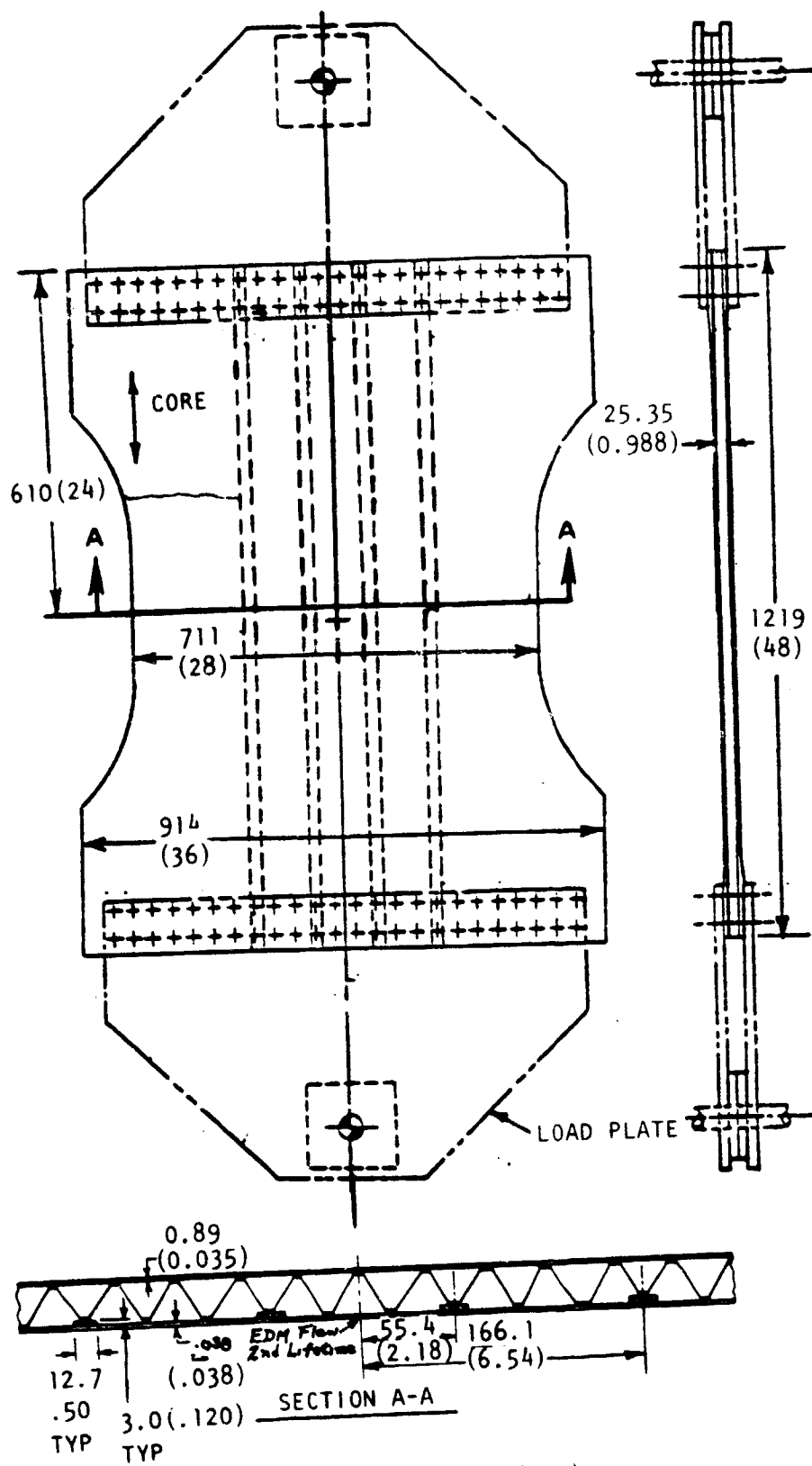
Figure 78. Fatigue Structural Performance Panel

116
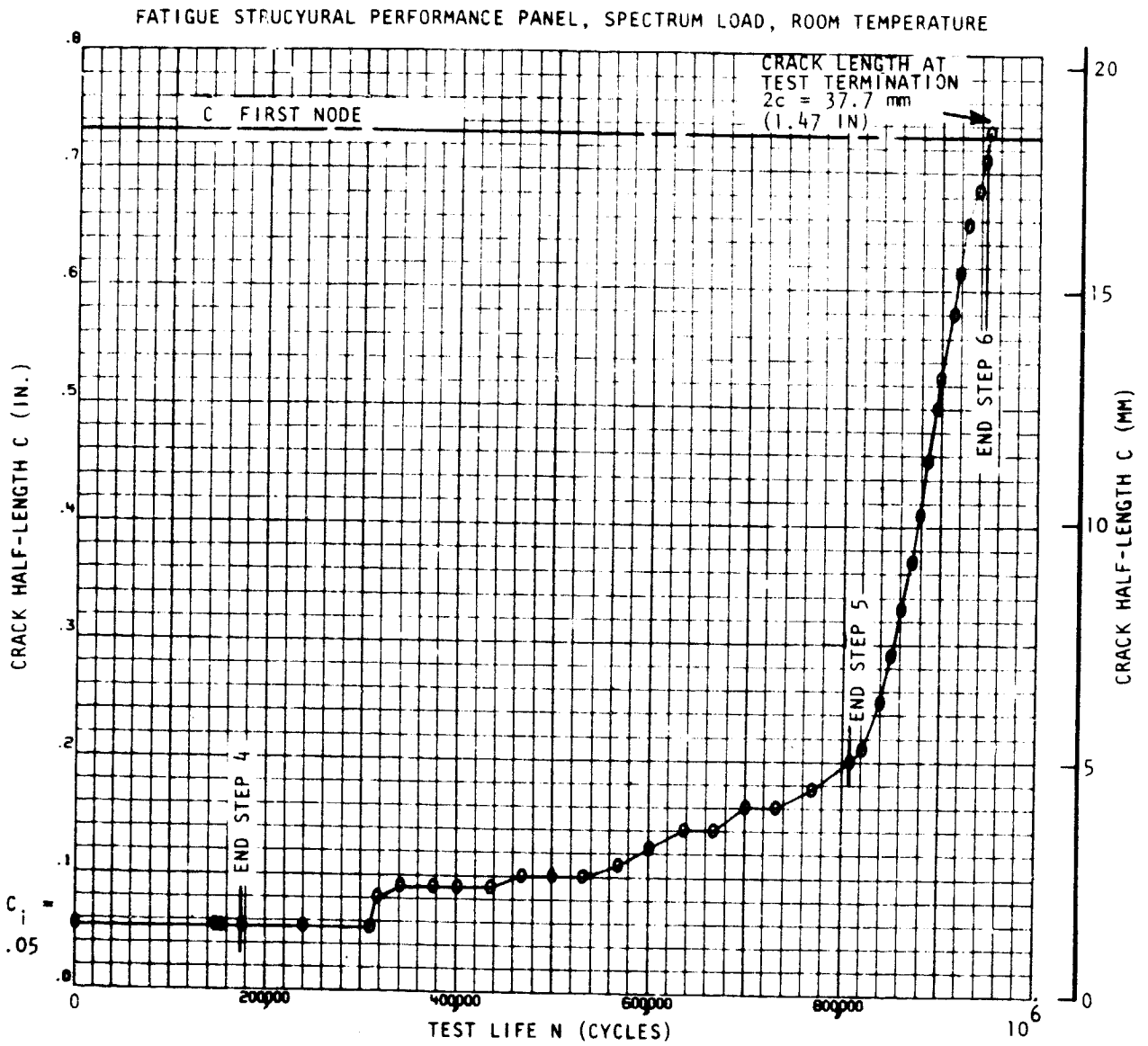
Figure 79. Crack Growth Curve for the Structural Performance Panel

Table I

LOADING SYSTEM AND PANELS SUBDIVISION

Spanwise (Ns) ←
Chordwise (Nc) ↑

| 460 |
| 451 |
| 448 |
| 441 |

*Loads in KN/m (kips/in.)

	Subpanel No.	Ns*	Nc*	Nsc*	Ns_max*	Nsc*
Original subpanel loads — Upper cover	460	-1.221 (-6.973)	-.392 (-2.239)	-.302 (1.725)		
	451	-1.207 (-6.892)	-.359 (-2.050)	-.326 (1.864)		
	448	-1.216 (-6.943)	-.336 (-1.921)	.324 (1.849)		
	441 441	-1.062 (-6.064)	-.475 (-2.712)	.378 (2.159)		
Original subpanel loads — Lower cover	460	-.183 (-1.047)	-.372 (-2.122)	.257 (1.466)	.517 (2.950)	.163 (.933)
	451	-.173 (-.988)	-.624 (-3.561)	.192 (1.097)	.538 (3.071)	.199 (1.137)
	451	-.138 (-.789)	-.568 (-3.245)	.043 (.246)	.499 (2.852)	.199 (1.139)
	488					
	441	-.152 (-.866)	-.538 (3.075)	-.004 (-.0206)	.624 (3.561)	.269 (1.538)
Averaged panel loads	Upper cover	-1.177 (-6.72)	-.390 (-2.23)	.333 (1.90)		
	Lower cover	-.161 (-.92)	-.525 (-3.00)	.122 (.70)	.545 (3.11)	.208 (1.19)
		Used for static design			Used for fatigue design	

Table II

RADIOGRAPHIC INSPECTION RESULTS

Discrepancy Type	Panel Number					
	1	2	3	4	5	6
Core rupture		$X^{(4)}$		$X^{(6)}$		$X^{(5)}$
Core thinning		$X^{(4)}$		$X^{(7)}$		X
Core distortion	$X^{(1)}$	X	X	X	$X^{(8)}$	$X^{(9)}$
Core spacing	X		X		X	
Nonbonds	$X^{(2)}$	$X^{(2)}$		$X^{(3)}$	$X^{(2)}$	

NOTES:
1. Edge only

2. 6 to 12 mm (1/4 to 1/2 inch) diameter

3. 152 mm (6 inches) diameter

4. At node termination only

5. 5% of panel area

6. 20% of panel area

7. 60% of panel area

8. 60% of panel area. Distortion not perceptible to visual examination of cut specimens

9. 70% of panel area

Table III

STATIC TEST PLAN (UPPER PANEL)
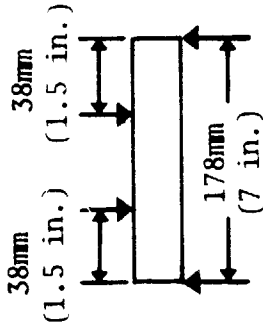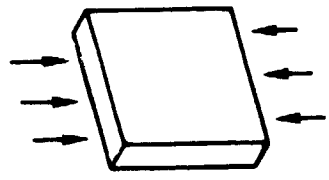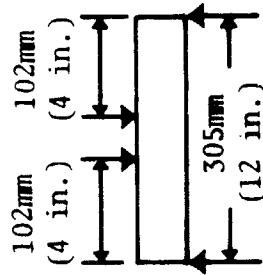
	Core shear beam			Short column			Bending beam		
Test type	Core shear beam			Short column			Bending beam		
Core direct	L&T			L&T			L&T		
Test temperature	-54° C (-65° F)	RT	260° C (500° F)	-54° C (-65° F)	RT	260° C (500° F)	-54° C (-65° F)	RT	260° C (500° F)
Specimen No. L	SCLL	SCLR1 SCLR2 SCLR3	SCLH1 SCLH2 SCLH3	CSLL	CSLR1 CSLR2 CSLR3	CSLH1 CSLH2 CSLH3	BBLL	BBLR1 BBLR2 BBLR3	BBLH
T	SCTL	SCTR1 SCTR2 SCTR3	SCTH1 SCTH2 SCTH3	CSTL	CSTR1 CSTR2 CSTR3	CSTH1 CSTH2 CSTH3	BBTL	BBTR1 BBTR2 BBTR3	BBTH

Core shear beam dimensions: 38mm (1.5 in.), 38mm (1.5 in.), 178mm (7 in.)

Bending beam dimensions: 102mm (4 in.), 102mm (4 in.), 305mm (12 in.)

Table IV

MATERIAL PROPERTIES

Temperature	-54° C	RT	260° C
F_{cy} (MPa)	932.9	813.6	488.2
E_c (GPa)	115.90	113.08	96.19

NOTE The use of nondifferential chem-milling of the panels, with consequently heavier than designed faces, caused the buckling stress level for the longitudinally tested specimens to be pushed into the plastic range and introduced the influence of the plasticity correction factor into the prediction of the buckling stresses. New data should be obtained in the elastic range (low-level stress) to eliminate the plasticity factor influence.

Table V

SHORT COLUMN LONGITUDINAL TEST EVALUATION

SPECIMEN	STRESSES						MODULUS OF ELASTICITY						
	PREDICTED		TEST		T/P		PREDICTED	TEST STRAIN GAGE			T/P STRAIN GAGE		
	F_{cr}	F_{cs}	f_{cr}	f_{ult}	$\frac{f_{cr}}{F_{cr}}$	$\frac{f_{ult}}{F_{cs}}$		#1	#2	Average	#1	#2	Average
SCLL	754	754	821	867	1.09	1.18	115.9	125.21	109.08	117.14	1.08	.94	1.01
SCLR1	717	704	704	751	.98	1.07	113.1	109.91	112.18	111.04	.97	.99	.98
SCLR2	736	727	671	732	.94	1.01	113.1	99.01	111.70	105.36	.88	.99	.93
SCLR3	647	680	739	801	1.06	1.18	113.1	115.49	105.98	110.74	1.02	.94	.98
SCLH1	479	490	466	484	.97	.99	96.2	111.91	97.50	104.70	1.16	1.01	1.09
SCLH2	465	470	476	494	1.00	1.05	96.2	111.63	110.66	111.14	1.16	1.15	1.16
SCLH3	458	466	478	504	1.04	1.08	96.2	102.39	104.87	103.63	1.06	1.09	1.08
Average					1.01	1.08					1.05	1.02	1.03

Stresses in MPa

Modulus of Elasticity in GPa

TABLE VI

SHORT COLUMN TRANSVERSE TEST EVALUATION

Specimen	Stress (MPa)					Compression Modulus - E_c (GPa)				
	Predicted	Test		Test/Predicted		Predicted	Test	T/P	Test Reduced by 1.64	T(Reduced)/P
	F_{cr}	f_{cr}	f_{ult}	f_{cr}/F_{cr}	$f_{ult}/1.2\ F_{cr}$					
SCTL	270	268	346	.99	1.07	115.9	170.9	1.47	104.2	.90
SCTR1	392	288	451	.73	.97	113.1	183.0	1.62	111.59	.99
SCTR2	314	249	428	.79	1.14	113.1	171.8	1.52	104.8	.93
SCTR3	341	256	408	.75	1.00	113.1	173.3	1.53	105.7	.93
SCTH1	228	200	276	.88	1.02	96.2	182.0	1.89	111.0	1.15
SCTH2	237	217	292	.92	1.03	96.2	162.8	1.69	99.3	1.03
SCTH3	253	210	282	.83	.93	96.2	168.2	1.75	102.6	1.07
Average				.84	1.02			1.64		1.00

TABLE VII

CORE SHEAR LONGITUDINAL TEST EVALUATION

Specimen	Stress (MPa)					Core Shear Modulus (GPa)		
	Predicted	Test		Test/Predicted		Predicted	Test	Test/Predicted
	F'_{s_L}	f'_{cr_s}	f'_{ult_s}	$\dfrac{f'_{cr_s}}{F'_{s_L}}$	$\dfrac{f'_{ult_s}}{F'_{s_L}}$			
CSLL	27.1	17.53	23.40	0.65	0.86	1239	1042	0.84
CSLR1	22.9	16.14	23.18	0.71	1.01	1033	910	0.88
CSLR2	23.8	16.88	22.86	0.71	0.95			
CSLR3	24.3	14.47	21.99	0.60	0.90	1297	969	0.75
CSLH1	14.0	6.38	8.79	0.45	0.63	933	1091	1.17
CSLH2	13.9	9.88	13.39	0.71	0.96	863	1742	2.02
CSLH3	14.1	9.06	10.96	0.64	0.78	916	1364	1.49
Average				0.64	0.87			1.157

NOTE: The prime (') superscript denotes equivalent shear stresses normalized to a hypothetical homogeneous core.

124

TABLE VIII

CORE SHEAR TRANSVERSE TEST EVALUATION

| Specimen | Stress (MPa) | | | | | Shear Modulus - G'_{c_T} (GPa) | | |
| | Predicted | Test | | T/P | | Predicted | Test | T/P |
	F'_{s_T}	f'_{cr_s}	f'_{ult_s}	f'_{cr_s}/F'_{s_T}	f'_{ult_s}/F'_{s_T}			
CSTL	18.5	7.7	9.8	0.41	0.53	1.44	0.86	0.60
CSTR1	14.0	4.5	6.0	0.32	0.43	1.45	1.03	0.71
CSTR2	17.9	7.7	9.8	0.43	0.55	1.42	1.05	0.72
CSTR3	14.5	5.0	7.3	0.34	0.51	1.39	1.41	1.01
CSTH1	11.3	4.3	5.0	0.38	0.44	1.19	0.42	0.35
CSTH2	9.8	4.8	5.7	0.49	0.58	1.15	0.68	0.59
CSTH3	10.7	6.5	7.7	0.61	0.72	1.18	1.06	0.89
Average				0.43	0.54		.70	

NOTE: The prime (') superscript denotes equivalent shear stresses normalized to a hypothetical homogeneous core.

125

TABLE IX

BENDING BEAM LONGITUDINAL TEST EVALUATION

Specimen	Predicted Stress (MPa)		Test Stress (MPa)		Test/Predicted	
	F_{cr}	F_{cs}	f_{cr}	f_{cs}	$(T/P)_{cr}$	$(T/P)_{cs}$
BBLL	689	707	775	1047	1.12	1.48
BBLR1	610	660	759	1074	1.24	1.62
BBLR2	724	719	669	945	.92	1.31
BBLR3	674	537	455	550	.95	1.02
BBLH	810	770	854	895	1.05	1.16

TABLE X

BENDING BEAM TRANSVERSE TEST EVALUATION

Specimen	Predicted Stress F_{cr} (MPa)	Test Stress f_{cr} (MPa)	T/P
BBLT	295	445	1.51
BBTR1	287	477	1.66
BBTR2	276	412	1.49
BBTR3	319	395	1.24
BBTH	231	306	1.32
Average			1.44

TABLE XI

SPECIMEN LIST FOR THE CRACK GROWTH TESTS

Specimen No.	Core Node Direct.	Crack Arrest Strip	Test Temperature	Type Load	Maximum Load KN (Kips)	Maximum Stress MPa (ksi)	Initial Crack Size mm (in.)	Test Life
F-05	L	Yes	21° C (70° F)	Constant Amplitude	135.7 (30.5)	219 (31.7)	3.6 (0.14)	66,000 N
F-07	L	No	21° C (70° F)	Constant Amplitude	122.3 (27.5)	218 (31.6)	3.3 (0.13)	80,000 N
F-09	L	No	-54° C (-65° F)	Constant Amplitude	122.3 (27.5)	218 (31.6)	4.1 (0.16)	83,000 N
F-10	L	No	260° C (500° F)	Constant Amplitude	122.3 (27.5)	214 (31.1)	4.3 (0.17)	78,000 N
F-11	T	Yes	21° C (70° F)	Constant Amplitude	84.5 (19.0)	200 (29.0)(1)	3.6 (0.14)	72,000 N
F-12	T	No	21° C (70° F)	Constant Amplitude	71.2 (16.2)	199 (28.8)(1)	3.3 (0.13)	64,000 N
F-13	T	No	-54° C (-65° F)	Constant Amplitude	70.3 (15.8)	186 (27.0)(1)	3.6 (0.14)	100,000 N
F-14	T	No	260° C (500° F)	Constant Amplitude	73.4 (16.5)	205 (29.7)(1)	3.8 (0.15)	93,000 N
F-06	L	Yes	21° C (70° F)	Spectrum	143.2 (32.2)	231 (33.5)	4.1 (0.16)	1,709,000 N

(1) For the transverse core tests, the listed maximum stress equals the load divided by the areas of the face sheets, and crack arrest strips when appropriate. No core material was assumed effective. See Table XIII for specimen dimensions.

128

TABLE XII

CRACK GROWTH TEST SPECIMEN DIMENSIONS

Specimen No.	Nominal Drawing Dimension				Actual Dimension			
	t_{F_1}	t_{F_2}	t_{strip}	t_N	t_{F_1}	t_{F_2}	t_{strip}	t_N
F-05	0.84 (.033)	0.84 (.033)	3.05 (.120)	1.12 (.044)	0.84 (.033)	1.07 (.042)	2.84 (.112)	1.12 (.044)
F-07					1.04 (.041)	0.79 (.031)	-	
F-09					1.04 (.041)	0.79 (.031)	-	
F-10					0.81 (.032)	1.07 (.042)	-	
F-11			3.05 (.120)		0.94 (.037)	1.04 (.041)	2.84 (.112)	
F-12					0.86 (.034)	1.04 (.041)	-	
F-13			-		0.91 (.036)	1.07 (.042)	-	
F-14			-		0.79 (.031)	1.09 (.043)	-	
F-06	0.84 (.033)	0.84 (.033)	3.05 (.120)	1.12 (.044)	0.84 (.033)	1.07 (.042)	2.84 (.112)	1.12 (.044)

Listed thickness dimensions are in mm (in.)
Panel width was 190.5 mm (7.50 in.), length 610 mm (24 in.)

TABLE XIII

TEST SPECTRUM

Step	Mission Segment	Gross Area Stress				% Load		Cycles per Lifetime
		Mean 1G Stress, MPa (KSI)	Alternating Load, Δ G	Maximum Stress, MPa (KSI)	Minimum Stress, MPa (KSI)	Max %	Min %	
1	Cruise	129 (18.75)	+.14G	147.4 (21.37)	111.2 (16.12)	63.8	48.1	147,700
2	Cruise	129 (18.75)	+.24G	160.3 (23.25)	98.3 (14.25)	69.4	42.5	5,275
3	Cruise	129 (18.75)	+.34G	173.2 (25.12)	85.3 (12.37)	75.0	36.9	970
4	GRO-AIR-GRO	--	--	147.4 (21.37)	6.9 (1.00)	63.8	3.0	21,100
5	Climb	172 (25)	+.14G	196.5 (28.50)	148.2 (21.50)	85.0	64.2	632,789
6	Climb	172 (25)	+.24G	213.7 (31.00)	131.0 (19.00)	92.5	56.7	136,960
7	Climb	172 (25)	+.34G	231.0 (35.50)	113.8 (16.50)	100	49.2	25,320
8	Descent	103 (15)	+.14G	117.9 (17.1)	88.9 (12.90)	51.0	38.5	198,340
9	Descent	103 (15)	+.24G	128.2 (18.6)	78.6 (11.40)	55.5	34.0	9,495
10	Descent	103 (15)	+.34G	138.6 (20.10)	68.3 (9.90)	60.0	29.6	802
11	Check Flights	121 (17.5)	+.14G	137.6 (19.95)	103.8 (15.05)	59.6	44.9	80,068
12	Check Flights	121 (17.5)	+.24/-.14G	149.6 (21.70)	103.8 (15.05)	64.8	44.9	20,237
13	Check Flights	121 (17.5)	+.34/-.24G	161.7 (23.45)	91.7 (13.30)	70.0	39.7	4,891
14	Check Flights	121 (17.5)	+.44/-.24G	173.7 (25.20)	91.7 (13.30)	75.2	39.7	1,760
15	Check Flights	121 (17.5)	+.54/-.34G	185.8 (26.95)	79.6 (11.55)	80.4	34.5	582
16	Check Flights	121 (17.5)	+.64/-.44G	197.9 (28.70)	67.6 (9.80)	85.7	29.2	159
17	Check Flights	121 (17.5)	+.74/-.54G	209.9 (30.45)	55.5 (8.05)	90.9	24.0	75

NOTES:

1. This table constitutes one lifetime of 21,100 flights.

2. The 100 percent test load for specimen F-06 was 143.2 KN (32,200 pounds.)

3. The 100 percent test load for the structural performance panel was 525 KN (118,000 pounds).

130

END

DATE

FILMED

MAY 11 1982